The Quasi-Steady-State Approximation for Computational Acceleration of Single Particle Modeling in Polyolefin Processes

by

Mohammed Al-Khayyat

A thesis submitted in partial fulfillment of the requirements for the degree of

Master of Science

in

Chemical Engineering

Department of Chemical and Materials Engineering

University of Alberta

Abstract

In the field of polymer reactor engineering, accurately modeling the complex kinetics and mass transfer mechanics of a supported-catalyst reaction is essential for designing efficient and scalable polymerization processes. However, mesoscale modeling, which involves detailed single-particle models, is often overlooked due to its mathematical complexity, where the dynamic numerical solution of the partial differential equations that describe the intraparticle reaction-diffusion phenomena are computationally demanding. The quasi-steady-state approximation (QSSA) presented in this thesis provides an alternative computationally efficient approach to solving the polymer flow model, which is an established numerical model for understanding the dynamics of polymer particle growth. In both homopolymerization and copolymerization setups, the developed QSSA model is compared with the corresponding dynamic solutions assuming both uniform and nonuniform radial distribution of active sites in the growing particle. The simulations demonstrate that, after a very short initial period, the QSSA provides a perfect match with the dynamic solution when active sites are uniformly distributed within the particle. However, if the dynamic solution accounts for the local dilution of catalyst fragments in the produced polymer, resulting in a non-uniform distribution of active sites decreasing with radial position, the QSSA shows promising performance only at low to medium Thiele moduli. As the Thiele modulus increases, the QSSA solution starts to deviate more from the dynamic solution due to the pronounced concentration gradient of active sites. These high Thiele modulus values correspond to high levels of mass transfer limitations, which are undesirable and often avoided in real processes.

Preface

The work in this thesis has been submitted for publication in two parts. This thesis is an original work by Mohammed Al-Khayyat, except for the homopolymerization dynamic model with uniform active sites distribution (section 3.2.4) which was mainly developed and coded by Dr. Arash Alizadeh and has been presented in his Ph.D. Thesis.

Acknowledgements

First and foremost, I want to express my gratitude to Allah, the source of my life and all that I have experienced. It is through His provisions — fortitude, tolerance, and the affection of others — that I have been sustained.

I owe my deepest gratitude to my supervisor, Professor Joao Soares. His continuous encouragement, support, and trust have been instrumental to my academic work, allowing me to explore and develop my skills and ideas. I would also like to extend my sincerest gratitude to Dr. Arash Alizadeh, who has been a very exceptional mentor. His guidance and teachings have had a significant impact on my work, and his insights and dedication have significantly contributed to the success of my research, for that, I am exceedingly appreciative. This thesis would not have been possible without them.

I would like to express my deepest love to my parents and siblings. Their unwavering support and encouragement have been a source of inspiration for me. I particularly thank them for tolerating my extensive daily calls.

Finally, I am thankful to all my friends, both domestic and international, from Canada, Bahrain, Brazil, France, and beyond, for their continuous cheering and support.

Contents

List of Figures

List of Abbreviations

A_c	Surface area of catalyst particle
A	Discretization parameter
B	Discretization parameter
C	Discretization parameter
$[C_0]$	Concentration of active sites
C_1	Constant
C_2	Constant
$D_{e,1}$	Effective diffusion coefficient for monomer
$D_{e,2}$	Effective diffusion coefficient for comonomer
F_1	Variable transformation definition
F_c	Complementary solution
F_p	Particular solution
$f(r)$	Ordinary differential equation solution
$M_{w,1}$	Monomer molecular weight
$M_{w,2}$	Comonomer molecular weight
m_i	Mass of polymer produced in shell
$[M_1]$	Concentration of monomer

$[M_2]$	Concentration of comonomer
$\overline{[M_1]}$	Average concentration of monomer at shell i
$\overline{[M_2]}$	Average concentration of comonomer at shell i
M_T	Total concentration
M	Molecular weight of polymer
N	Total number of grids
$[M_1]_s$	Monomer concentration at surface of particle
$[M_2]_s$	Comonomer concentration at surface of particle
m_{tot}	Total mass of polymer
R_0	Initial radius of catalyst
R_p	Rate of polymerization
R_v	Volumetric rate of homopolymerization
$R_{v,1}$	Volumetric rate of monomer copolymerization
$R_{v,2}$	Volumetric rate of comonomer copolymerization
R	Time-dependent radius of growing polymer particle
r	Radial position in polymer particle
V_c	Volume of catalyst particle
V_{tot}^{t}	Previous volume of particle
$V_{tot}^{t+\Delta t}$	Updated volume of particle
V_{tot}	Volume of particle
$W_{logM,ins}$	Instantaneous molecular weight distribution
W_{logM}	Cumulative molecular weight distribution
$w_M(i)$	Flory most probable distribution

$[M_L]$	Concentration of living polymer chains
ρ_p	Density of polymer

List of Acronyms

PFM	Polymer Flow Model
QSSA	Quasi-Steady-State Approximation
QSSA-Vf	Quasi-Steady-State Approximation, variable monomer fraction
QSSA-AF	Quasi-Steady-State Approximation, average monomer fraction
RS	Rigorous Solution
DS	Dynamic Solution

List of Tables

Chapter 1

Introduction

1.1 Motivation and Objectives

Polyolefins synthesized by supported catalysts have become a dominant class of synthetic polymers around us. They are commonly produced by polymerizing olefins like ethylene and propylene as the main monomers, with α-olefins as comonomers. The polyolefin market is expected to grow more than 2% during 2024-2026. This is attributed to the polyolefins' excellent mechanical and physical properties, coupled with their low production cost and versatility. Examples of polyolefins products include food packaging, automotive parts, textiles, and household goods. Polyethylene is commercially produced as copolymers of ethylene reacted with varying fractions of α-olefins. The complexity of this process lies in the many layers of chemical and physical phenomena that must be considered. From the macroscale of the reactor to the mesoscale of polymer particle and the microscale of the catalyst site. While many models have been developed for the micro- and macroscale, the mesoscale described by the single-particle models is often ignored due to its complex numerical and demanding computational needs. This complexity drastically escalates when these levels are combined and integrated with Monte Carlo simulations and computational fluid dynamic models. This thesis aims to present a simple, computationally efficient, accurate alternative to model the single polymer particles. By applying the quasi-steady-state approximation, we will drive novel analytical and approximate solutions that solve the Polymer Flow Model problem in both homopolymerization and copolymerization systems.

1.2 Thesis Outline

This thesis consists of 6 chapters. Chapter 1 presents a brief overview of the aim and objectives of the thesis. Chapter 2 presents an overview on polyolefin types, common catalyst systems, reactor configurations and modelling. The most common single particle models are presented in this chapter with an overview of their advantages and disadvantages. The chapter also discusses the complexity of polyolefin reaction modelling and the multiple scales associated with it. Chapter 3 presents the mathematical modeling of the polymer flow model for homo- and copolymerization reactions explaining the basis of particle discretization and growth. The chapter also presents and explains the differences between two common solutions for catalyst dilution phenomena in the particle. In Chapter 4, the mathematical derivation and modeling of the quasi-steady-state approximation for homo- and copolymerization reactions are presented. This chapter demonstrates the simplicity of developing the quasi-steady-state approximation and clarifies the assumptions made to attain this solution. Chapter 5 showcases the comparison criteria followed when evaluating the model. This chapter discusses the results and their practical importance. Chapter 6 presents the conclusion and recommendations for future work.

Chapter 2

Literature Review

2.1 Polyethylene

Polyolefins are made of monomers connected in a chain. They are derived from a set of simple olefins. While these monomers can essentially be any kind of olefin, the most popular polyolefins in the market are polyethylene and polypropylene with the most produced plastic being polyethylene. It is a polymer that is mostly utilized in packaging, such as bottles, plastic bags, and films. In 2017, the yearly production of polyethylene resins exceeded 100 million tonnes, making about 34 percent of the global plastics market.[1, 2]

A significant breakthrough in the commercial manufacture of polyethylene occurred with the advent of catalysts that allowed polymerization to occur at low pressures and temperatures. First, there were chromium trioxide catalysts, which were invented in 1951 at Phillips Petroleum by Robert Banks and J. Paul Hogan. Karl Ziegler later created a catalytic system based on organoaluminium compounds and titanium halides in 1953 that functioned even more subtly than the Phillips catalyst. Even though the Phillips catalyst is easier to use and more affordable, by the late 1950s, both approaches had become widely used in industry to produce high-density polyethylene (HDPE). Figure 2.1 shows the Developments of polyolefins catalysts over the years.[3] Polyethylene resins will be the focus of this thesis. Polyethylene (PE) resins are divided into three types: low-density (LDPE), linear low-density (LLDPE), and high-density (HDPE). As the names imply, polyethylene resins are classified according to their density range. Low-density polyethylene is produced in autoclaves or tubular reactors in the presence of oxygen traces under high pressures, where the presence of oxygen leads to the formation of free radicals.

LDPEs have long-chain branches (LCB) and short-chain branches (SCB) formulated on the backbone of the polymer. The long chain branches are generated due to backbiting reactions during chain growth. While the short-chain branches are a result of chain transfer reactions to the

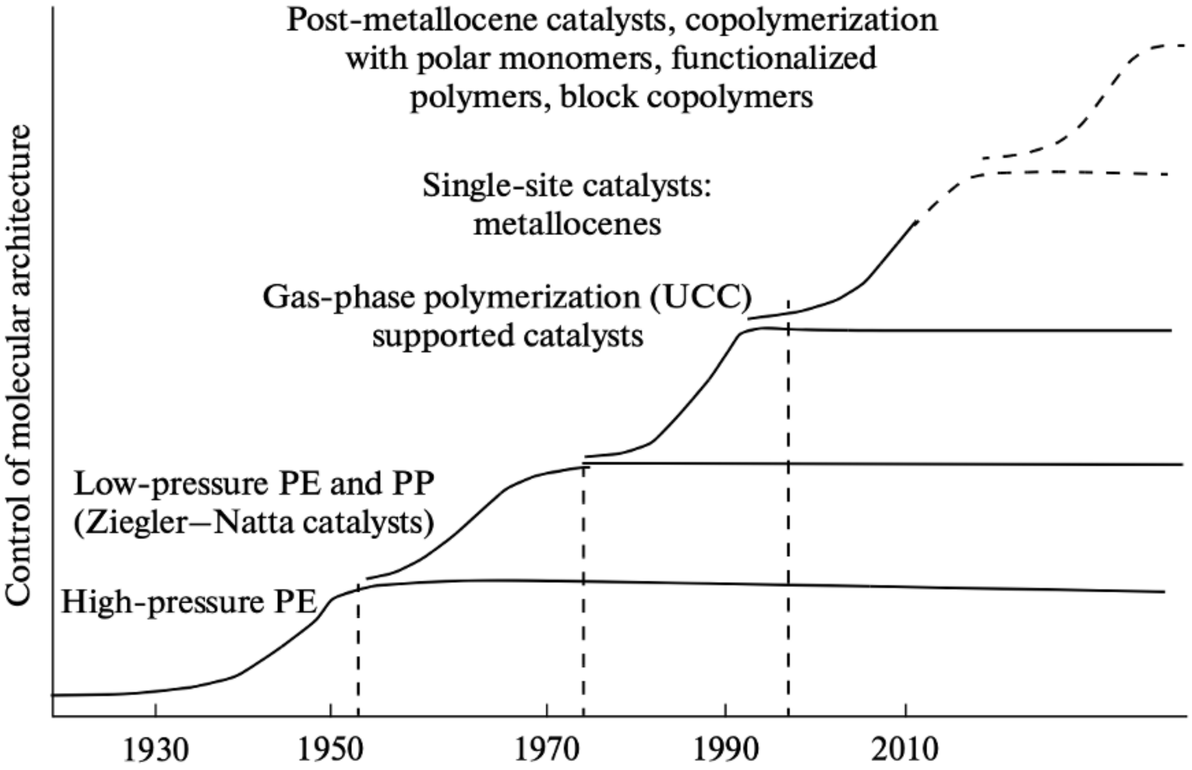

Figure 2.1: Developments of polyolefins catalysts over the century.[4]

polymer. High-density and linear low-density polyethylene, on the other hand, are formed using coordination catalysts, which help in producing the polymers under low temperature and pressure conditions with more control over the density and chain growth mechanism.[3, 4, 5]

Even though the "polyethylene" name suggests that it is only made of ethylene; However, commercial polyethylene resins are usually produced by copolymerizing ethylene with α-olefins. The density of the polyethylene is determined by the number of short branches formed on the backbone (Figure 2.2), as they act like a defect in the polymer that makes it form less crystalline regions. For example, HDPE's density is attributed to the low fraction of α-olefins incorporated into the backbone, and for this reason, HDPE is commonly used for products requiring increased stiffness and low flexibility. LLDPE on the other hand has a higher comonomer incorporation, making them ideal for flexible packaging applications. The heterogeneous Ziegler-Natta catalysts on the other hand are insoluble in the reactor medium and they usually have more than one type of active site, which results in broad, nonuniform molecular weight distribution.

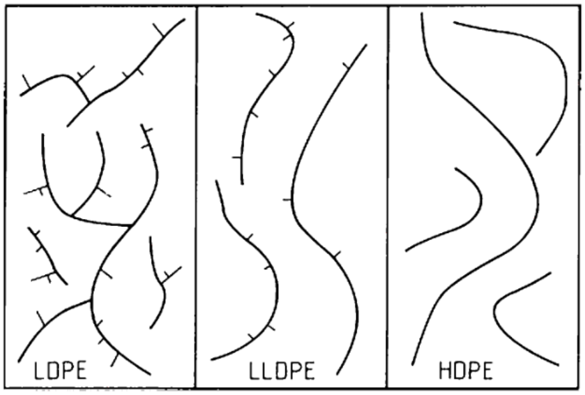

Figure 2.2: Comparison of LDPE, LLDPE, and HDPE.[6]

2.2 Polymerization Catalysis

The discovery of coordination catalysts by Karl Ziegler and Giuseppe Natta in the 1950s sparked the growth of commercial polyethylene. There are three major groups of catalysis: Ziegler-Natta, Phillips, and metallocene catalysts. Ziegler-Natta catalysts, which include titanium and vanadium from groups IV-VIII, work with metal alkyls from groups I-III as co-catalysts. The active sites for polymerization are generated through alkylation and reduction. These can be subdivided into homogeneous and heterogeneous groups. The homogeneous is usually associated with vanadium-based catalysts which are soluble in the reactor. With their single type of active site, they make polyolefins with uniform microstructures.[4, 7] The heterogeneous Ziegler-Natta catalysts on the other hand are insoluble in the reactor medium and they usually have more than one type of active site, which results in broad, nonuniform molecular weight distribution. Phillips catalysts are typically made of chromium oxide (CrO3) or vanadium oxide (VO2) on a silica base and are activated by ethylene during polymerization, without needing a co-catalyst. Phillips catalysts have generally low tendency for α-olefins incorporation, and for this reason, they are not suitable for LLDPE resins. Metallocene catalysts are composed of transition metal atoms such as Zr, Ti, or Hf, positioned between two cyclopentadienyl rings, which can be connected by various bridges. These catalysts are activated by methylaluminoxane (MAO). The structure and type of ligands, including their shape, geometry, and chemical nature, influence the catalyst's behavior, such as activity and selectivity. Metallocene catalysts can be customized by altering the chemical substituents and bridging groups, making them versatile for different polymerization applications.[4, 8]

2.3 Polymerization Processes

Polyethylene (and other polyolefins) can be produced in a wide range of processes using all the different types of catalysts. These processes are slurry, solution, and gas-phase polymerization. The slurry-based (heterogeneous) polymerization process utilizes inert diluents to suspend the polymer particles. These diluents are commonly hydrocarbons, and they are used to offer better heat transfer capabilities. However, removing and recycling the diluent back to the polymerization reactors adds more operational costs to the reactor, and can sometimes add potential hazard risk to the environment. Autoclaves and loop reactors are often used for slurry polymerization, operating under mild conditions.[9, 10, 11, 12, 13] The solution-based polymerization (homogeneous) utilizes homogenous metallocenes, where all the components of the reaction are soluble in the reactor medium. Solution polymerization operates at a very high temperature and pressure to ensure that the polymer chains remain dissolved in the solvent. These conditions offer high polymerization rates and shorter residence times. Autoclaves, tubular, and loop reactors are often used for solution polymerization.[14, 15] Finally, the gas-phase polymerization reactions utilize heterogeneous catalysis, where the catalyst particles are suspended by the upward flow of gases or mechanical agitation (latter only used for polypropylene). The gas-phase polymerization (heterogeneous) method was the latest to be created among the three main groups. They provide a cost-effective and energy-efficient alternative to liquid-phase polymerization. The gas phase of the monomer allows for facile separation of the polymer and unreacted monomer.[16, 17, 12] Typically, the gas-phase polymerization reactors are used with heterogeneous Ziegler-Natta catalysts where the polymerization occurs at the Ti active sites distributed throughout the porous support. In this thesis, we will only focus on the heterogeneous polymerization of supported catalysts in the gas-phase.

2.4 Fragmentation and Particle Growth

When the catalyst is injected into the reactor, the monomers, and other components that are present in the reactor start diffusing from the reactor's continuous phase into the boundary layer around the catalyst and then into the catalyst pores. As soon as the monomers reach the active sites, the polymerization reaction starts, and the generated polymer layers eventually accumulate inside the pores of the catalysts. The accumulated polymer then builds up mechanical stress on the pores and the support, and when the stress exceeds the threshold, the catalyst undergoes a process referred to as "fragmentation".[18, 19, 20, 21] Fragmentation is a process that happens in a short period at the very start of the reaction, where the catalyst fragments very quickly into a series of disconnected substructures that get held together by a polymer phase (Figure 2.3) generated during the reaction. This very rapid process plays a significant role in how the reaction is carried out during particle growth. As the monomer in the bulk phase must now diffuse through the pores

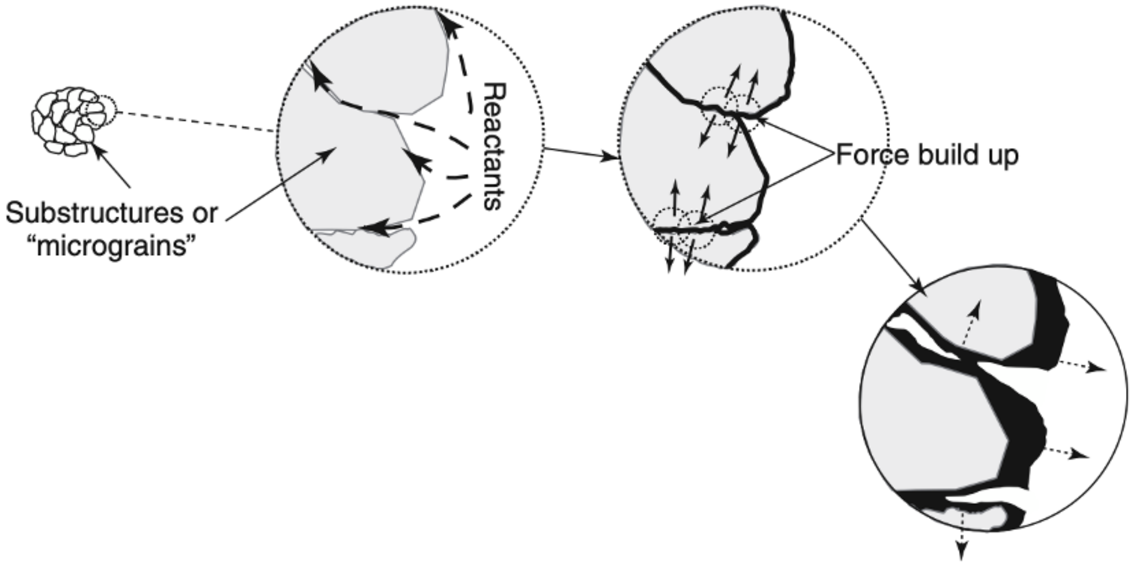

Figure 2.3: Catalyst fragmentation and particle growth.[25]

of the particle and get sorbed into the polymer phase before reaching the active sites. As a result, the new polymer generated on the active sites covers the old polymer layers, causing the particle to expand in size. This process continues as the particles keep growing until it is removed from the reactor.[22, 23, 20, 24] A critical aspect of polymerization is that both the concentration of active sites and monomers influences the polymerization rate. Therefore, the fragmentation process is a favorable phenomenon that maximizes the number of monomers diffusing to the active sites. Finally, it is commonly assumed that the monomers can only diffuse through the amorphous phase but not the crystalline phase of generated polymer.[3, 25]

2.5 Single Particle Modeling

Particle growth is a complex process involving various chemical and physical phenomena that occur simultaneously. These processes do not only influence the particle morphology but also affect the microstructure of the polymer. Several single-particle models have been used. The most commonly employed models include the polymer flow model and the multigrain model, both of which are known for their practicality and accuracy.[23, 26, 27, 22]

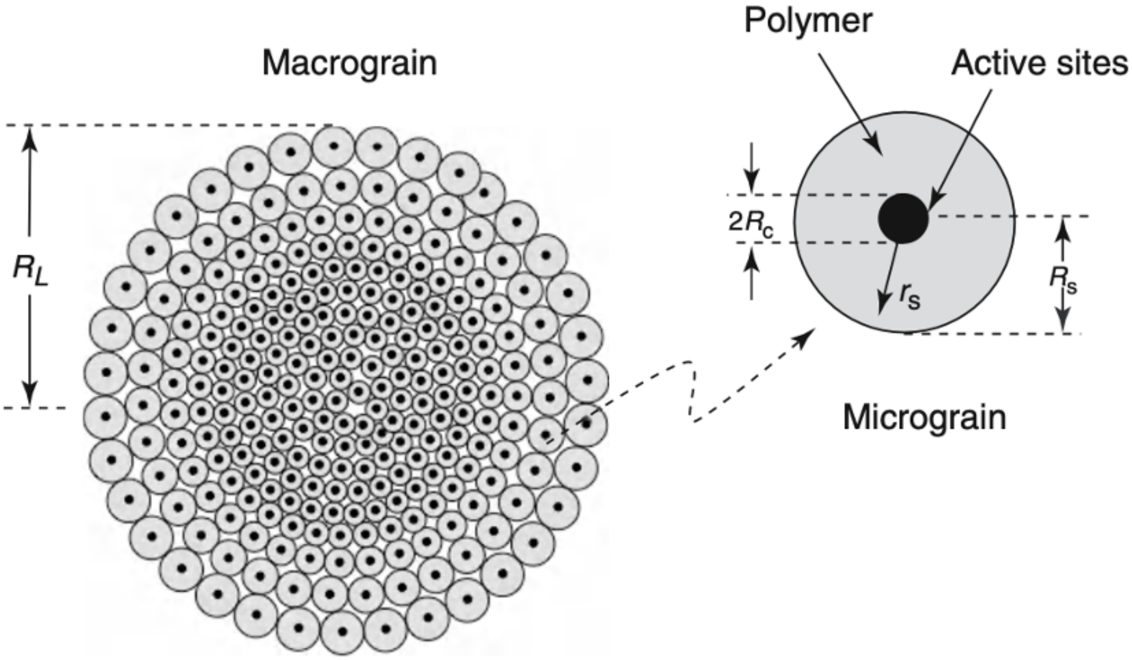

Figure 2.4: Schematic of the multigrain model.[25]

2.5.1 Multigrain Model

The multigrain model is considered to be one of the first efforts to simulate particle growth and its dynamics. The multigrain model divides the polymer particle into two levels: macrograin and microparticles; it models the whole particle as a sphere containing numerous uniformly distributed microparticles. Each of these spherical microparticles consists of the polymer phase that has developed around the catalyst fragments. As displayed in Figure 2.4, the multigrain model mimics the behavior of monomers diffusing through the pores by the consideration of the macrograin. While the micrograins represent the polymer phase the absorbed monomers have to diffuse into, so they reach the active sites. While the multigrain model can be usefully adopted in many situations, its major limitation is that it assumes the polymer particle structure to mimic the structure of the catalyst particle. Which is not always the case for every supported polymerization reaction. Also, the multigrain model frequently results in predictions that are close to simpler models that only consider diffusion processes at the macroscale, like the polymer flow model.[28, 29, 30]

2.5.2 Polymer Flow Model

The main assumption of the polymer flow model (PFM) is that resistances to heat and mass transport at the level of the micrograins are insignificant. The polymer flow model considers the expanding polymer particle, consisting of catalyst fragments, pores, and polymer chains, as a pseudo-homogeneous spherical medium. It measures intraparticle mass transfer using an effective diffusion coefficient that relies on the monomer diffusivity in the polymer phase and in the pores. The polymer flow model is presently more common for olefin polymerization modeling research because of its simplicity and faster computation than the multigrain model. Several variations of the PFM were developed over the years, the most notable is the random pore model, which incorporates the randomness and complexity of actual porous materials.[31]

2.6 Multi-Scale Reactor Modeling

Polymerization reactors contain multiscale processes starting from the catalyst site microscale, the polymer particle mesoscale, and the polymerization reactor macroscale. In polyolefin reactors, several chemical and physical processes that take place at these scales are implicated and each affects the polymerization kinetics, polymer microstructure, and characteristics. The mesoscale, described with different single-particle models as explained earlier, is often ignored due to its mathematical complexity.[32] This is because the dynamic nature of the numerical solution for partial differential equations is computationally demanding. The single particle model describes the intraparticle reaction-diffusion problem with moving-boundary conditions, which is the particle growing with time. The existing models such as the polymer flow model and multigrain model solve the problem by discretizing the differential equations into grids. Because the numerical solution is an approximation to the exact solution, the particle must be discretized to many grids such that the approximate error is reduced. The high number of grids (along with other factors that will be discussed later) causes the simulations to take a very long time. Single-particle modeling becomes particularly challenging when we want to describe a large number of polymer particles. For example, when modeling a significant sample of catalyst particles being fed to an industrial reactor, each catalyst particle needs to be simulated individually, which significantly increases the computation time. This mathematical complexity is further amplified when the reactor is used for olefin copolymerization containing both reactive species of monomers as well as comonomers.

Chapter 3

Mathematical Modeling of the Polymer Flow Model for Homo- and Copolymerization Reactions

The objective of this thesis is to develop and compare the analytical solutions of the PFM based on the quasi-steady-state approximation with the numerical solutions. While there are several references for the mathematical development of the PFM solution, most of the available models would complicate the comparison process as they consider non-isothermal particle with modeling variations on diffusion, porosity, number of sites, and other factors. For this reason, the models developed in this thesis assume that the growing polymer particle is isothermal, with constant porosity, and constant monomer and comonomer effective diffusivity. The presented Polymer Flow Model in this thesis is adequate for ease of adjustment, with few modifications, it can consider different active sites dilution behavior, with the ability to add multiple components and multiple site types (by modeling superpositions of n single-site catalysts). The list of assumptions is summarized as follows:

- The growing polymer particle is assumed to be isothermal.
- The porosity of the polymer particle is constant.
- The monomer and comonomer effective diffusivities are constant.
- The model assumes that the concentration at the boundary is at equilibrium, equal to the surface concentration, thereby neglecting any convective transport effects.

3.1 Model Development for Homopolymerization

3.1.1 Polymerization Kinetics

The molar balance for the living polymer chains, $[Y_0]$, is given by,

$$\frac{d[Y_0]}{dt} = -k_d[Y_0] \tag{3.1}$$

subject to the following initial condition,

$$[Y_0]_{(\forall r,t=0)} = [C_0^*] \tag{3.2}$$

where t is time, r is the radial position in the polymer particle, $[C_0^*]$ is the concentration of active sites at time zero, and k_d is the deactivation rate constant.

Assuming that the catalyst activation is instantaneous, the concentration of living chains as a function of time are given as a function of active sites concentration,

$$[Y_0] = [C_0^*]e^{-k_d t} \tag{3.3}$$

this does not affect the conclusions derived from our comparison, since it only affects how fast the polymerization rate reaches its maximum value.

Note that the concentration of active sites and living polymer chains are identical, as we are assuming that each live polymer chain is coupled to an active site and that the rate of initiation of an active site (following a chain transfer process) is extremely quick.

The rate of homopolymerization is given by,

$$R_p = k_p[M_1][Y_0] = k_p[M_1][C_0^*]e^{-kdt} \tag{3.4}$$

where $[M_1]$ is the concentration of monomer and k_p is the propagation rate constant.

3.1.2 Mass Balance

The mass balance equation for the reaction-diffusion problem at spherical coordinates describes the temporal and radial gradient in monomer concentration in the growing particle by,

$$\frac{\partial[M_1]}{\partial t} = \frac{1}{r^2}\frac{\partial}{\partial r}(D_{e,1}r^2\frac{\partial[M_1]}{\partial r}) - R_v \tag{3.5}$$

the following boundary and initial conditions are true when assuming the boundary layer to be free of external mass transfer resistances:

$$[M_1]_{(r=R,\forall t)} = [M_1]_s \tag{3.6}$$

$$\left.\frac{\partial [M_1]}{\partial r}\right|_{(r=0,\forall r)} = 0 \tag{3.7}$$

$$[M_1]_{(\forall r,t=0)} = 0 \tag{3.8}$$

where $[M_1]_s$ is the monomer concentration at the surface of the particle, R_v is the volumetric rate of polymerization for the total particle volume ($\frac{mol}{m^3 total.sec}$), $D_{e,1}$ is the effective diffusion coefficient for the monomer, and R is the time-dependent radius of the growing polymer particle.

In the coming section, we will look at the simplest solution for the polymer flow model, which we will call the *dynamic solution* (DS). The dynamic solution assumes that the concentration of active sites is a function of time rather than radial position, meaning that at a specific polymerization time, the concentration of active sites is constant throughout the polymer particle. This method is important for the study, because the proposed quasi-steady-state model also assumes that the catalyst concentration is independent of the radial position in the particle. The other version of the polymer flow model is referred to as the *rigorous solution* (RS). The partial differential equation is solved rigorously by accounting for the catalyst concentration radial profile caused by the catalysts' dispersion in the polymer that is produced. The catalyst fragments become more diluted in the generated polyolefin from the center to the surface of the polymer particle as a result of an increase in monomer concentration, which raises the local polymerization rate as one moves from the particle center to the surface. As a result, the particle's active site concentration is evolving both radially and temporally, with the highest concentration at the center and the lowest at the surface. This solution is more realistic than the dynamic solution and it is also more computationally demanding.

3.2 Numerical Method for The Rigorous and The Dynamic Solution - Homopolymerization

3.2.1 Particle Grid

A schematic representation of the polymer flow model is shown in Figure 3.1. The single particle is discretized into concentric spherical shells. The monomer concentrations at the boundaries of each shell are calculated using 3-point Lagrange interpolation polynomial. The average monomer

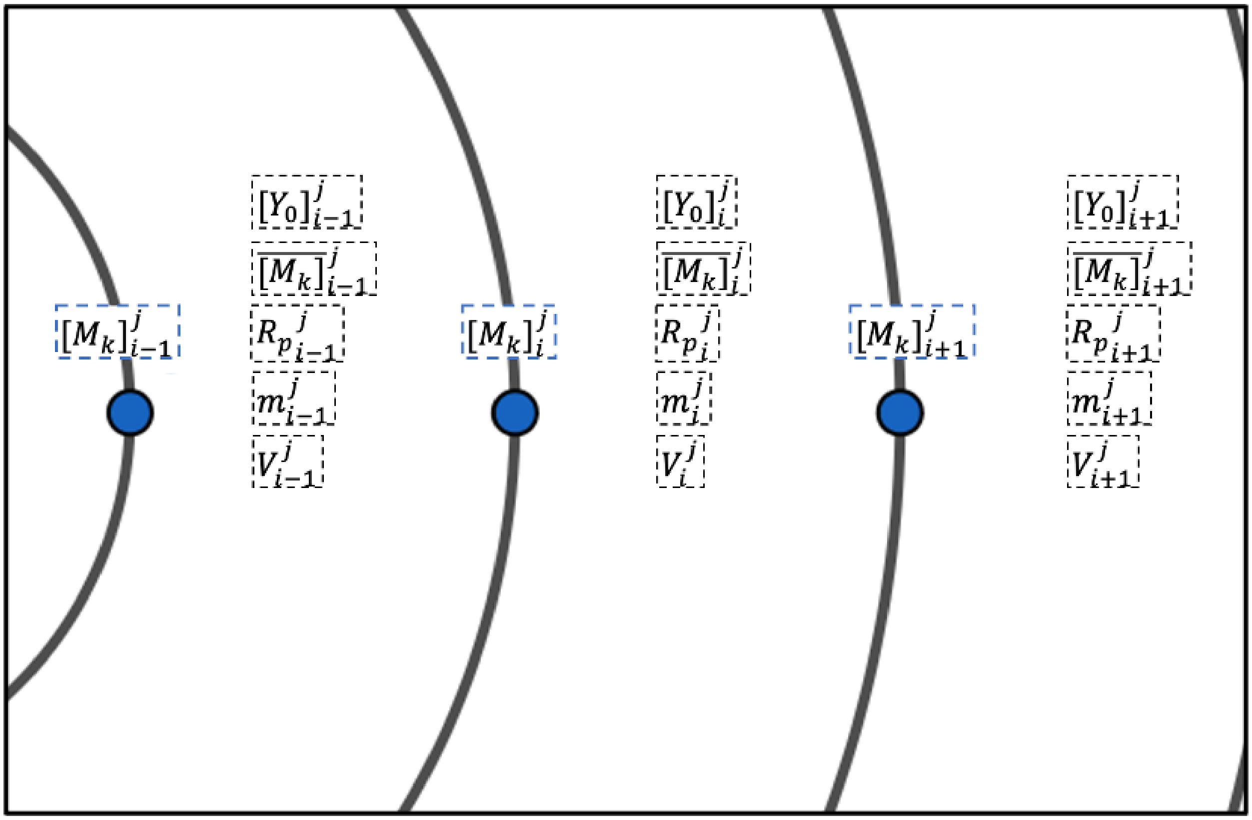

Figure 3.1: Particle discretization of polymer flow model.

concentration is then used to calculate the growing polymer properties and parameters. The polymerization sites, on the other hand, are activated at time zero in all shells, and as the reaction proceeds, these sites start to deactivate and dilute in the growing particle. The subscript i represents the radial location (the grid number), while superscript j indicates the time step. k represents the component type, where $k = 1$ for the monomer and $k = 2$ for the comonomer. The number of grids used in this thesis is 50. This value was determined by incrementally increasing the number of grids until the concentration profile showed no significant change.

3.2.2 Numerical Discretization

First, the monomer radial profile is calculated using a 3-point Lagrange interpolating polynomial,

$$[M_1](r) = \sum_{i=1}^{3} l_i\,(r)\,M_1(r_i) \tag{3.9}$$

$$l_i\,(r) = \frac{p_3(r)}{(r - r_i)p_3(r_i)} \tag{3.10}$$

$$p_3(r) = (r - r_{i-1})(r - r_i)(r - r_{i+1}) \tag{3.11}$$

the first and second derivative of the monomer concentration are written as,

$$\begin{aligned}\frac{d[M_1]}{dr}(r) = &\frac{(r - r_i) + (r - r_{i+1})}{(r_{i-1} - r_i)(r_{i-1} - r_{i+1})}[M_1]_{i-1} \\ &+ \frac{(r - r_{i+1}) + (r - r_{i-1})}{(r_i - r_{i-1})(r_i - r_{i+1})}[M_1]_i \\ &+ \frac{(r - r_{i-1}) + (r - r_i)}{(r_{i+1} - r_{i-1})(r_{i+1} - r_i)}[M_1]_{i+1}\end{aligned} \tag{3.12}$$

$$\begin{aligned}\frac{d^2[M_1]}{dr^2}(r) = &\frac{2}{(r_{i-1} - r_i)(r_{i-1} - r_{i+1})}[M_1]_{i-1} \\ &+ \frac{2}{(r_i - r_{i-1})(r_i - r_{i+1})}[M_1]_i \\ &+ \frac{2}{(r_{i+1} - r_{i-1})(r_{i+1} - r_i)}[M_1]_{i+1}\end{aligned} \tag{3.13}$$

substituting equations (3.13) and (3.13) in equation (3.5) gives,

$$\frac{d[M_1]}{dt}(r_i) = 2D_{e,1}\left(A_i[M_1]_{i-1} + B_i[M_1]_i + C_i[M_1]_{i+1}\right) - R_{v_i} \tag{3.14}$$

with,

$$A_i = \frac{2r_i - r_{i+1}}{r_i(r_{i-1} - r_i)(r_{i-1} - r_{i+1})} \tag{3.15}$$

$$B_i = \frac{3r_i - r_{i+1} - r_{i-1}}{r_i(r_i - r_{i-1})(r_i - r_{i+1})} \tag{3.16}$$

$$C_i = \frac{2r_i - r_{i-1}}{r_i(r_{i+1} - r_{i-1})(r_{i+1} - r_i)} \tag{3.17}$$

where $i = 1, 2, 3, \ldots, N - 2$. N is the total grid points (i.e., number of shells + 1).

Using forward Euler method,

$$\frac{[M_1]_i^{j+1} - [M_1]_i^j}{\Delta t} = 2D_{e,1}\left(A_i[M_1]_{i-1}^j + B_i[M_1]_i^j + C_i[M_1]_{i+1}^j\right) - R_{v_i}^j \tag{3.18}$$

as equation (3.14) is undefined when $r = 0$ ($i = 0$). We need to apply L'Hospital rule to the derivative term,

$$\frac{\partial [M_1]}{\partial t} = 3D_{e,1}\frac{\partial^2 [M_1]}{\partial r^2} - R_{v_i} \tag{3.19}$$

using Taylor series around the origin and substituting the boundary conditions,

$$\frac{\partial^2 [M_1]}{\partial r^2}(r_0) = 2\frac{[M_1]_1 - [M_1]_2}{(r_1 - r_0)^2} \tag{3.20}$$

the discretized monomer profile at the center of the particle is,

$$\frac{d[M_1]}{dt}(r_0) = \frac{-6D_{e,1}}{(r_1 - r_0)^2}\left([M_1]_0 - [M_1]_1\right) - R_{v_0} \tag{3.21}$$

using the forward Euler method,

$$\frac{[M_1]_0^{j+1} - [M_1]_0^j}{\Delta t} = \frac{-6D_{e,1}}{(r_1 - r_0)^2}\left([M_1]_0^j - [M_1]_1^j\right) - R_{v_0}^j \tag{3.22}$$

finally, the polymerization rate of reaction ($\frac{mol}{m^3 total.sec}$) at shell i is given by,

$$R_{p_i}^j = k_p [M_1]_i^j [Y_0]_i^j \tag{3.23}$$

the concentration of monomer inside the shell is the average of two adjacent grids,

$$\overline{[M_1]}_i^j = \frac{[M_1]_i^j + [M_1]_{i+1}^j}{2} \tag{3.24}$$

3.2.3 Particle Growth Calculation

The mass of polymer produced inside each shell is needed to find the volume of polymer generated, the mass at shell i is given by,

$$m_i^{j+1} = M_{W,1} V_i^j \Delta t \, k_p \overline{[M_1]}_i^j [Y]_i^j \tag{3.25}$$

where V_i^j is the volume of shell i, and $M_{W,1}$ is the monomer molecular weight.

At the start of the simulation, the initial catalyst volume V_c is discretized into equal shell volumes. This method is more stable numerically compared to the usual convention of discretizing the particle into equally spaced shells (equal Δr). The initial volume of each shell is equal to,

$$V_{0,1,2,\ldots,N}^0 = \frac{V_c}{N} \tag{3.26}$$

the initial radius positions can be found using:

$$r_i^0 = \left(\frac{3}{4\pi}V_i^0 + (r_{i-1}^0)^3\right)^{1/3} \tag{3.27}$$

where $r_0^0 = r_0^j = r_0^{j+1} = r_0^{j+2} = \ldots = 0$.

After calculating the mass generated in each shell using equation 3.25, the new volume of each shell can be found with:

$$V_i^{j+1} = \frac{m_i^{j+1}}{(1-\epsilon)\rho_p 1000} + V_i^j \tag{3.28}$$

where ρ_p is the density of the polymer, and ϵ is the porosity of the polymer particle. Finally, the radius of each grid can be calculated for the new volume update:

$$r_i^{j+1} = \left(\frac{3}{4\pi}V_i^{j+1} + (r_{i-1}^{j+1})^3\right)^{1/3} \tag{3.29}$$

The total mass of polymer generated at time step $j+1$ can be calculated by adding the masses generated inside all shells:

$$m_{tot}^{j+1} = \sum_{i=1}^{N} m_i^{j+1} \tag{3.30}$$

The new radial locations and volumes are then used to calculate the monomer profiles again. These steps are repeated until the end of the simulation.

3.2.4 Calculation of The Active Sites: The Dynamic Solution

The dynamic solution assumes that the active sites are not a function of the radial position, meaning the active sites are deactivating and diluting at each time step uniformly. The simplification can be written as,

$$[Y_0] = [C_0^*]e^{-k_d t}\left(\frac{1-\epsilon}{\alpha^3}\right) \tag{3.31}$$

upon discretization,

$$[Y_0]^{j+1} = [C_0^*]\, e^{-k_d t}\left(\frac{1-\epsilon}{(\alpha^j)^3}\right) \tag{3.32}$$

where α is the growth factor, calculated by dividing the radius of the particle over the initial radius of the catalyst, R_0,

$$\alpha^j = \frac{R^j}{R_0} = \frac{r_N^j}{R_0} \tag{3.33}$$

note that the active sites $[Y_0]^{j+1}$ are not changing radially, combining with the rate of reaction gives,

$$R^j_{v_i} = R^j_{p_i}\left(\frac{1-\epsilon}{(\alpha^j)^3}\right) = k_p[M_1]^j_i\,[C^*_0]\,e^{-k_d t}\left(\frac{1-\epsilon}{(\alpha^j)^3}\right) \tag{3.34}$$

3.2.5 Calculation of The Active Sites: The Rigorous Solution

The active sites in the rigorous solution are a function of the radial position and time. They are diluted radially while deactivating, which is more realistic to how the particle behaves. The active sites concentration is calculated as the following,

$$[Y_0]^j_i = [C^*_0]\,e^{-k_d t}\cdot\frac{V^0_i}{V^j_i} \tag{3.35}$$

combining with the rate of reaction gives:

$$R^j_{v_i} = R^j_{p_i}\,(1-\epsilon) = k_p\,[M_1]^j_i\,[Y_0]^j_i\,(1-\epsilon) = k_p\,[M_1]^j_i\,[C^*_0]\,e^{-k_d t}\cdot\frac{V^0_i}{V^j_i}(1-\epsilon) \tag{3.36}$$

The calculation of active sites concentration is embedded in the particle growth steps. Depending on the approach (dynamic or rigorous), the active sites are updated after calculating the new grid volumes. The resulting new active sites concentration is then substituted in equation (3.22). Equation (3.34) and (3.36) show that the volumetric rate of reaction $R^j_{v_i}$ ($\frac{mol}{m^3\text{total}\cdot\text{sec}}$) is calculated by multiplying the polymerization rate $R^j_{p_i}$ ($\frac{mol}{m^3\text{cat}\cdot\text{sec}}$) with the ratio between catalyst volume and total particle volume.

3.3 Numerical Stability

Since the monomer concentration in the discretized solution of both the dynamic and rigorous methods must remain positive, the maximum allowed time step, Δt, must be determined before every step to avoid numerical instabilities. The formula for calculating the maximum allowed time step depends on how one discretizes the growing particle. Generally, the maximum allowed time step for shell i, Δt_i, is directly proportional to the shell thickness and inversely proportional to the effective diffusion coefficient, propagation rate constant, and active sites concentration. The time step for shell i can be found by solving the discretized terms for positive Δt_i with the following steps:

1. The rate of reaction, equation (3.34), is substituted into the discretized solution, equation

(3.37),

$$\frac{[M_1]_i^{j+1} - [M_1]_i^j}{\Delta t} = 2D_{e,1}\left(A_i\,[M_1]_{i-1}^j + B_i\,[M_1]_i^j + C_i\,[M_1]_{i+1}^j\right) - k_p\,[M_1]_i^j\,[Y_0]_i^j \tag{3.37}$$

2. separating variables,

$$[M_1]_i^{j+1} = [M_1]_i^j\left(2D_{e,1}B_i\Delta t - k_p\Delta t\,[Y_0]_i^j + 1\right) + [M_1]_{i-1}^j\,(2D_{e,1}A_i\Delta t) + [M_1]_{i+1}^j\,(2D_{e,1}C_i\Delta t) \tag{3.38}$$

3. for $[M_1]_i^{j+1}$ to be positive, the following condition applies,

$$\left(2D_{e,1}B_i\Delta t - k_p\Delta t\,[Y_0]_i^j + 1\right) \geq 0 \tag{3.39}$$

$$\Delta t \leq \frac{1}{2D_{e,1}B_i - k_p\,[Y_0]_i^j} \tag{3.40}$$

4. for the center of the particle, the rate of reaction, equation (3.34), is substituted into the discretized solution, equation (3.22),

$$\frac{[M_1]_0^{j+1} - [M_1]_0^j}{\Delta t} = \frac{-6D_{e,1}}{(r_1 - r_0)^2}\left([M_1]_0^j - [M_1]_1^j\right) - k_p\,[M_1]_0^j\,[Y_0]_0^j \tag{3.41}$$

5. separating variables,

$$[M_1]_0^{j+1} = [M_1]_0^j\left(\frac{-6D_{e,1}}{(r_1 - r_0)^2}\Delta t - k_p\,[Y_0]_0^j\,\Delta t + 1\right) + [M_1]_1^j\left(\frac{6D_{e,1}}{(r_1 - r_0)^2}\Delta t\right) \tag{3.42}$$

6. for $[M_1]_0^{j+1}$ to be positive, the following condition applies,

$$\left(\frac{-6D_{e,1}}{(r_1 - r_0)^2}\Delta t - k_p\Delta t\,[Y_0]_0^j + 1\right) \geq 0 \tag{3.43}$$

$$\Delta t \leq \frac{1}{\frac{-6D_{e,1}}{(r_1 - r_0)^2} - k_p\,[Y_0]_0^j} \tag{3.44}$$

equations (3.40) and (3.44) are used to set the value of Δt at each time step during simulation. Where Δt is:

$$\Delta t_{max,i}^j = \frac{1}{2D_{e,1}B_i - k_p\,[Y_0]_i^j} \tag{3.45}$$

$$\Delta t^j_{max,center} = \frac{1}{\frac{-6D_{e,1}}{(r_1-r_0)^2} - k_p \left[Y_0\right]^j_0} \tag{3.46}$$

$$\Delta t^j_i = \min\left(\Delta t^j_{max,i}, \Delta t^j_{max,center}\right) \tag{3.47}$$

3.4 Model Development for Copolymerization

The polymer flow model can be adjusted to account for copolymerization by defining a kinetic model and calculating the diffusion of each component independently. The most commonly used kinetic models are the Bernoullian and terminal model. The Bernoullian model has the simplest mechanism which does not consider steric and electronic effects on the propagation step by the active site; it has two kinetic propagation constants and assumes that the chain end does not affect the relative polymerization rate of both monomers. The terminal model involves four possibilities of chain propagation; it assumes that the propagating monomers at the end of the polymer chain influence the polymerization rate. This model is more commonly used when modeling olefin copolymerization as it provides accuracy over the simple Bernoullian model. The terminal model reaction mechanism is summarized in table 3.1.

Model type	Propagation step	Rate constant
Terminal	$P^1_r + M_1 \rightarrow P^1_{r+1}$	$k_{p,11}$
	$P^1_r + M_2 \rightarrow P^2_{r+1}$	$k_{p,12}$
	$P^2_r + M_1 \rightarrow P^1_{r+1}$	$k_{p,21}$
	$P^2_r + M_2 \rightarrow P^2_{r+1}$	$k_{p,22}$

Table 3.1: Copolymerization mechanism for ethylene/α-olefin using the terminal model.

3.4.1 Polymerization Kinetics

The copolymerization rate is defined by,

$$R_{p,1} = \left(k_{p,11}\varnothing_1 + k_{p,21}\varnothing_2\right)[M_1][Y_0] \tag{3.48}$$

$$R_{p,2} = (k_{p,12}\varnothing_1 + k_{p,22}\varnothing_2)\,[M_2][Y_0] \tag{3.49}$$

where $[M_2]$ is the concentration of comonomer, $k_{p,11}$, $k_{p,21}$, $k_{p,12}$, and $k_{p,22}$ are the propagation constants for each respective mechanism.

The molar fraction of the living chain terminated by monomer 1, $\varnothing_1$, is given by:

$$\varnothing_1 = \frac{k_{p,21} f_1}{k_{p,21} f_1 + k_{p,12} f_2} \tag{3.50}$$

with,

$$\varnothing_2 = 1 - \varnothing_1 \tag{3.51}$$

the molar fraction of monomer and comonomer, f_1 and f_2, respectively, is given by,

$$f_1 = \frac{[M_1]}{[M_1] + [M_2]} \tag{3.52}$$

$$f_2 = 1 - f_1 \tag{3.53}$$

finally, the total concentration is given by:

$$[M_T] = [M_1] + [M_2] \tag{3.54}$$

3.4.2 Mass Balance

The monomer and comonomer concentrations are described by the mass balance equations for the reaction-diffusion problem in spherical coordinates:

$$\frac{\partial [M_1]}{\partial t} = \frac{1}{r^2}\frac{\partial}{\partial r}\left(D_{e,1} r^2 \frac{\partial [M_1]}{\partial r}\right) - R_{v,1} \tag{3.55}$$

$$\frac{\partial [M_2]}{\partial t} = \frac{1}{r^2}\frac{\partial}{\partial r}\left(D_{e,2} r^2 \frac{\partial [M_2]}{\partial r}\right) - R_{v,2} \tag{3.56}$$

with the following boundary and initial conditions:

$$[M_1]_{(r=R,\forall t)} = [M_1]_s \tag{3.57}$$

$$\left[M_2\right]_{(r=R,\forall t)} = \left[M_2\right]_s \tag{3.58}$$

$$\left.\frac{\partial\left[M_1\right]}{\partial r}\right|_{(r=0,\forall t)} = \left.\frac{\partial\left[M_2\right]}{\partial r}\right|_{(r=0,\forall t)} = 0 \tag{3.59}$$

$$\left[M_1\right]_{(\forall r,t=0)} = \left[M_2\right]_{(\forall r,t=0)} = 0 \tag{3.60}$$

where $\left[M_2\right]_s$ is the comonomer concentration at the surface of the particle, and $D_{e,1}$ and $D_{e,2}$ are the effective diffusion coefficients of each component, respectively. $R_{v,1}$ and $R_{v,2}$ are the respective volumetric rates of reactions considering the dilution of active sites in the generated semi-crystalline polyolefin. The modeling of active sites $[Y_0]$ remains unchanged.

3.5 Numerical Method for The Rigorous and The Dynamic Solution – Copolymerization

3.5.1 Numerical Discretization

The discretization applied to homopolymerization is also applied for the copolymerization mass transfer equations and kinetics. Using the forward Euler method, the discretized equations are:

$$\frac{\left[M_1\right]_i^{j+1} - \left[M_1\right]_i^j}{\Delta t} = 2D_{e,1}\left[A_i\left[M_1\right]_{i-1}^j + B_i\left[M_1\right]_i^j + C_i\left[M_1\right]_{i+1}^j\right] - \left(R_{v,1}\right)_i^j \tag{3.61}$$

$$\frac{\left[M_2\right]_i^{j+1} - \left[M_2\right]_i^j}{\Delta t} = 2D_{e,2}\left[A_i\left[M_2\right]_{i-1}^j + B_i\left[M_2\right]_i^j + C_i\left[M_2\right]_{i+1}^j\right] - \left(R_{v,2}\right)_i^j \tag{3.62}$$

The discretized monomer profile at the center of the particle is:

$$\frac{\left[M_1\right]_0^{j+1} - \left[M_1\right]_0^j}{\Delta t} = \frac{-6D_{e,1}}{\left(r_1 - r_0\right)^2}\left[\left[M_1\right]_0^j - \left[M_1\right]_1^j\right] - \left(R_{v,1}\right)_0^j \tag{3.63}$$

$$\frac{\left[M_2\right]_0^{j+1} - \left[M_2\right]_0^j}{\Delta t} = \frac{-6D_{e,2}}{\left(r_1 - r_0\right)^2}\left[\left[M_2\right]_0^j - \left[M_2\right]_1^j\right] - \left(R_{v,2}\right)_0^j \tag{3.64}$$

The rate of polymerization is given by:

$$(R_{p,1})_i^j = \left(k_{p,11}\varnothing_{1,i}^j + k_{p,21}\varnothing_{2,i}^j\right)[M_1]_i^j[Y_0]_i^j \tag{3.65}$$

$$(R_{p,2})_i^j = \left(k_{p,12}\varnothing_{1,i}^j + k_{p,22}\varnothing_{2,i}^j\right)[M_2]_i^j[Y_0]_i^j \tag{3.66}$$

As explained in the homopolymerization section, equation (3.34) for the dynamic solution or equation (3.36) for the rigorous solution are used to convert the polymerization rate of reaction $R_{p,1}$ and $R_{p,2}$ to the volumetric rate of reaction $R_{v,1}$ and $R_{v,2}$.

Finally, the average concentrations inside each shell are given by,

$$\overline{[M_1]}_i^j = \frac{[M_1]_i^j + [M_1]_{i+1}^j}{2} \tag{3.67}$$

$$\overline{[M_2]}_i^j = \frac{[M_2]_i^j + [M_2]_{i+1}^j}{2} \tag{3.68}$$

3.5.2 Particle Growth Calculation

The combined mass of polymer produced at shell i is given by,

$$m_i^{j+1} = V_i^j \Delta t \left(M_{W,1}(R_{p,1})_i^j + M_{W,2}(R_{p,2})_i^j\right) \tag{3.69}$$

where $M_{W,2}$ is the molecular weight of comonomer.

The total mass of polymer generated at time step j can be calculated by adding the masses generated inside all shells:

$$m_{tot}^{j+1} = \sum_{i=1}^{N} m_i^{j+1} \tag{3.70}$$

The time step for shell i can be found by solving the discretized terms for positive Δt_i.

$$\Delta t_{max,i,1}^j = \frac{1}{\left(2D_{e,1}B_i - (k_{p,11}\varnothing_{1,i}^j + k_{p,21}\varnothing_{2,i}^j)\,[Y_0]_i^j\right)} \tag{3.71}$$

$$\Delta t_{max,center,1}^j = \frac{1}{\frac{-6D_{e,1}}{(r_1-r_0)^2} - (k_{p,11}\varnothing_{1,0}^j + k_{p,21}\varnothing_{2,0}^j)\,[Y_0]_0^j} \tag{3.72}$$

$$\Delta t^{j}_{max,i,2} = \frac{1}{\left(2D_{e,2}B_i - (k_{p,12}\varnothing^{j}_{1,i} + k_{p,22}\varnothing^{j}_{2,i})\,[Y_0]^{j}_{i}\right)} \tag{3.73}$$

$$\Delta t^{j}_{max,center,2} = \frac{1}{\frac{-6D_{e,2}}{(r_1-r_0)^2} - (k_{p,12}\varnothing^{j}_{1,0} + k_{p,22}\varnothing^{j}_{2,0})\,[Y_0]^{j}_{0}} \tag{3.74}$$

Finally, Δt each step is selected with:

$$\Delta t^{j} = \text{Minimum}(\Delta t^{j}_{max,1}, \Delta t^{j}_{max,2}, \Delta t^{j}_{max,3}, \Delta t^{j}_{max,4}) \tag{3.75}$$

The rigorous solution code is validated by comparing it with the following references [33, 17].

Chapter 4

Mathematical Derivation and Modeling of The Quasi-Steady-State Approximation for Homo- and Copolymerization Reactions

The quasi-steady-state approximation (QSSA) can effectively be applied when the system conditions are changing slowly enough that the relations among the various parameters can be solved as if the system were at the steady state, despite ongoing changes. In the reaction engineering realm, the quasi-steady-state assumption is applied particularly to complex reaction networks involving multiple chemical species and intermediate steps. The application of the quasi-steady-state assumes that the concentrations of certain reactive intermediates in a reaction pathway change very rapidly compared to the overall rate of the reaction. The analysis of complex reaction mechanisms can be carried out by effectively "freezing" the concentrations of these reactive intermediates at their quasi-steady-state values. This allows for the derivation of simplified rate expressions and facilitates the study of the overall reaction kinetics without having to explicitly track the dynamics of every intermediate species. In our case, the quasi-steady-state is a simplification that is valid when the timescale for both polymerization and diffusion rates is smaller than the timescale for particle growth. In other words, the monomer concentration profile reaches steady state before the polymer particle grows considerably. When the QSSA is applied to the particle growth problem, we are assuming that each time step (before the volume is updated) is fast enough that it remains at the steady state. The results obtained from the steady-state step is used to update the next particle volume. The main advantage of QSSA is that it offers faster simulation of particle growth compared to the numerical methods, as it is only an integration of a series of analytical solutions over time.

4.1 Model Development - Homopolymerization

In the quasi-steady-state approximation, the monomer accumulation term is set to zero and the partial differential equation is reduced to an ordinary differential equation:

$$0 = \frac{1}{r^2}\frac{d}{dr}\left(r^2 D_{e,1}\frac{d[M_1]}{dr}\right) - k_p[Y_0]\,[M_1] \tag{4.1}$$

The analytical solution for the above equation can be obtained with the following steps:

1. Differentiate equation (4.1) using the product rule:

$$\frac{D_{e,1}}{r^2}\left(r^2\frac{d^2[M_1]}{dr^2} + 2r\frac{d[M_1]}{dr}\right) = k_p[Y_0][M_1] \tag{4.2}$$

2. Rearranging:

$$\frac{d^2[M_1]}{dr^2} + \frac{2}{r}\frac{d[M_1]}{dr} = \frac{k_p[Y_0]}{D_{e,1}}[M_1] \tag{4.3}$$

   Equation (4.3) is a non-homogeneous 2^{nd} order ordinary differential equation. Variable transformation is applied to solve the ODE.

$$[M_1] = \frac{F_1}{r} \tag{4.4}$$

$$\frac{d[M_1]}{dr} = \frac{1}{r}\frac{dF_1}{dr} - \frac{F_1}{r^2} \tag{4.5}$$

3. Substituting into equation (4.1):

$$0 = \frac{1}{r^2}\frac{d}{dr}\left(r^2 D_{e,1}\left(\frac{1}{r}\frac{dF_1}{dr} - \frac{F_1}{r^2}\right)\right) - k_p[Y_0]\frac{F_1}{r} \tag{4.6}$$

4. Differentiating and arranging:

$$\frac{d^2F_1}{dr^2} - \frac{k_p}{D_{e,1}}[Y_0]F_1 = 0 \tag{4.7}$$

5. Equation (4.7) is a homogeneous linear 2^{nd} order ODE. The general solution is given by:

$$F_1 = C_1e^{r\sqrt{\beta}} + C_2e^{-r\sqrt{\beta}} \tag{4.8}$$

6. Since $F = r[M_1]$, then:

$$[M_1] = \frac{C_1 e^{r\sqrt{\beta}}}{r} + \frac{C_2 e^{-r\sqrt{\beta}}}{r} \tag{4.9}$$

7. Apply the boundary and initial conditions given in equations (3.6), (3.7), and (3.8) to find C_1 and C_2 constants. The analytical solution is obtained as follows:

$$[M_1] = [M_1]_s \frac{R}{r} \frac{\sinh r\sqrt{\beta}}{\sinh R\sqrt{\beta}} \tag{4.10}$$

   with:

$$\beta = \frac{k_p[Y_0]}{D_{e,1}} = \frac{k_p[C_0^*]e^{-k_d t}\left(\frac{1-\epsilon}{\alpha^3}\right)}{D_{e,1}} \tag{4.11}$$

The mass of polymer produced can be calculated analytically by integrating the rate of reaction:

$$m_{tot} = \frac{M_{w,1}k_p[Y_0]}{\alpha^3}\left(\int_0^R [M_1]dV\right)\Delta t \tag{4.12}$$

The total mass of polymer is calculated using the volume of the pure polymer by excluding the porosity term $(1-\epsilon)$.

Replacing $[M_1]$ with equation (4.10) and using the volume of a sphere:

$$m_{tot} = \frac{M_{w,1}k_p[Y_0]}{\alpha^3}\left(\int_0^R [M_1]_s \frac{R}{r}\frac{\sinh r\sqrt{\beta}}{\sinh R\sqrt{\beta}}\, d\left(\frac{4}{3}\pi r^3\right)\right)\Delta t \tag{4.13}$$

integrating,

$$m_{tot} = \frac{4\pi M_{w,1}k_p[Y_0]}{\alpha^3}[M_1]_s \frac{R(R\sqrt{\beta}\coth(R\sqrt{\beta})-1)}{\beta}\Delta t \tag{4.14}$$

and the volume of the particle is found with:

$$V_{tot}^{t+\Delta t} = V_{tot}^{t} + \frac{m_{tot}}{(1-\epsilon)\rho_p} \tag{4.15}$$

Finally, the radius of the resulting particle is calculated,

$$R = \left(\frac{3}{4\pi}V_{tot}^{t+\Delta t}\right)^{1/3} \tag{4.16}$$

4.2 Model Development – Copolymerization

4.2.1 Quasi-Steady-State, Variable Monomer Fraction Solution

When describing the copolymerization with the terminal model, the following ordinary differential equations are obtained,

$$0 = \frac{1}{r^2}\frac{\partial}{\partial r}\left(r^2 \frac{\partial}{\partial r}(D_{e,1}[M_1])\right) - (k_{p,11}\varnothing_1 + k_{p,21}(1-\varnothing_1))[M_1][Y_0] \tag{4.17}$$

$$0 = \frac{1}{r^2}\frac{\partial}{\partial r}\left(r^2 \frac{\partial}{\partial r}(D_{e,2}[M_2])\right) - (k_{p,12}\varnothing_1 + k_{p,22}(1-\varnothing_1))[M_2][Y_0] \tag{4.18}$$

substituting $\varnothing_1$ with equation (3.50) and (3.52) gives,

$$\frac{1}{r^2}\frac{\partial}{\partial r}\left(r^2 \frac{\partial}{\partial r}(D_{e,1}[M_1])\right) = \frac{(k_{p,11}k_{p,21}[M_1] + k_{p,21}k_{p,12}[M_2])}{k_{p,21}[M_1] + k_{p,12}[M_2]}[M_1][Y_0] \tag{4.19}$$

$$\frac{1}{r^2}\frac{\partial}{\partial r}\left(r^2 \frac{\partial}{\partial r}(D_{e,2}[M_2])\right) = \frac{(k_{p,12}k_{p,21}[M_1] + k_{p,22}k_{p,12}[M_2])}{k_{p,21}[M_1] + k_{p,12}[M_2]}[M_2][Y_0] \tag{4.20}$$

obtaining an analytical solution for this system is not possible; there are no solutions that satisfy the system as long as it contains nonlinear terms. We can modify the above system to obtain a linear combination that has an approximate solution,

$$\frac{1}{r^2}\frac{\partial}{\partial r}\left(r^2 \frac{\partial}{\partial r}(D_{e,1}[M_1])\right) = \frac{(\frac{k_{p,11}k_{p,21}[M_1]}{k_{p,21}[M_1]} + \frac{k_{p,21}k_{p,12}[M_2]}{k_{p,21}[M_1]})}{1 + \frac{k_{p,12}[M_2]}{k_{p,21}[M_1]}}[M_1][Y_0] \tag{4.21}$$

$$\frac{1}{r^2}\frac{\partial}{\partial r}\left(r^2 \frac{\partial}{\partial r}(D_{e,2}[M_2])\right) = \frac{k_{p,12}(\frac{k_{p,21}[M_1]}{k_{p,21}[M_1]} + \frac{k_{p,22}[M_2]}{k_{p,21}[M_1]})}{1 + \frac{k_{p,12}[M_2]}{k_{p,21}[M_1]}}[M_2][Y_0] \tag{4.22}$$

when the active sites are low in reactivity towards α-olefin, $k_{p,21}$ will be much higher than both $k_{p,12}$ and $k_{p,22}$. In this situation, the above system can be reduced to:

$$\frac{1}{r^2}\frac{\partial}{\partial r}\left(r^2 \frac{\partial}{\partial r}(D_{e,1}[M_1])\right) = (k_{p,11}[M_1] + k_{p,12}[M_2])[Y_0] \tag{4.23}$$

$$\frac{1}{r^2}\frac{\partial}{\partial r}\left(r^2 \frac{\partial}{\partial r}(D_{e,2}[M_2])\right) = k_{p,12}[M_2][Y_0] \tag{4.24}$$

The following solution is obtained,

$$[M_1] = \frac{[M_1]_s - [M_2]_s}{\frac{D_{e,1}}{D_{e,2}} - \frac{k_{p,11}}{k_{p,12}}} \frac{R}{r} \frac{\sinh r\sqrt{\beta_{11}}}{\sinh R\sqrt{\beta_{11}}} + \frac{[M_2]_s}{\frac{D_{e,1}}{D_{e,2}} - \frac{k_{p,11}}{k_{p,12}}} \frac{R}{r} \frac{\sinh r\sqrt{\beta_{12}}}{\sinh R\sqrt{\beta_{12}}} \tag{4.25}$$

$$[M_2] = [M_2]_s \frac{R}{r} \frac{\sinh r\sqrt{\beta_{12}}}{\sinh R\sqrt{\beta_{12}}} \tag{4.26}$$

The steps for obtaining the analytical solution are provided in Appendix A. The applicability of this solution can be evaluated by writing the insignificant terms that were removed during simplification. Since the largest value $[M_1]$ can exhibit is $[M_1]_s$, the accuracy of the solution can be determined with:

$$\aleph_1 = \frac{k_{p,12}[M_2]_s}{k_{p,21}[M_1]_s} \tag{4.27}$$

$$\aleph_2 = \frac{k_{p,22}[M_2]_s}{k_{p,21}[M_1]_s} \tag{4.28}$$

The parameters $\aleph_1$ and $\aleph_2$ serve as the indicators to assess the accuracy of equation (4.25) and equation (4.26). Lower values of $\aleph_1$ and $\aleph_2$ correspond to less errors associated with the simplification. The analytical solution derived by this approach specifically holds true when $k_{p,21}$ is higher than $k_{p,12}$, $k_{p,22}$, and the comonomer concentration is less than the monomer concentration at the particle surface. The distinguishing feature of this solution is that it allows the molar fractions of monomer and comonomer to vary radially. We will refer to this approach as the quasi-steady-state solution with variable monomer fraction (QSSA-Vf).

4.2.2 Quasi-Steady-State, Average Monomer Fraction Solution

Another possible approximation for the system can be achieved by modifying the nonlinear terms. If we assume the monomer fraction to be constant radially, that is averaged over the radius, the system can be solved. This is similar to how the actives sites are assumed to be homogenously distributed along the particle.

First, the average molar fraction of monomer across the particle is calculated,

$$\overline{f_1} = \frac{[\dot{M}_1]}{[\dot{M}_1] + [\dot{M}_2]} \tag{4.29}$$

where $[\dot{M}_1]$ and $[\dot{M}_2]$ are the average concentrations of monomer and comonomer inside the entire particle at a given time, respectively. Subsequently, the average fraction of living chains is obtained by,

$$\overline{\varnothing_1} = \frac{k_{p,21}\overline{f_1}}{k_{p,21}\overline{f_1} + k_{p,12}(1-\overline{f}_1)} \tag{4.30}$$

substituting in equations (4.17) and (4.18),

$$0 = \frac{1}{r^2}\frac{\partial}{\partial r}\left(r^2 \frac{\partial}{\partial r}(D_{e,1}[M_1])\right) - \left(k_{p,11}\overline{\varnothing_1} + k_{p,21}(1-\overline{\varnothing_1})\right)[M_1][Y_0] \tag{4.31}$$

$$0 = \frac{1}{r^2}\frac{\partial}{\partial r}\left(r^2 \frac{\partial}{\partial r}(D_{e,2}[M_2])\right) - \left(k_{p,12}\overline{\varnothing_1} + k_{p,22}(1-\overline{\varnothing_1})\right)[M_2][Y_0] \tag{4.32}$$

since the average fraction of living chains does not depend on the radial position, the following analytical solution can be derived,

$$[M_1] = [M_1]_s \frac{R}{r}\frac{\sinh r\sqrt{\beta_1}}{\sinh R\sqrt{\beta_1}} \tag{4.33}$$

$$[M_2] = [M_2]_s \frac{R}{r}\frac{\sinh r\sqrt{\beta_2}}{\sinh R\sqrt{\beta_2}} \tag{4.34}$$

with,

$$\beta_1 = \frac{\left(k_{p,11}\overline{\varnothing_1} + k_{p,21}(1-\overline{\varnothing_1})\right)[Y_0]\left(\frac{1-\epsilon}{\alpha^3}\right)}{D_{e,1}} \tag{4.35}$$

$$\beta_2 = \frac{\left(k_{p,12}\overline{\varnothing_1} + k_{p,22}(1-\overline{\varnothing_1})\right)[Y_0]\left(\frac{1-\epsilon}{\alpha^3}\right)}{D_{e,2}} \tag{4.36}$$

this approach works by calculating the average monomer and comonomer concentrations from the particle center to its surface. The average concentrations are then used to calculate the average monomer fraction, equation (4.29), and average living chain fraction, equation (4.30). The monomer and comonomer concentration profiles are subsequently calculated using equations (4.33) and (4.34). The newly established profiles are used to find the average monomer fraction for the next time step. This computational cycle is repeated until the reaction time is reached. We will refer to this approach as the quasi-steady-state solution with averaged monomer fraction (QSSA-Af) in the upcoming sections. The flowchart in Figure 4.1 summarizes each of the presented solutions.

Similar to homopolymerization, the mass of polymer produced can be calculated analytically. For the QSSA-Vf, the rate of reaction is integrated considering both components:

$$m_{tot,1} = \frac{M_{w,1}[Y_0]}{\alpha^3}\left(\int_0^R k_{p,11}[M_1]dV\right)\Delta t \tag{4.37}$$

$$m_{tot,2} = \frac{M_{w,2}\,[Y_0]}{\alpha^3}\left(\int_0^R k_{p,12}[M_2]dV\right)\Delta t \tag{4.38}$$

replacing $[M_1]$ and $[M_2]$ and using the volume of a sphere,

$$m_{tot,1} = \frac{M_{w,1}\,[Y_0]}{\alpha^3}\left(\int_0^R k_{p,11}\left(A\frac{R}{r}\frac{\sinh r\sqrt{\beta_{11}}}{\sinh R\sqrt{\beta_{11}}} + B\frac{R}{r}\frac{\sinh r\sqrt{\beta_{12}}}{\sinh R\sqrt{\beta_{12}}}\right)d\left(\frac{4}{3}\pi r^3\right)\right)\Delta t \tag{4.39}$$

$$m_{tot,2} = \frac{M_{w,2}\,[Y_0]}{\alpha^3}\left(\int_0^R k_{p,12}[M_2]_s\frac{R}{r}\frac{\sinh r\sqrt{\beta_{12}}}{\sinh R\sqrt{\beta_{12}}}d\left(\frac{4}{3}\pi r^3\right)\right)\Delta t \tag{4.40}$$

integrating,

$$m_{tot,1} = \frac{4\pi M_{w,1}k_{p,11}\,[Y_0]}{\alpha^3}\left(A\frac{R\left(R\sqrt{\beta_{11}}\coth\left(R\sqrt{\beta_{11}}\right)-1\right)}{\beta_{11}} + B\frac{R\left(R\sqrt{\beta_{12}}\coth\left(R\sqrt{\beta_{12}}\right)-1\right)}{\beta_{12}}\right)\Delta t \tag{4.41}$$

$$m_{tot,2} = \frac{4\pi M_{w,2}k_{p,12}\,[Y_0]}{\alpha^3}[M_2]_s\frac{R\left(R\sqrt{\beta_{12}}\coth\left(R\sqrt{\beta_{12}}\right)-1\right)}{\beta_{12}}\Delta t \tag{4.42}$$

where,

$$A = \frac{[M_1]_s - [M_2]_s}{\frac{D_{e,1}}{D_{e,2}} - \frac{k_{p,11}}{k_{p,12}}}, \quad B = \frac{[M_2]_s}{\frac{D_{e,1}}{D_{e,2}} - \frac{k_{p,11}}{k_{p,12}}} \tag{4.43}$$

For the QSSA-Af, the mass produced is calculated by:

$$m_{tot,1} = \frac{M_{w,1}\,[Y_0]}{\alpha^3}\left(\int_0^R \left(k_{p,11}\overline{\varnothing_1} + k_{p,21}(1-\overline{\varnothing_1})\right)[M_1]dV\right)\Delta t \tag{4.44}$$

$$m_{tot,2} = \frac{M_{w,2}\,[Y_0]}{\alpha^3}\left(\int_0^R \left(k_{p,12}\overline{\varnothing_1} + k_{p,22}(1-\overline{\varnothing_1})\right)[M_2]dV\right)\Delta t \tag{4.45}$$

Finally, the total mass is calculated,

$$m_{tot} = m_{tot,1} + m_{tot,2} \tag{4.46}$$

the new volume and radius of the particle is calculated using equation (4.15) and (4.16), respectively.

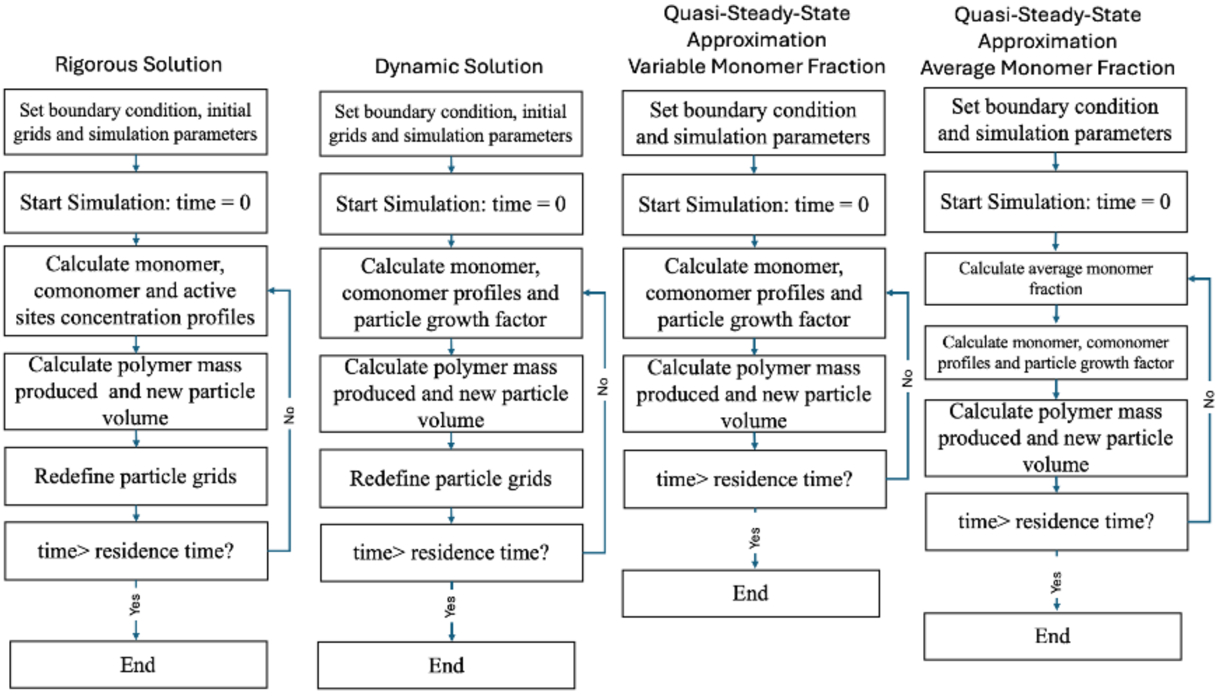

Figure 4.1: Flowchart for the rigorous solution, the dynamic solution, the quasi-steady-state approximation with variable monomer fraction, and the quasi-steady-state approximation with average monomer fraction.

Chapter 5

Results and Discussion

5.1 Comparison Criteria

The QSSA models are compared with the RS and DS methods using the following criteria: (*i*) monomer and comonomer mass transfer efficiency, (*ii*) instantaneous rate of polymerization, (*iii*) particle growth factor, (*iv*) polymer molecular weight distribution, and (*v*) short chain branching distribution.

The efficiency factor is a measure of the resistance to monomer transport through the particle. It is a convenient metric to quantify how steep the monomer radial profile is throughout the polymerization. It is calculated by,

$$\eta_k = \frac{\int [M_k]\ dV}{[M_k]_s V_{tot}} \tag{5.1}$$

the mass transfer efficiency is calculated numerically for the RS and DS,

$$\eta_k^j = \frac{\sum_i^N [M_k]_i^j V_i^j}{[M_k]_s V_{tot}} \tag{5.2}$$

the analytical efficiency factor for the QSSA can be found by substituting the respective monomer equation. For example, in case of homopolymerization, equation (4.10) is substituted in equation (5.1),

$$\eta_k = \frac{\int_0^R [M_k]_s \frac{R}{r} \frac{\sinh r\sqrt{\beta_k}}{\sinh R\sqrt{\beta_k}} d\left(\frac{4}{3}\pi r^3\right)}{[M_k]_s V_{tot}} = 4\pi R \frac{\left(R\sqrt{\beta_k}\coth\left(R\sqrt{\beta_k}\right) - 1\right)}{\beta_k V_{tot}} \tag{5.3}$$

the rate of polymerization is a crucial metric for this study since the rigorous solution handles the active sites distribution differently from the dynamic solution and quasi-steady-state methods. The instantaneous rate of polymerization is given by,

$$R_p^{ins} = \frac{m_{tot}}{\Delta t \rho_c V_c} \tag{5.4}$$

while the instantaneous rate of polymerization gives insight on the instantaneous differences between the models, the growth factor on the other hand is a measure of the average difference between the compared models; it can be viewed as a cumulative error for the quasi-steady-state solution. The growth factor is calculated using equation (3.33).

Comparing the polymer molecular weight distributions (MWDs) predicted with these different models gives an additional metric to evaluate how close the simplified QSSA model approaches the stricter RS simulations. In the RS model, the MWD of polymer made in each shell follows the Flory's MWD instantaneously, given by:

$$w_{logM,j}^{i} = ln(10)M^2\left(\tau_j^i\right)^2 e^{-M\tau_j^i} \tag{5.5}$$

The parameter τ in the Flory's most probable distribution is defined as,

$$\tau_j^i = \frac{k_{tM} + \left(k_{tH,1}\varnothing_{1,i}^{j} + k_{tH,2}\varnothing_{2,i}^{j}\right)[H_2]}{\hat{k_p}\left([M_1]_i^j + [M_2]_i^j\right)} \tag{5.6}$$

where k_{tM} is the rate constant for transfer to monomer, $k_{tH,1}$ and $k_{tH,2}$ are the monomer and comonomer transfer rates to hydrogen, and $[H_2]$ is the hydrogen concentration. $\hat{k_p}$ is the pseudo-kinetic constant, given by:

$$\hat{k_p} = k_{p,11}\varnothing_1 f_1 + k_{p,12}\varnothing_1(1-f_1) + k_{p,21}(1-\varnothing_1)f_1 + k_{p,21}(1-\varnothing_1)(1-f_1) \tag{5.7}$$

In the case of homopolymerization, equation (5.6) is reduced to:

$$\tau = \frac{k_{tM} + k_{tH,1}[H_2]}{k_p\,[M_1]_i^j} \tag{5.8}$$

Since each shell experiences a different monomer concentration, the MWDs will vary from shell to shell at a given polymerization time. These distributions across the shells must be averaged radially to get the instantaneous MWD for the whole particle at a given time,

$$w^j_{logM} = \frac{\sum_{i=1}^{N} m_i^j w^j_{logM,i}}{\sum_{i=1}^{N} m_i^j} \tag{5.9}$$

finally, the instantaneous MWDs are integrated temporally, which yields the cumulative MWD,

$$w_{logM} = \frac{\sum_{j=0}^{time} R_v^j w^j_{logM} \Delta t}{\sum_{j=0}^{time} R_v^j \Delta t} \tag{5.10}$$

finally, we will be comparing the models based on the initial value of the Thiele modulus, since it quantifies the relative importance of diffusion and reaction rates in porous catalysts. The general form of Thiele modulus developed by Petersen[34] is,

$$\Phi_i = \frac{V_c}{A_c} \frac{(-r_i)_{int}|_{C_{i,s}}}{\left[2D_{e,i}\int_0^{C_{i,s}}(-r_i)_{int}dC_i\right]^{1/2}} \tag{5.11}$$

where $(-r_i)_{int}$ is the intrinsic rate of reaction for component i, and $(-r_i)_{int}|_{C_{i,s}}$ is the rate of reaction at the surface of the particle, $C_{i,s}$, A_c is the surface area of the catalyst particle. Substituting the rate of reaction with equation (3.48) and (3.49) gives,

$$\Phi_1 = \frac{V_c}{A_c}\sqrt{\frac{(k_{p,11}\varnothing_1 + k_{p,21}(1-\varnothing_1))\,[Y_0]\left(\frac{1-\epsilon}{\alpha^3}\right)}{D_{e,1}}} = \frac{R_0}{3}\sqrt{\beta_1} \tag{5.12}$$

$$\Phi_2 = \frac{V_c}{A_c}\sqrt{\frac{(k_{p,12}\varnothing_1 + k_{p,22}(1-\varnothing_1))\,[Y_0]\left(\frac{1-\epsilon}{\alpha^3}\right)}{D_{e,2}}} = \frac{R_0}{3}\sqrt{\beta_2} \tag{5.13}$$

initially a numerical value is assigned to Φ_1 and Φ_2, and then we calculate $D_{e,1}$ and $D_{e,2}$ based on other parameters of the polymer flow model as provided in Table 5.1.

In the case of homopolymerization, Φ_1 is reduced to:

$$\Phi_1 = \frac{V_c}{A_c}\sqrt{\frac{k_p\,[Y_0]\left(\frac{1-\epsilon}{\alpha^3}\right)}{D_{e,1}}} = \frac{R}{3}\sqrt{\beta} \tag{5.14}$$

Equations (5.12), (5.13) and (5.14) shows that for a first order rate of reaction, Thiele modulus is independent of surface concentration. For a simple non-growing particle, the Thiele modulus simplifies the analysis of reaction and diffusion by providing a dimensionless number that does not change with concentration. It allows comparison between systems or conditions with different concentrations but similar relative reaction and diffusion characteristics. Since we are concerned with a growing particle problem, the surface concentration plays a significate role in determining the amount of polymer generated, particle growth and how fast can particle reach the steady state. We will show the effect of surface concentration on the quasi steady state approximation accuracy independently of Thiele modulus, which is concerned with the catalyst part of the reaction, not the entire process conditions.

Parameter	**Value**	**Unit**
k_{p11}	500	m^3 mol s^{-1}
k_{p21}	500	m^3 mol s^{-1}
r_1	8	-
r_2	0.3	-
k_d	1×10^{-4}	s^{-1}
$k_{tH,1}$	0.01	s^{-1}
$k_{tH,2}$	0.01	s^{-1}
k_{tM}	0.60	s^{-1}
R_0	2.5×10^{-5}	m
ϵ	0.05	-
$[C_0^*]$	5	mol m^{-3}
$[M_1]_s$	170	mol m^{-3}
$[M_2]_s$	50	mol m^{-3}
$[H_2]$	50	mol m^{-3}
Simulation time	15000	s

Table 5.1: Simulation parameters.

Before starting the comparison of the models, it is important to realize that they will always differ at the beginning of the simulations. Figure 5.1 compares the monomer concentration profiles for three different times and Thiele modulus of $\Phi_1 = 0.5$. The QSSA solution predicts a monomer concentration profile even at $t = 0$, which is the profile that the monomer would reach at steady state if the radius of the catalyst particle did not change (no particle growth). This is certainly not the case for olefin polymerizations with heterogeneous coordination catalysts, but we will see below that this difference becomes less relevant for longer polymerization times. In contrast, both the DS and RS methods, which apply the initial condition $[M]|_{\forall r,t=0} = 0$, predict that no monomer is present inside the catalyst particle at $t = 0$. After 3 seconds, the DS and RS predictions approach each other, and after only 100 seconds, the DS catches up to the QSSA solution, since both methods assume that the concentration of active sites in the particle is uniform. The monomer profiles predicted by the RS method eventually catch up to the QSSA and DS predictions at 300s.

5.2 Comparison Between the Quasi-Steady-State Approximation and Dynamic Solution Methods, Homopolymerization

Figure 5.2 shows that the polymerization rate, mass transfer efficiency, and growth factor predicted with the QSSA and DS methods match for all cases over a wide range of Thiele moduli. These results are enlightening because both the QSSA and the DS methods assume that the concentration of active sites in the polymer particle does not depend on the radial position, but the QSSA also assumes that the monomer concentration profile reaches steady state during a short time interval dt. The latter simplification is valid only when the timescale for polymerization/diffusion rates is much smaller than the timescale for particle growth. In other words, the monomer concentration profile reaches steady state before the polymer particle can grow considerably.

Figure 5.3 shows the concentration change over time in each shell. The numerical derivative of the profiles affirms the validity of the steady-state assumption made, as it reveals that as time progresses, the accumulation of unreacted monomers approaches zero, as depicted in Figure 5.4.

In the previous section, it was proved that the simulation results obtained with the QSSA and DS methods matched for all case studies. In this section, will compare the RS method predictions with those from the QSSA method, which is equivalent to comparing the DS with the RS predictions. Since the RS considers that the concentration of active sites in the particle varies as a function of radial position, the overall polymerization kinetics for the whole particle will reflect how fast the QSSA and RS methods converge to the same solution. Figure 5.5 shows that the polymerization kinetic curves predicted by the QSSA and RS methods match faster when the active sites deactivate. If the active sites do not deactivate, the polymerization rate will reach a plateau, but the QSSA simulations (and consequently the DS simulations) will get there faster because it assumes a uniform concentration of active sites in the particle.

Figure 5.6 shows that the QSSA model is accurate for $\Phi_1 < 3$ but diverges from the RS model predictions for higher Thiele moduli. Even though the monomer concentration profiles predicted by the RS and QSSA method differ at the beginning of the polymerizations, they quickly converge after short polymerization times, as illustrated in Figure 5.7.a and Figure 5.7.b when $\Phi_1 < 3$. Figure 5.7.c and Figure 5.7.d show that the concentration of active sites predicted by the QSSA model is the average of those predicted by the RS model, considering that the volumes of the outer shells are larger than those of the inner shells. Figure 5.8 shows how decreasing the monomer concentration at the surface, starting from the same Φ_1 of 3, slighly increases the differences between the QSSA and RS predictions. This is because the monomer concentration at the surface effect how much polymer is getting generated and the extent of polymer swelling. This is an external property of the system that does not have a huge impact on the as the surface concentration itself doesn't play a significant role in the diffusion-reaction problem alone and it is canceled out when the particle

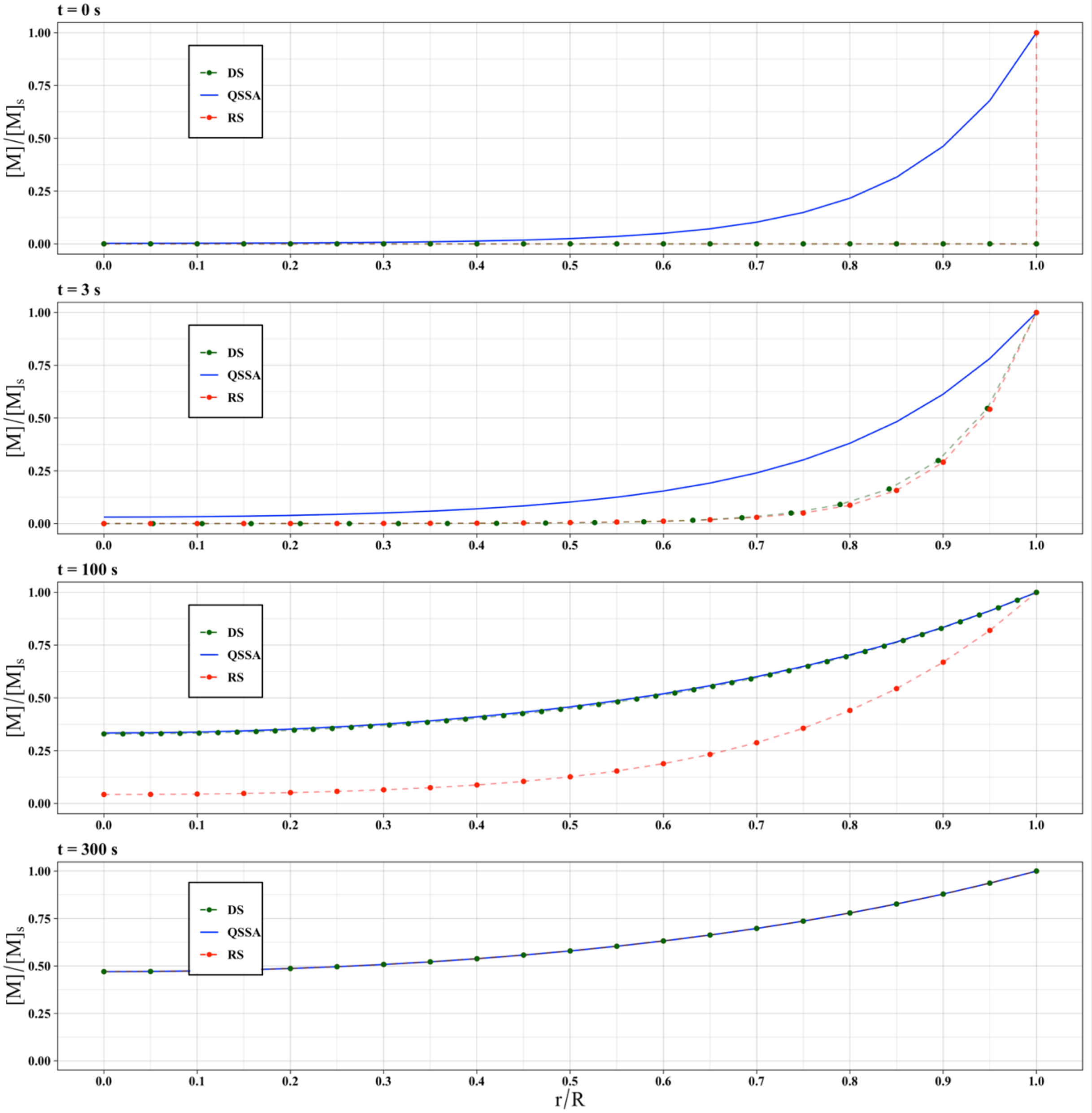

Figure 5.1: Comparison between the monomer radial profiles predicted by the quasi-steady-state approximation, dynamic solution, and rigorous solution, from t = 0 to t =300 s, at Φ_1=0.5

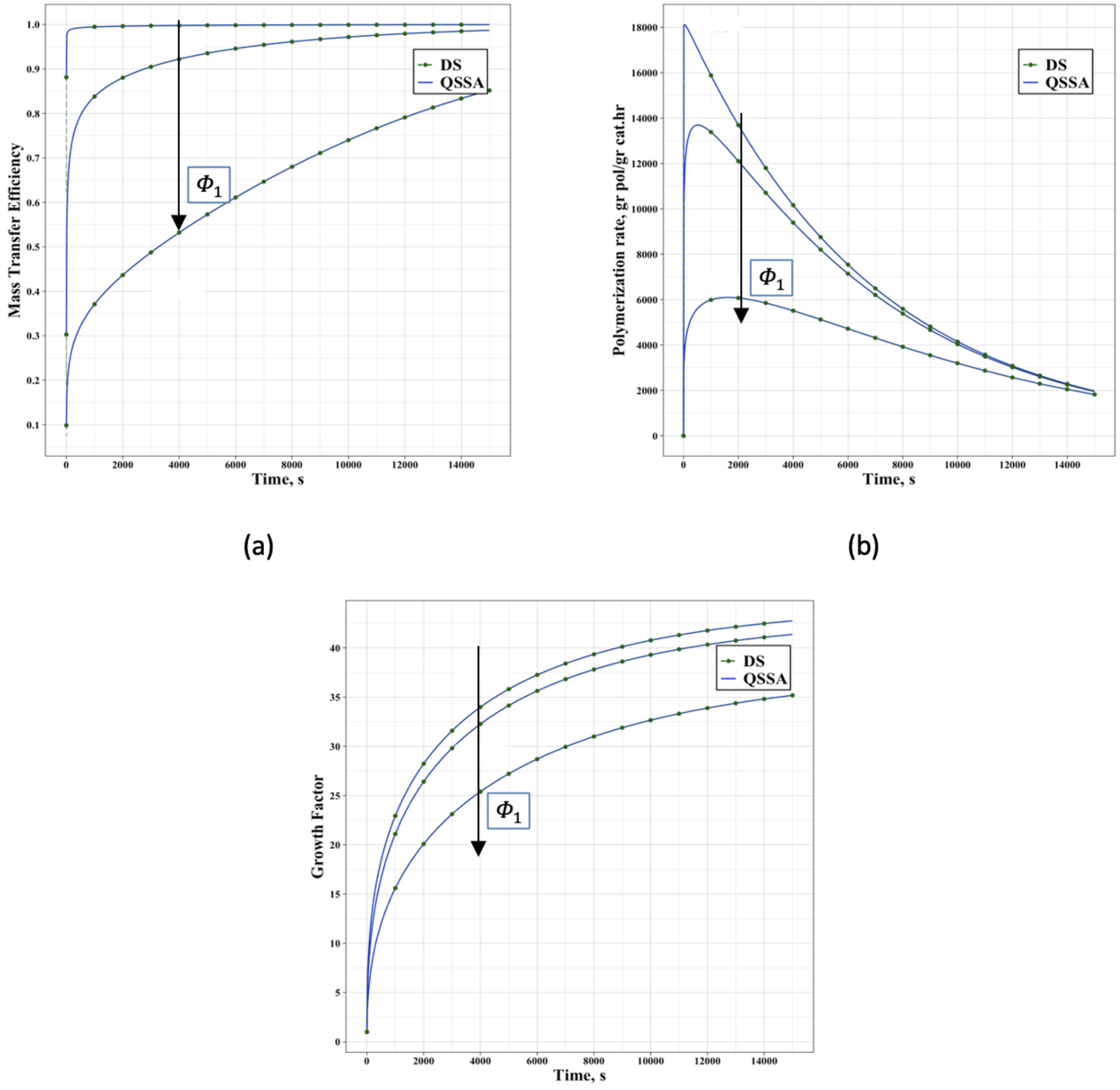

(a)

(b)

(c)

Figure 5.2: Comparison between the quasi-steady-state approximation and dynamic solution for three different Thiele moduli Φ_1=0.5, 3, and 10 for: a) mass transfer efficiency, b) rate of polymerization, and c) particle growth.

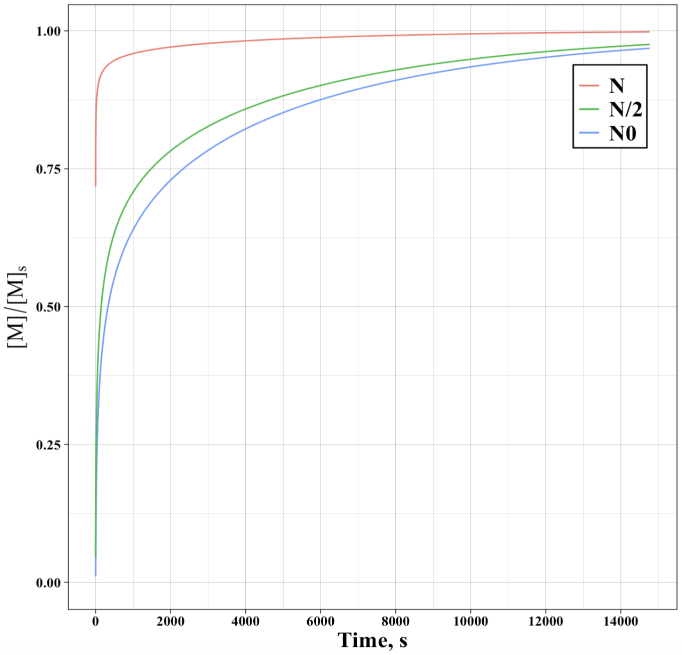

Figure 5.3: Monomer concentration evolution with time at three shell locations, starting from the particle center (N0) to the surface (N).

doesn't grow. But because our particle is growing, changing the concentration at the surface affects the time at which the particle reaches steady state and how much it grows.

Figure 5.9.a shows how the MWD develops for polymer made with Thiele modulus of 3, using the polymerization kinetics parameters given in Table 2. The MWD predicted by the RS method after 1000 seconds of polymerization is a little broader since the steeper monomer concentration profile (Figure 5.7.b) leads to the production of polymer populations with lower molecular weight averages that are not predicted by the QSSA model. As the polymerization goes on, the monomer concentration profile predicted by the QSSA model approaches the predictions of the RS model which, in turn, make the MWDs predicted by both models look increasingly more alike. Figure 5.9.b compares the predicted polydispersity index for both models. Even though the RS and QSSA model predictions converge for higher polymerization times, the QSSA always predicts a slightly more narrow MWD than the RS model.

5.3 Comparison Between Quasi-Steady-State and Dynamic Solutions, Copolymerization

Figure 5.10 shows that the predicted monomer efficiency and comonomer efficiency for mass transfer at $\Phi_2 = 3$ match for all Φ_1 values. The quasi-steady-state method in its core is a simplification to

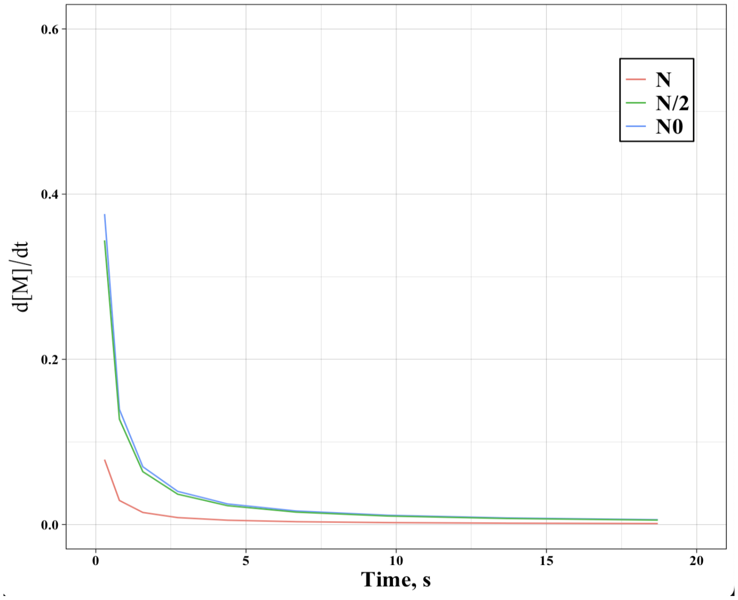

Figure 5.4: Monomer concentration accumulation at three shell locations, starting from the particle center (N0) to the surface (N).

the dynamic solution, where it assumes that the monomer profile is increasing at a steady rate. This is similar to the results obtained for the homopolymerization case. The addition of a comonomer adds further complexity to the equations, as the kinetics of the reaction depends on the monomer fraction, which is a variable that changes within the particle radius. Figure 5.11 shows a contour plot comparing the quasi-steady-state solution assuming constant monomer fraction and variable monomer fraction with the dynamic solution. The figure shows that when the quasi-steady-state method assumes an averaged monomer fraction through the particle, the model matches with the dynamic solution with a very slight difference at the start that eventually disappears as the reaction proceeds. This indicates that averaging the monomer fraction is not an inappropriate approximation for the quasi-steady-state solution. When the particle exhibits a high Thiele moduli value regardless of the component, the respective monomer profile at a specific time is very steep along the radius, which makes the averaged monomer fraction deviate from the actual case. As the reaction proceeds, the Thiele modulus of each component reduces, and the monomer profile inside the particle flattens out which reduces the error induced by averaging. Although the difference in significance is very minor, this finding will be helpful in analyzing the rigorous solution comparison as we will see later. On the other hand, the variable monomer fraction model does perform slightly better as it is an analytical solution of the particle under conditions that are met. In later sections, we will demonstrate how this model can perform very poorly when it is taken out of the required conditions. Additional plots are included in Appendix B, showcasing the comparison between the models predicting: monomer mass transfer efficiency, comonomer mass transfer efficiency, polymerization

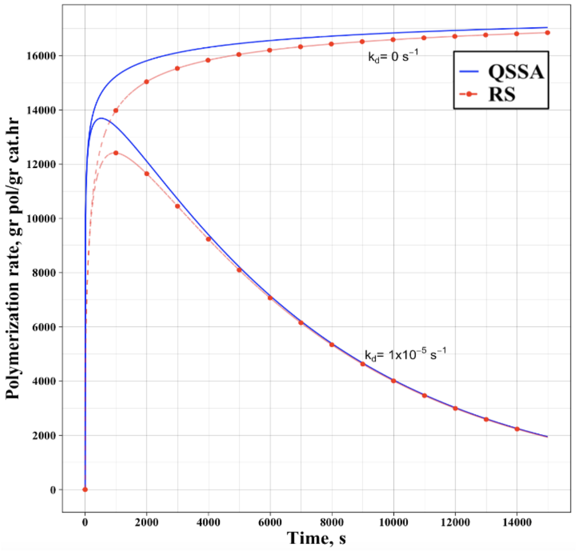

Figure 5.5: Comparison between the quasi-steady-state approximation and rigorous solution with and without active sites deactivation at Φ_1= 3.

rate, and particle growth factor.

In this section, we will compare the analytical quasi-steady-state and approximate quasi-steady-state methods with the rigorous solution, equivalent to comparing the dynamic solution with the rigorous solution. The rigorous solution considers that the concentration of active sites varies as a function of radial position. This is a significant consideration that we investigated in the homopolymerization section, as the differences between the quasi-steady-state and rigorous solutions become larger with higher Thiele values. In Figure 5.12, the predicted monomer mass transfer efficiency by the rigorous solution matches with the quasi-steady-state solution with variable monomer fraction at the monomer Thiele value lower than 3. As for the comonomer mass transfer efficiency, the difference is higher, as the comonomer Thiele value is kept at high at 3. Figure 5.13 shows a clear perspective on how varying the comonomer Thiele value at a constant monomer Thiele modulus affects the differences between the models. These results indicate that the monomer has a greater effect on the polymerization rate and particle properties than the comonomer. Since the accuracy of the quasi-steady-state approximation depends on the particle state (i.e., with less diffusion limitation resulting in higher accuracy), an increase in the monomer Thiele value has a more significant impact on the quasi-steady-state predictions than the comonomer. The major difference between the two quasi-steady-state models and the rigorous solution is the active sites profile; in the steady-state models the active sites are homogenously diluted, and they are not a function of particle radius. In the rigorous solution, the active sites are radially diluted, and they are a function of particle radius. When the particle is at a low Thiele moduli region, the particle grows uniformly

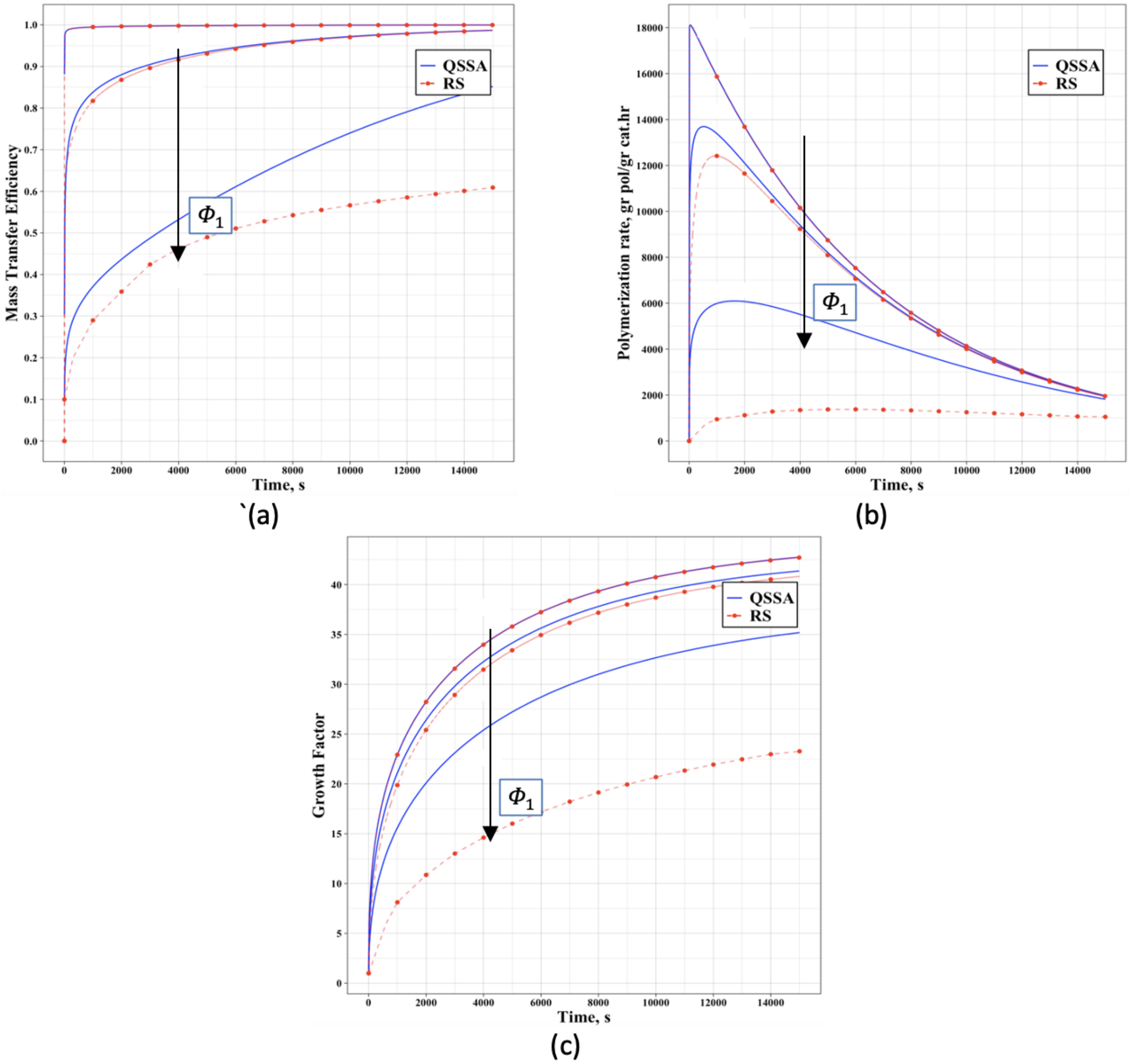

`(a)

(b)

(c)

Figure 5.6: Comparison between the quasi-steady-state approximation and rigorous solution at three different Thiele moduli, Φ_1= 0.5, 3 , and 10: a) mass transfer efficiency, b) rate of polymerization, and c) particle growth factor.

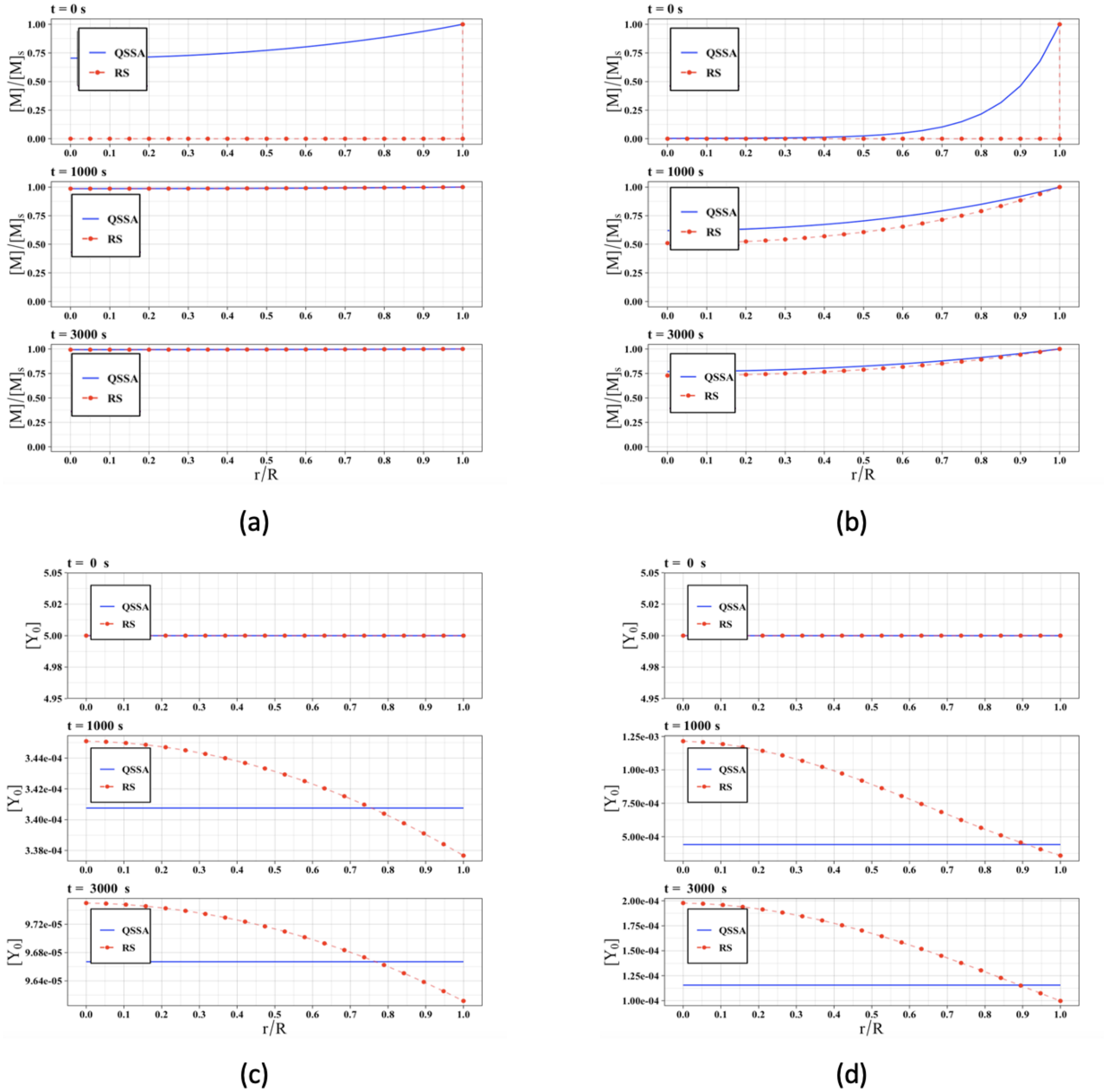

Figure 5.7: Comparison between the development of the quasi-steady-state approximation and rigorous solution from t = 0 to t = 3000 s: for monomer concentration, a)Φ_1= 0.5 and b) Φ_1= 3, and for active sites concentration, c) Φ_1= 0.5 and d) Φ_1= 3.

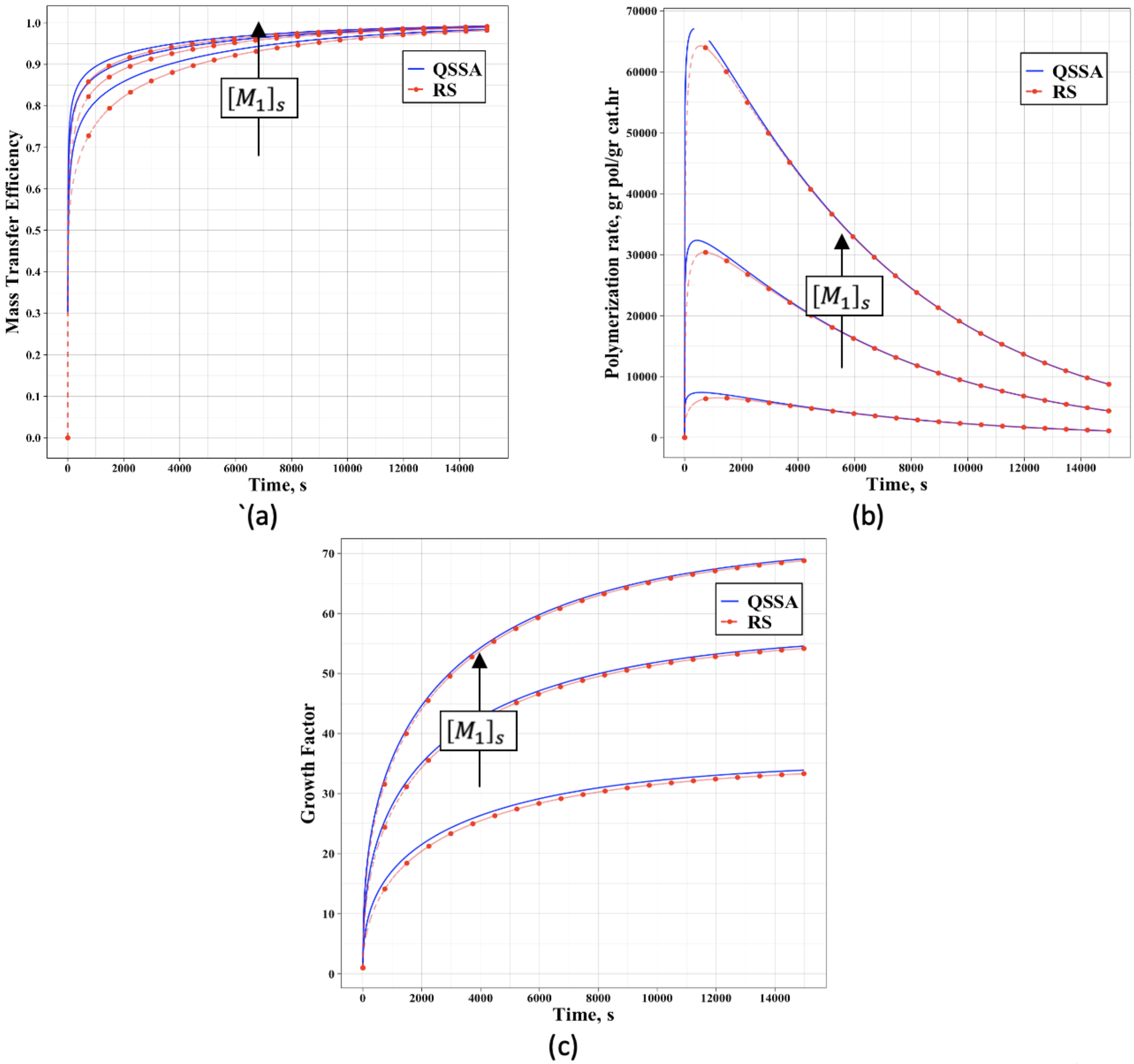

Figure 5.8: Comparison between the quasi-steady-state approximation and rigorous solution at three different monomer surface concentration, $[M_1]_s = 100$, 200 and 400 a) mass transfer efficiency, b) rate of polymerization, and c) particle growth factor.

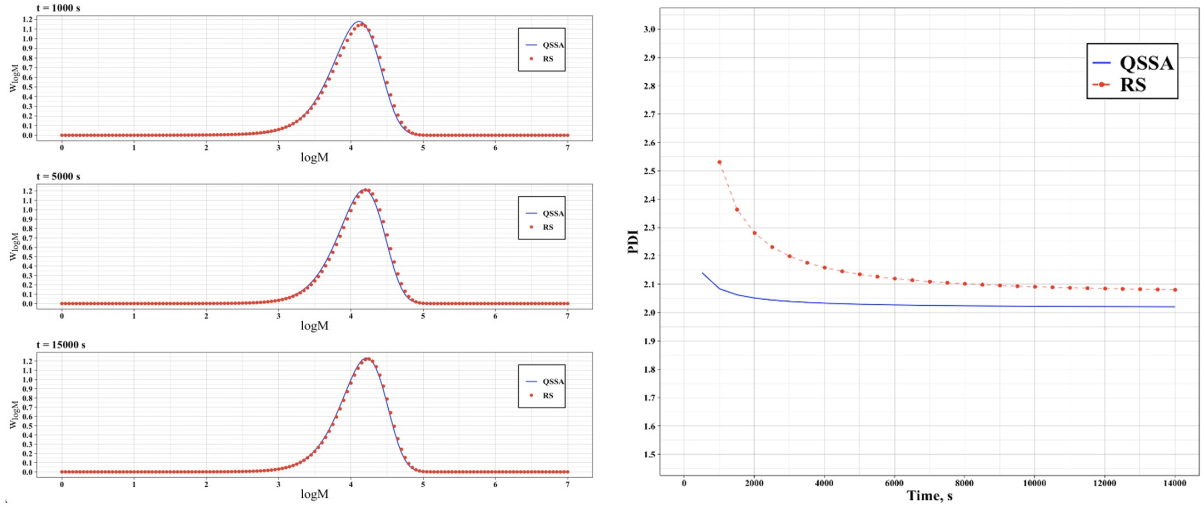

(a)

(b)

Figure 5.9: Comparison between the quasi-steady-state approximation and rigorous solution for: a) MWD as a function of time, b) polydispersity index as a function of time.

equally inside-out as there is enough supply of monomer and a high rate of reaction.

When increasing the Thiele moduli of the models, the steady-state models will always over-predict the particle growth and concentration profiles due to its relatively high kinetics caused by non-radial active sites dilution. The active sites profile becomes significantly more important as the particle gets more diffusion-limited, where the inner shells grow much slower than the outer shells. This causes the active sites profile to be steep, inducing the difference between the steady-state and rigorous solutions.

Finally, Figure 5.14 shows that the predicted results by both the quasi-steady-state models are close to the rigorous solution prediction at the low Thiele modulus regions, with a relative difference less than %1. Similar to the findings of the previous section, the steady-state solution considering variable monomer fraction is slightly better than its counterpart. The figure also shows how the monomer Thiele moduli have a higher effect on the differences than the comonomer Thiele moduli. This is because the comonomer contribute less to the reaction as it exhibits lower propagation kinetics than the monomer. This is generally true in polyolefins engineering, as the amount of the comonomer in the polymer generated is significantly lower than the main monomer which makes up the backbone of the polymer. Just as in homopolymerization, the concentration of monomer and comonomer did not have a noticable effect. The accuracy of the QSSA simulation for most polyolfien processes will be hindered by the monomer thiele modulus because the monomer contributes more

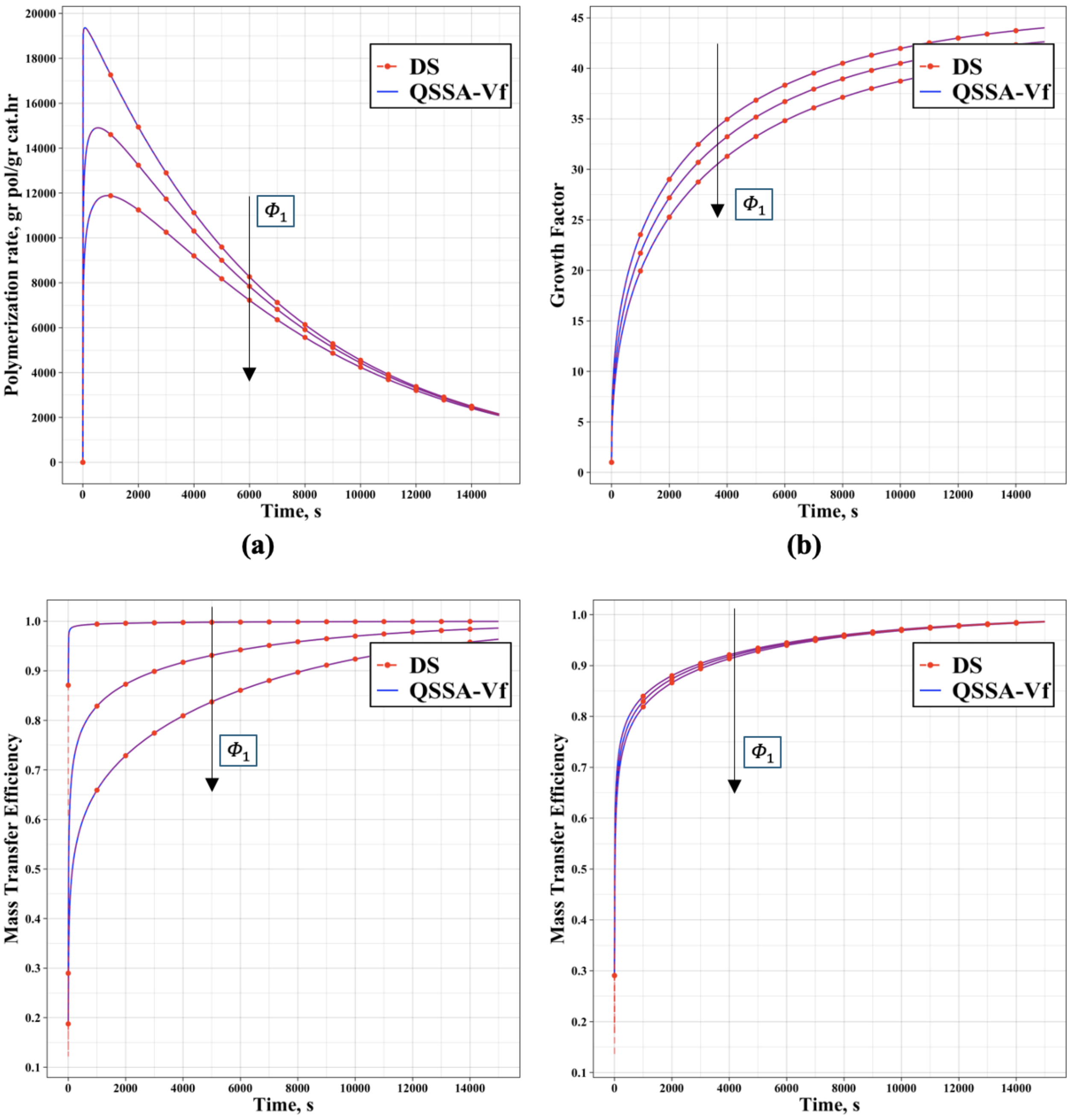

(a) (b)

(c) (d)

Figure 5.10: Comparison between the quasi-steady-state variable monomer fraction (QSSA-Vf) and dynamic solution (DS) at three different monomer Thiele moduli, Φ_1= 0.5, 3, and 5, at a constant comonomer Thiele moduli, Φ_2=3, for: a) rate of polymerization, b) particle growth factor, c) monomer mass transfer efficiency, and d) comonomer mass transfer efficiency.

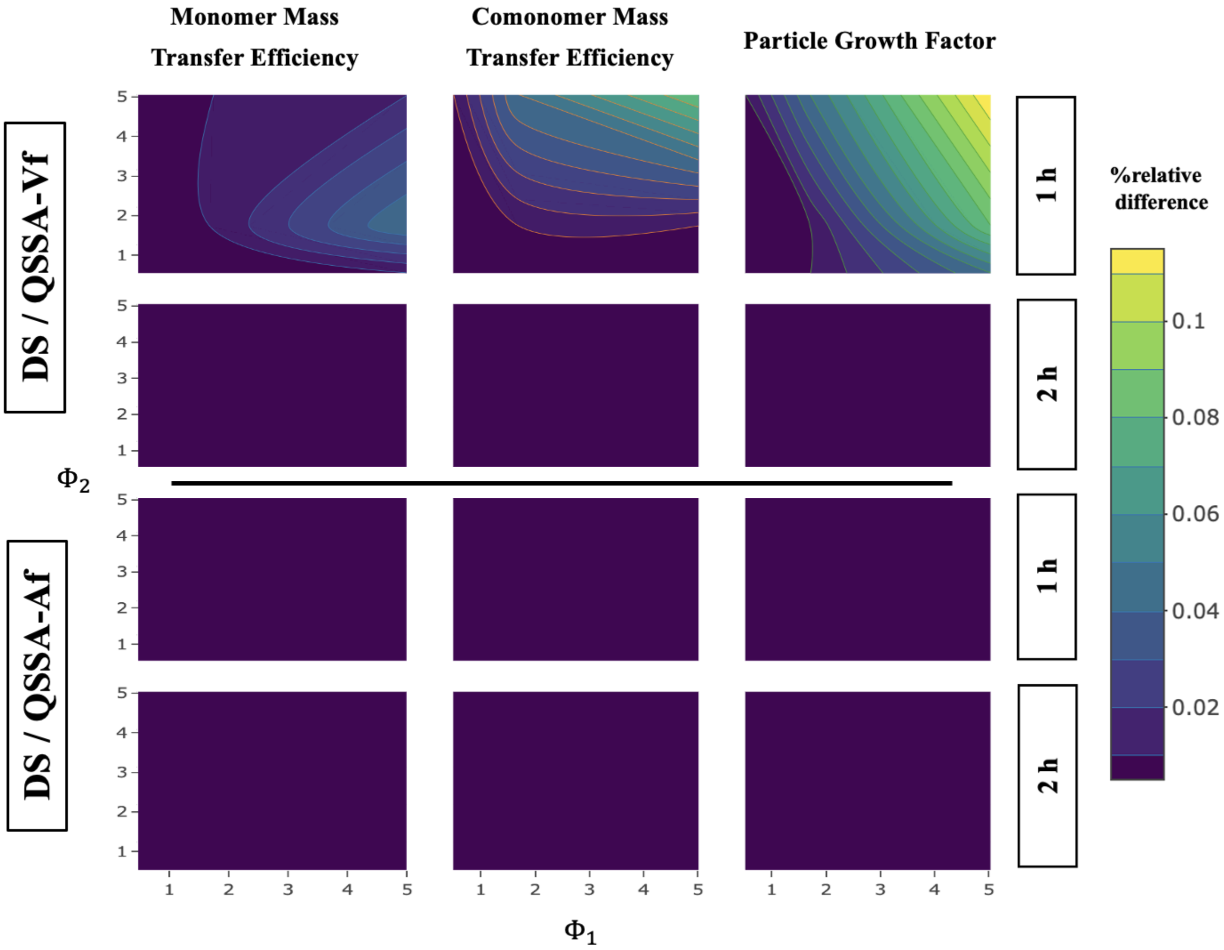

Figure 5.11: Comparison between the quasi-steady-state variable monomer fraction, the quasi-steady-state average monomer fraction, and the dynamic solution.

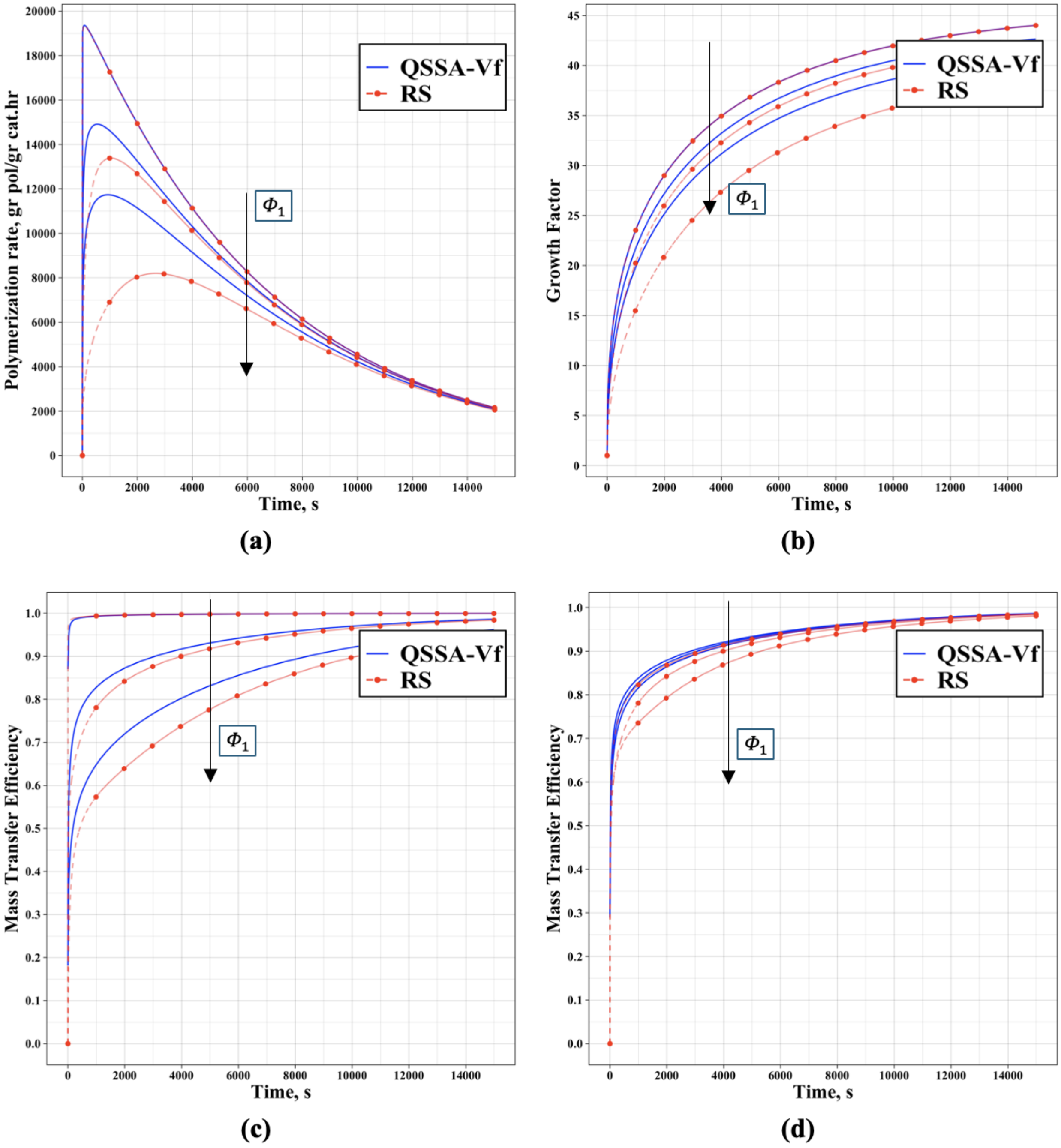

Figure 5.12: Comparison between the quasi-steady-state variable monomer fraction and rigorous solutions at three different monomer Thiele moduli, Φ_1= 0.5, 3, and 5, at constant comonomer Thiele moduli, Φ_2=3, a) rate of polymerization, b) particle growth factor, c) monomer mass transfer efficiency, and d) comonomer mass transfer efficiency.

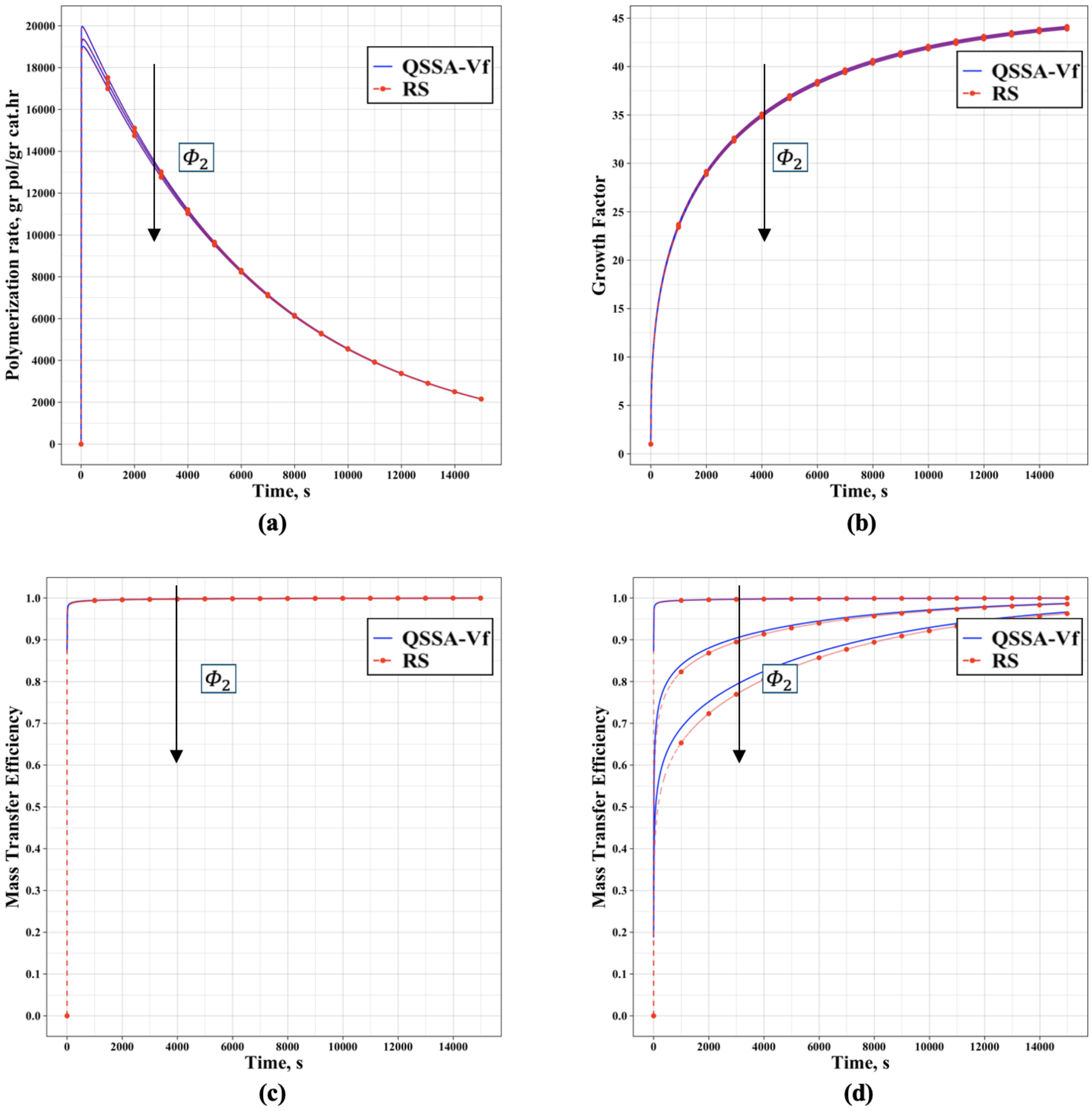

(a) (b) (c) (d)

Figure 5.13: Comparison between the quasi-steady-state variable monomer fraction and rigorous solutions at three different comonomer Thiele moduli, Φ_2= 0.5, 3 and 5, at constant monomer Thiele moduli, Φ_1= 3, for: a) rate of polymerization, b) particle growth factor, c) monomer mass transfer efficiency, and d) comonomer mass transfer efficiency.

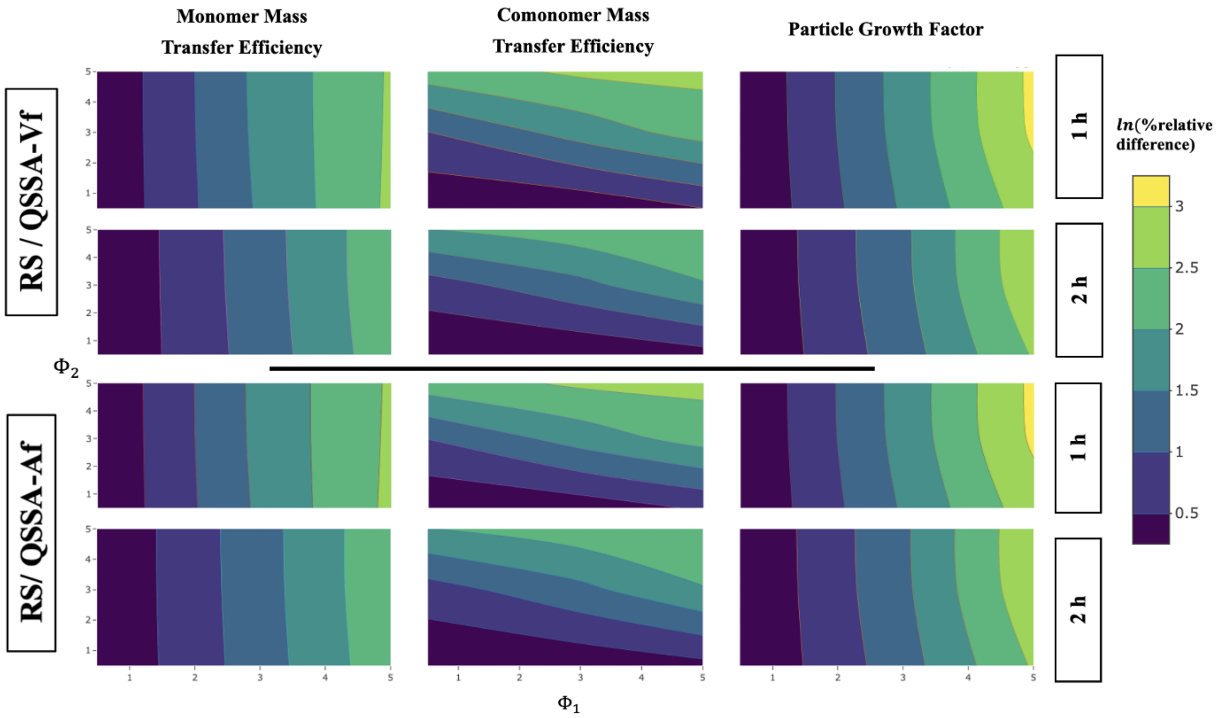

Figure 5.14: Comparison between the quasi-steady-state variable monomer fraction, the quasi-steady-state average monomer fraction, and rigorous solutions.

to the kinetics of the reaction than the comonomer.

Figure 5.16 shows the number and weight average chain lengths predicted by the rigorous solution, steady-state model considering variable monomer fraction, and steady-state model considering constant monomer fraction. Generally, both steady-state models predict N_n and N_w well at the low monomer Thiele moduli where the comonomer Thiele moduli has a slight effect on the relative differences. Furthermore, the steady-state models fail to predict the number average molecular weight at the high Thiele modulus region, as it neglects the lower end of the molecular weight distribution when the particle is starved.

Figure 5.17 illustrates the short chain branches (SCB) predicted by the rigorous solution and the steady-state models. At the low Thiele region, the SCB predicted by the steady-state models almost matches the rigorous solution with a flat distribution across the molecular weights as a result of low Thiele moduli and high mass transfer efficiencies for monomer and comonomer. When the monomer Thiele moduli is increased, the monomer to comonomer ratio increases along the particle radius which causes a decrease in the likelihood of short branches insertion in the backbone of the polymer chain.

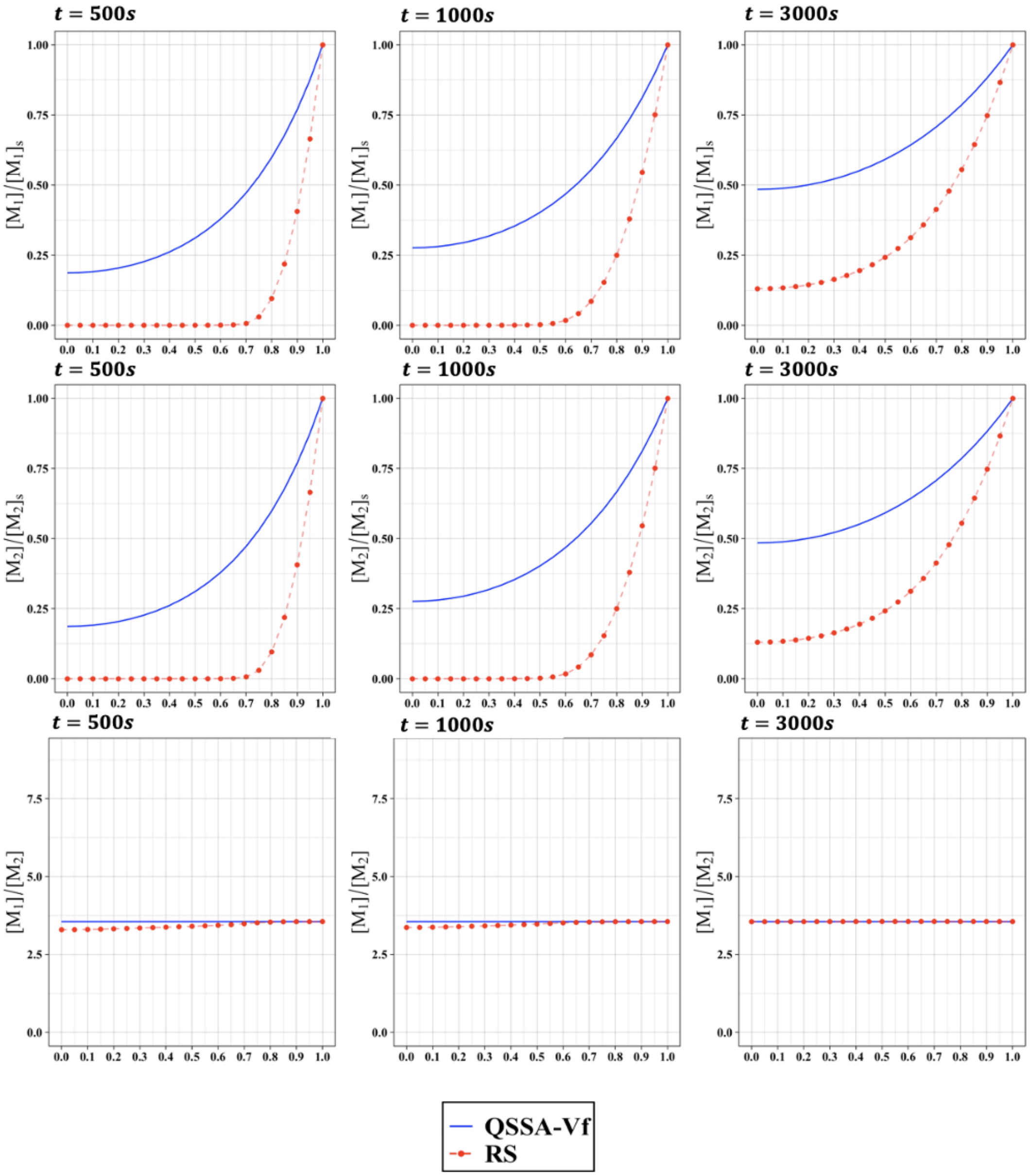

Figure 5.15: Radial concentration profiles for monomer, comonomer, and their ratios at three different times. Φ_1= 5, Φ_2= 5

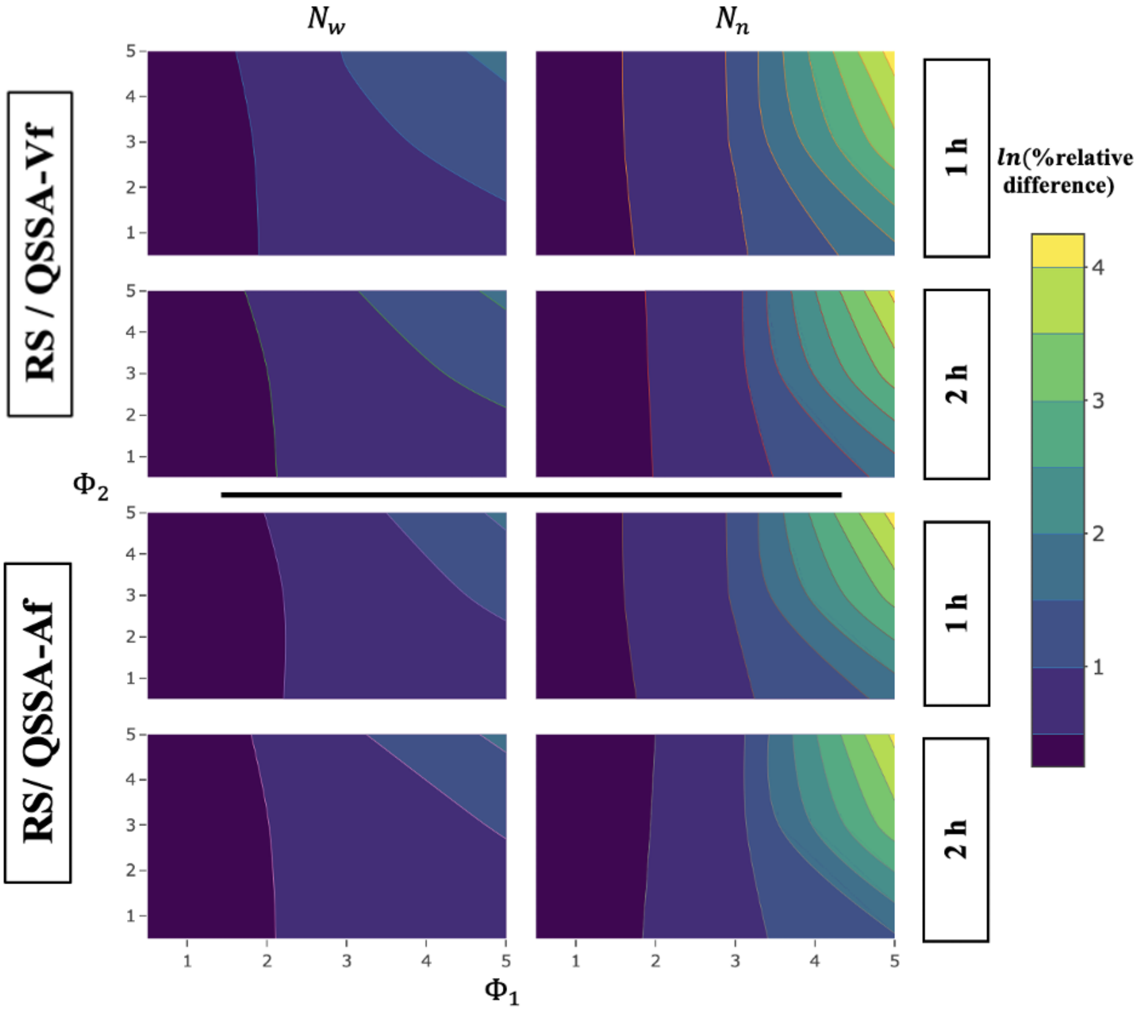

Figure 5.16: Comparison of the weight average chain lengths predicted by the rigorous solution and the steady-state models.

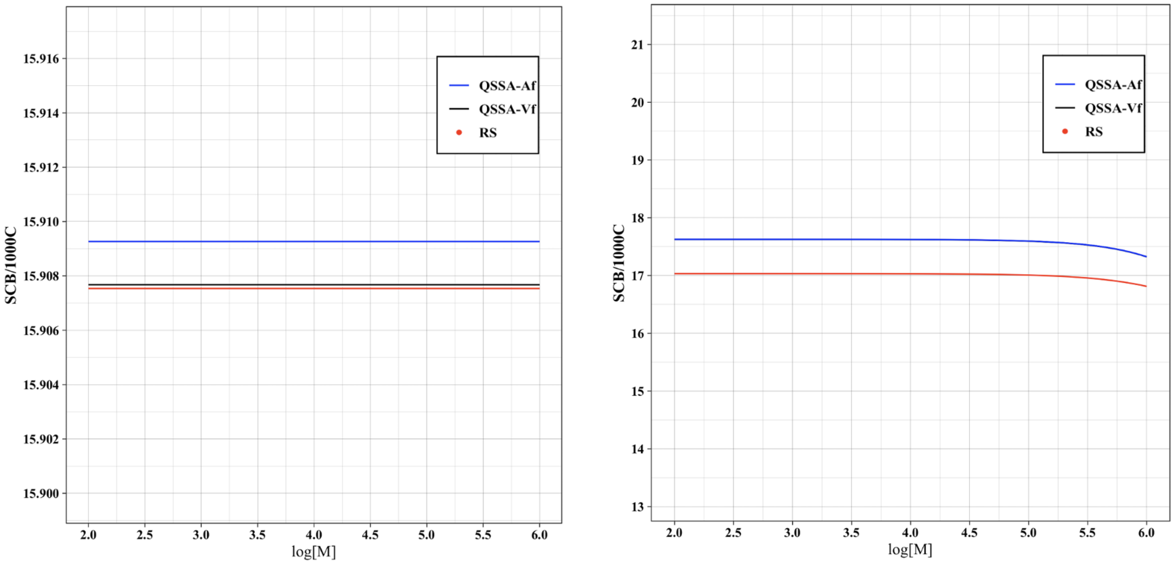

(a) (b)

Figure 5.17: Comparison of the short chain branching distribution of the quasi-steady-state variable monomer fraction and average monomer fraction solutions with the rigorous solution, for: a) Φ_1=0.5, Φ_2=0.5, b) Φ_1=3, Φ_2= 0.5

Because there are many possible combinations of Φ_1 and Φ_2, each yielding different results for the QSSA accuracy, some which are not relevant to common industrial practices, going through all the possibilities will be endless. While the contour plots provide a general guidance on the QSSA performance, additional plots for the rigorous solution are provided in the appendix.

5.4 Monte Carlo Simulation

Both the quasi-steady-state models and the rigorous solution programs are written in C++ language, as it offers high-speed computation through compiled execution. In a prior publication from our team, we created a framework to analyze the performance of polyolefin reactors utilizing Monte Carlo simulation. The main challenge with the Monte Carlo simulation was the extensive computation time.[35] To assess the computational speed of quasi-steady-state models, a simple Monte Carlo simulation framework was integrated with the QSSA. Table 5.2 shows that both steady-state models are significantly faster than the rigorous solution, especially when modeling a high number of particles. This is because the rigorous solution is significantly more demanding on computational power and because the distribution of particles and residence time is random; the rigorous solution speed is highly dependent on the model properties. On the other hand, the steady-state simulation is not affected by the state of the particle. The steady-state solution assuming average monomer

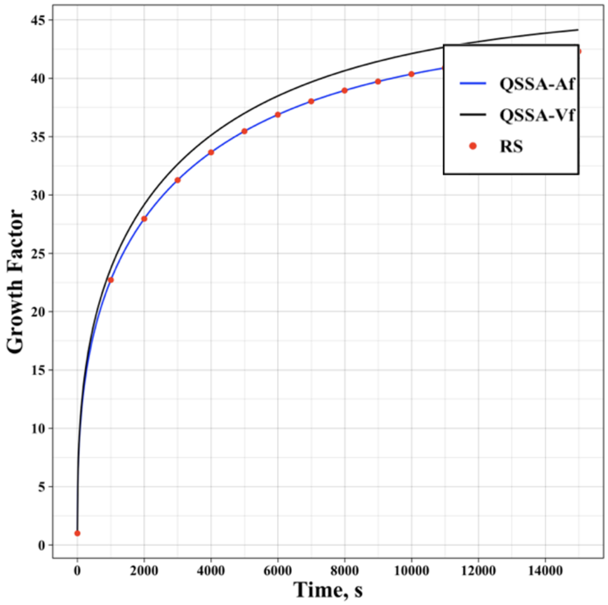

Figure 5.18: Comparison of the particle growth between the quasi steady-state variable monomer fraction (QSSA-Vf), average monomer fraction (QSSA-Af), and rigorous solution (RS), a) Φ_1=0.5, Φ_1=0.5, Φ_2=0.5, $k_{p21} = (100\frac{\mathrm{m}^3}{\mathrm{mol}\cdot\mathrm{s}})$

fraction does take slightly more time as it has to calculate the average of the concentration profiles during the simulation.

Number of particles	**1**	**50**	**100**	**200**
Rigorous solution, computational speed (seconds)	62	7123	14400	28300
QSSA-Vf, computational speed (seconds)	0.197	3.06	12.14	24.69
QSSA-Af, computational speed (seconds)	0.211	4.10	13.59	29.21

Table 5.2: Computation time of simulations.

Even though the steady-state model assuming variable monomer fraction is slightly better and faster than the one assuming constant monomer fraction, it can drastically fail when it is taken out of its conditions. For example, when we decrease the value of k_{p21} from 500 to 100 m^3 mol s^{-1}, the value of $\aleph_1$ and $\aleph_2$ becomes 0.175 and 0.028 which is high enough that model overpredicts the particle growth, as seen in Figure 5.18. While the steady-state model assuming variable monomer fraction can be employed if precision is essential, one should be careful to only utilize it when the prerequisites are satisfied.

Chapter 6

Conclusions and Recommendations

The mass transfer phenomenon in growing polymer particles has a major influence on the process of polymerization and the characteristics of polymers generated in polyolefin reactors. Several single particle models have been previously developed to solve the reaction-diffusion problem with moving boundary condition. However, the computing cost of the polymer flow models, even in their most basic versions, make it challenging to scale them up for modeling industrial reactors with a high number of particles.

In the current thesis, the quasi-steady-state approximation is applied as a computationally efficient method, to solve the polymer flow model. The QSSA results are compared to the dynamic solutions, assuming both uniform and nonuniform radial distribution of active sites. For the homopolymerization case, we have proposed a solution assuming uniform distribution of active sites. For the copolymerization case, we have proposed two viable alternatives: the first method assumes a constant monomer fraction throughout the particle, and the second one is an analytical solution applicable under certain conditions which is slightly faster and more accurate compared to the first method.

The performance of the developed models is evaluated based on various factors, including the calculated particle growth factor, monomer mass transfer efficiency, comonomer mass transfer efficiency, molecular weight distribution, weight-average chain length, number-average chain length, and short chain branches distribution. The catalyst Thiele modulus is used as the benchmark for this evaluation. Our simulations show that, after a brief initial period, the steady-state models achieve a precise alignment with the dynamic solution when the active sites are evenly distributed throughout the particle. If the dynamic solution takes into account the local dilution of catalyst fragments in the produced polymer, the distribution of active sites will be nonuniform in the growing particle, i.e., decreasing with the radial position. In this scenario, the steady-state models demonstrate favorable performance only throughout the range of low to medium monomer Thiele moduli, which reflect the regions that are realistically significant. The comonomer Thiele moduli has less influence on the findings as it contributes less to the polymer that is formed. As the Thiele modulus increases, the steady-state models start to deviate from the dynamic solution since the concentration gradient of active sites becomes more and more pronounced. These high Thiele modulus values equate to very high levels of mass transfer limitations that are unwanted and typically avoided in practical operations. Finally, the steady-state models are merged into the Monte Carlo framework with a high number of random particles, greatly increasing the computational speed and confirming this method as a scalable approach for single particle modeling of polyolefin reactors.

For future work, it is possible to expand on the QSSA model to account for multiple active site types, variable diffusion and porosity calculations. It is also possible to develop QSSA model with nonuniform distribution of active sites but the model will probably require fitting constants to get the correct active sites dilution effect. Finally, the QSSA improves our ability to simulate fill reactor modelling for commercial processes. We recommend using the QSSA in future reactor modeling studies, Monte Carlo simulations, and fluidized bed dynamics.

Bibliography

[1] Walter Kaminsky, “Trends in Polyolefin Chemistry”, *Macro Chemistry & Physics* **209**(5), pp. 459–466 (2008).

[2] Nicole K. Boaen and Marc A. Hillmyer, “Post-polymerization functionalization of polyolefins”, *Chem. Soc. Rev.* **34**(3), pp. 267–275 (2005), Publisher: The Royal Society of Chemistry.

[3] João B. P. Soares and Timothy F. L. McKenna, “Polyolefin Reaction Engineering: SOARES:POLYOLEFIN O-BK”, (2012).

[4] Ahmad Shamiri, Mohammed Harun Chakrabarti, Shah Jahan, Mohd Azlan Hussain, Werner Kaminsky, P.V. Aravind, and Wageeh A. Yehye, “The Influence of Ziegler-Natta and Metallocene Catalysts on Polyolefin Structure, Properties, and Processing Ability”, *Materials* (2014).

[5] J.T.M. Pater, G. Weickert, and Willibrordus Petrus Maria van Swaaij, “Optical and infrared imaging of growing polyolefin particles”, *Aiche Journal* (2003).

[6] Roman Hackl and Stephanie Perret, “Power production with Organic Rankine Cycle technology utilizing waste heat from a cracker and three polyethylene units” (2009).

[7] JR John Severn, JC John Chadwick, Robbert Duchateau, and Nic Friederichs, “”Bound but not gagged”–immobilizing single-site alpha-olefin polymerization catalysts.”, *Chemical Reviews* (2005).

[8] Vasileios Touloupidis, “Catalytic Olefin Polymerization Process Modeling: Multi-Scale Approach and Modeling Guidelines for Micro-Scale/Kinetic Modeling”, *Macromolecular Reaction Engineering* (2014).

[9] Arash Alizadeh, Vasileios Touloupidis, and João B. P. Soares, “Systematic Comparison of Slurry and Gas-Phase Polymerization of Ethylene: Part I Thermodynamic Effects”, *Macromolecular Reaction Engineering* (2021).

[10] Shuaifeng Zhang, Qinghua Zhang, Bo Hyun Kong, Chao Yang, and Rodney O. Fox, "An effectiveness factor model for slurry phase olefin polymerizations", *Chemical Engineering Science* (2022).

[11] Vassilis Kanellopoulos, E. Tsiliopoulou, Georgios Dompazis, V. Touloupides, and Costas Kiparissides, "Evaluation of the Internal Particle Morphology in Catalytic Gas-Phase Olefin Polymerization Reactors", *Industrial & Engineering Chemistry Research* (2007).

[12] Vassilis Kanellopoulos, Bill Gustafsson, and Costas Kiparissides, "Gas-Phase Olefin Polymerization in the Presence of Supported and Self-Supported Ziegler-Natta Catalysts", *Macromolecular Reaction Engineering* (2008).

[13] Arash Alizadeh, Farhad Sharif, Morteza Ebrahimi, and Timothy F. L. McKenna, "Modeling Condensed Mode Operation for Ethylene Polymerization: Part III. Mass and Heat Transfer", *Industrial & Engineering Chemistry Research* (2018).

[14] Charles R. Wilke and Pin Chang, "Correlation of diffusion coefficients in dilute solutions", *Aiche Journal* (1955).

[15] Isaac C. Sánchez and Robert H. Lacombe, "Statistical Thermodynamics of Polymer Solutions", *Macromolecules* (1978).

[16] Alan S. Michaels and Harris J. Bixler, "Flow of gases through polyethylene", *Journal of Polymer Science* (1961).

[17] Arash Alizadeh, "Study of Sorption, Heat and Mass Transfer During Condensed Mode Operation of Gas Phase Ethylene Polymerization on Supported Catalyst", (2014).

[18] Afsaneh Soleimani, Andreas Aigner, and Vasileios Touloupidis, "Single Particle Growth, Fragmentation and Morphology Modelling: A DEM Approach", *Macromolecular Reaction Engineering* (2022).

[19] Arash Alizadeh, Farhad Sharif, Morteza Ebrahimi, and Timothy F. L. McKenna, "Modeling Condensed Mode Operation for Ethylene Polymerization: Part III. Mass and Heat Transfer", *Ind. Eng. Chem. Res.* **57**(18), pp. 6097–6114 (2018).

[20] Timothy F. L. McKenna and Muhammad Ahsan Bashir, "Fragmentation, Particle Growth and Single Particle Modelling", (2019).

[21] Mohammad Mansouri, Gholam Hossein Zohuri, and Navid Ramezanian, "Effect of Ethylene Monomer Pressure on BCE Ziegler-Nata Catalyst Fragmentation in the Early Stage of Polymerization", (2018).

[22] Timothy F McKenna and Joao B P Soares, "Single particle modelling for oleÿn polymerization on supported catalysts: A review and proposals for future developments", *Chemical Engineering Science* (2001).

[23] Timothy F. L. McKenna, Audrey Di Martino, Guenter Weickert, and João B. P. Soares, "Particle Growth During the Polymerisation of Olefins on Supported Catalysts, 1 – Nascent Polymer Structures", *Macromolecular Reaction Engineering* (2010).

[24] Mohsen Najafi, Mahmoud Parvazinia, M. Parvazinia, Mir Hamid Reza Ghoreishy, and Costas Kiparissides, "Development of a 2D Single Particle Model to Analyze the Effect of Initial Particle Shape and Breakage in Olefin Polymerization", *Macromolecular Reaction Engineering* (2014).

[25] Joao B P Soares and Timothy F L McKenna, "Polyolefin Reaction Engineering".

[26] Timothy F. L. McKenna and João B. P. Soares, "Single particle modelling for olefin polymerization on supported catalysts: A review and proposals for future developments", *Chemical Engineering Science* (2001).

[27] Piet van Leeuwen, *Homogeneous Catalysis – Understanding the Art*, (2004).

[28] Philipp A. Mueller, John R. Richards, and John P. Congalidis, "Polymerization Reactor Modeling in Industry", *Macromolecular Reaction Engineering* (2011).

[29] Alan S. Michaels and Harris J. Bixler, "Solubility of gases in polyethylene", *Journal of Polymer Science* (1961).

[30] Soares J.B.P. and A. E. Hamielec, "GENERAL DYNAMIC MATHEMATICAL MODELING OF HETEROGENEOUS ZIEGLER-NATTA AND METALLOCENE CATALYZED COPOLYMERIZATION WITH MULTIPLE SITE TYPES AND MASS AND HEAT TRANSFER RESISTANCES", *Polymer Reaction Engineering* (1995).

[31] Vassileios Kanellopoulos, Georgios Dompazis, Bill Gustafsson, and Costas Kiparissides, "Comprehensive Analysis of Single-Particle Growth in Heterogeneous Olefin Polymerization: The Random-Pore Polymeric Flow Model", *Ind. Eng. Chem. Res.* **43**(17), pp. 5166–5180 (2004).

[32] João B. P. Soares and Timothy F. L. McKenna, "A conceptual multilevel approach to polyolefin reaction engineering", *Canadian Journal of Chemical Engineering* (2022).

[33] Yi Zhou, Arash Alizadeh, Boping Liu, and João B. P. Soares, "Development of an Integrated Framework for Multiscale, Multiphase Modeling of Industrial Slurry-Phase Reactors for Polyethylene Production", *Macro Reaction Engineering* **15**(1), pp. 2000043 (2021).

[34] E. E. Petersen, “A general criterion for diffusion influenced chemical reactions in porous solids”, *Chemical Engineering Science* **20**(6), pp. 587–591 (1965).

[35] Yi Zhou, Arash Alizadeh, Boping Liu, and João B. P. Soares, “Development of an Integrated Framework for Multiscale, Multiphase Modeling of Industrial Slurry-Phase Reactors for Polyethylene Production”, *Macromolecular Reaction Engineering* (2020).

Appendix A

The Method of Undetermined Coefficients is a technique used to solve non-homogeneous linear ordinary differential equations (ODEs). It involves guessing a particular solution based on the form of the non-homogeneous term, then determining the coefficients of this guess by substituting it into the ODE. The general steps are:

- Guess the Form: Based on the non-homogeneous term (e.g., polynomial, exponential, sine, cosine), propose a particular solution with undetermined coefficients.
- Substitute and Solve: Plug this guess into the original ODE and solve for the coefficients.
- Combine Solutions: Add the particular solution to the general solution of the corresponding homogeneous ODE to get the complete solution.

The following steps are followed to solve the copolymerization QSSA model with variable monomer fraction.

1. First, we solve the comonomer mass balance equation by applying variable transformation to equation (4.24),

$$[M_2] = \frac{F_2}{r} \tag{A.1}$$

$$\frac{d\,[M_2]}{dr} = \frac{1}{r}\frac{dF_2}{dr} - \frac{F_2}{r^2} \tag{A.2}$$

2. Equation (4.24) is then solved using the same steps given for the homopolymerization solution. The analytical solution for equation (4.24) is:

$$[M_2] = \frac{C_1 e^{r\sqrt{\beta_{12}}}}{r} + \frac{C_2 e^{-r\sqrt{\beta_{12}}}}{r} \tag{A.3}$$

where,

$$\beta_{12} = \frac{k_{p,12}[C_0^*]e^{-k_d t}\left(\frac{1-\epsilon}{\alpha^3}\right)}{D_{e,2}} \tag{A.4}$$

3. The solution of the comonomer, equation (A.3), is substituted into the monomer mass balance, equation (4.23),

$$\frac{1}{r^2}\frac{\partial}{\partial r}\left(r^2\frac{\partial}{\partial r}\left(D_{e,1}\left[M_1\right]\right)\right) = \left(k_{p,11}[M_1] + k_{p,12}\left(\frac{C_1 e^{r\sqrt{\beta_{12}}}}{r} + \frac{C_2 e^{-r\sqrt{\beta_{12}}}}{r}\right)\right)[Y_0] \tag{A.5}$$

4. Using variable transformation given in equation (4.4) for the monomer and rearranging gives,

$$\frac{d^2F_1}{dr^2} - \frac{[Y_0]}{D_{e,1}}\left(k_{p,11}F_1 + k_{p,12}\left(C_1 e^{r\sqrt{\beta_{12}}} + C_2 e^{-r\sqrt{\beta_{12}}}\right)\right) = 0 \tag{A.6}$$

5. Equation (A.6) is a non-homogeneous ordinary differential equation; thus, variable transformation alone is not sufficient to solve the above equation. We can solve the above equation using the method of undetermined coefficients. First, we solve for the complementary solution, $F_c(r)$, by removing the non-homogeneous term from equation (A.6).

$$\frac{d^2F_1}{dr^2} - \frac{[Y_0]}{D_{e,1}}\left(k_{p,11}F_1\right) = 0 \tag{A.7}$$

6. The solution of equation (A.7) is the complementary solution,

$$F_c(r) = C_3 e^{r\sqrt{\beta_{11}}} + C_4 e^{-r\sqrt{\beta_{11}}} \tag{A.8}$$

$$\beta_{11} = \frac{k_{p,11}[C_0^*]e^{-k_d t}\left(\frac{1-\epsilon}{\alpha^3}\right)}{D_{e,1}} \tag{A.9}$$

7. As for finding the particular solution, we first guess a solution by looking at the non-homogeneous term that was removed from equation (A.6). The guess for the particular solution is,

$$F_p(r) = a_1 e^{r\sqrt{\beta_{12}}} + a_2 e^{-r\sqrt{\beta_{12}}} \tag{A.10}$$

$$\frac{d^2F_p(r)}{dr^2} = \beta_{12}\left(a_1 e^{r\sqrt{\beta_{12}}} + a_2 e^{-r\sqrt{\beta_{12}}}\right) \tag{A.11}$$

8. where a_1 and a_2 are the undetermined coefficients. We then substitute the guess into equation (A.6),

$$\beta_{12}\left(a_1 e^{r\sqrt{\beta_{12}}} + a_2 e^{-r\sqrt{\beta_{12}}}\right) = \beta_{11}\left(a_1 e^{r\sqrt{\beta_{12}}} + a_2 e^{-r\sqrt{\beta_{12}}}\right) + \frac{[Y_0]}{D_{e,1}} k_{p,12}\left(C_1 e^{r\sqrt{\beta_{12}}} + C_2 e^{-r\sqrt{\beta_{12}}}\right) \tag{A.12}$$

9. Equalizing the terms,

$$\beta_{12} a_1 = \beta_{11} a_1 + \frac{[Y_0]}{D_{e,1}} k_{p,12} C_1 \tag{A.13}$$

$$\beta_{12} a_2 = \beta_{11} a_2 + \frac{[Y_0]}{D_{e,1}} k_{p,12} C_2 \tag{A.14}$$

10. Solving for a_1 and a_2 gives,

$$a_1 = \frac{\frac{[Y_0]}{D_{e,1}} k_{p,12} C_1}{\beta_{12} - \beta_{11}} \tag{A.15}$$

$$a_2 = \frac{\frac{[Y_0]}{D_{e,1}} k_{p,12} C_2}{\beta_{12} - \beta_{11}} \tag{A.16}$$

11. Substituting into equation (A.10),

$$F_p(r) = \frac{\frac{[Y_0]}{D_{e,1}} k_{p,12} C_1}{\beta_{12} - \beta_{11}} e^{r\sqrt{\beta_{12}}} + \frac{\frac{[Y_0]}{D_{e,1}} k_{p,12} C_2}{\beta_{12} - \beta_{11}} e^{-r\sqrt{\beta_{12}}} \tag{A.17}$$

12. The analytical solution for the equation (4.23) is the sum of the complementary and particular solutions:

$$f\left(r\right) = F_c\left(r\right) + F_p\left(r\right) \tag{A.18}$$

13. Substituting the complementary and particular solutions:

$$f\left(r\right) = C_3 e^{r\sqrt{\beta_{11}}} + C_4 e^{-r\sqrt{\beta_{11}}} + \frac{\frac{[Y_0]}{D_{e,1}} k_{p,12}}{\beta_{12} - \beta_{11}} C_1 e^{r\sqrt{\beta_{12}}} + \frac{\frac{[Y_0]}{D_{e,1}} k_{p,12}}{\beta_{12} - \beta_{11}} C_2 e^{-r\sqrt{\beta_{12}}} \tag{A.19}$$

14. Rearranging the coefficients:

$$\frac{\frac{[Y_0]}{D_{e,1}}k_{p,12}}{\beta_{12}-\beta_{11}} = \frac{k_{p,12}D_{e,2}}{k_{p,12}D_{e,1}-D_{e,2}k_{p,11}} = \left(\frac{D_{e,1}}{D_{e,2}} - \frac{k_{p,11}}{k_{p,12}}\right)^{-1} \tag{A.20}$$

Finally, the general solution is:

$$f\left(r\right) = C_3 e^{r\sqrt{\beta_{11}}} + C_4 e^{-r\sqrt{\beta_{11}}} + \frac{C_1}{\frac{D_{e,1}}{D_{e,2}} - \frac{k_{p,11}}{k_{p,12}}} e^{r\sqrt{\beta_{12}}} + \frac{C_2}{\frac{D_{e,1}}{D_{e,2}} - \frac{k_{p,11}}{k_{p,12}}} e^{-r\sqrt{\beta_{12}}} \tag{A.21}$$

Appendix B

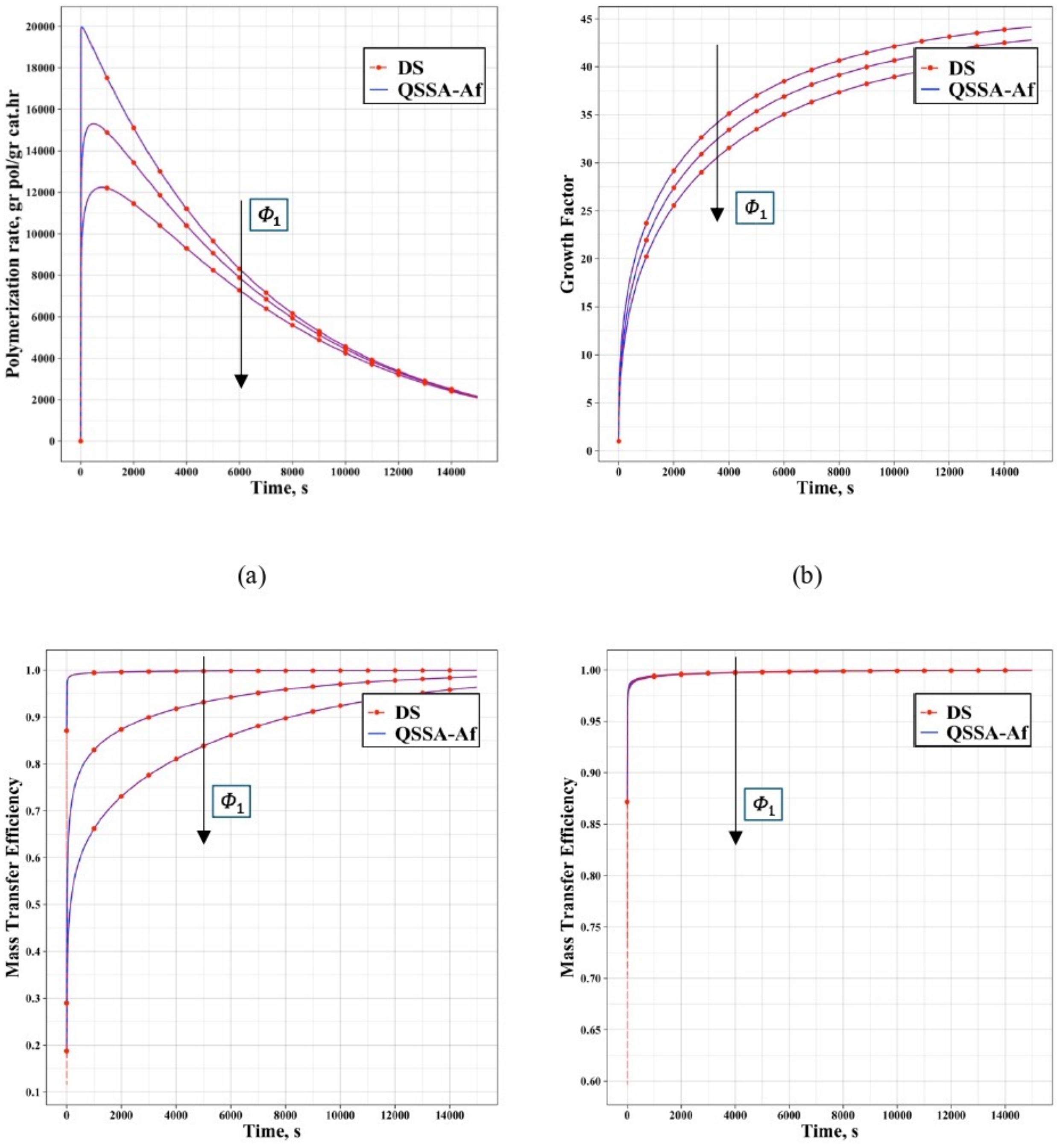

(a)

(b)

(c)

(d)

Figure B.1: Comparison between the quasi steady-state averaged monomer fraction (QSSA-Af) and dynamic solution (DS) at three different monomer Thiele moduli, Φ_1, at a constant comonomer Thiele moduli, Φ_2=0.5, a) rate of polymerization, b) particle growth, c) monomer mass transfer efficiency, and d) comonomer mass transfer efficiency.

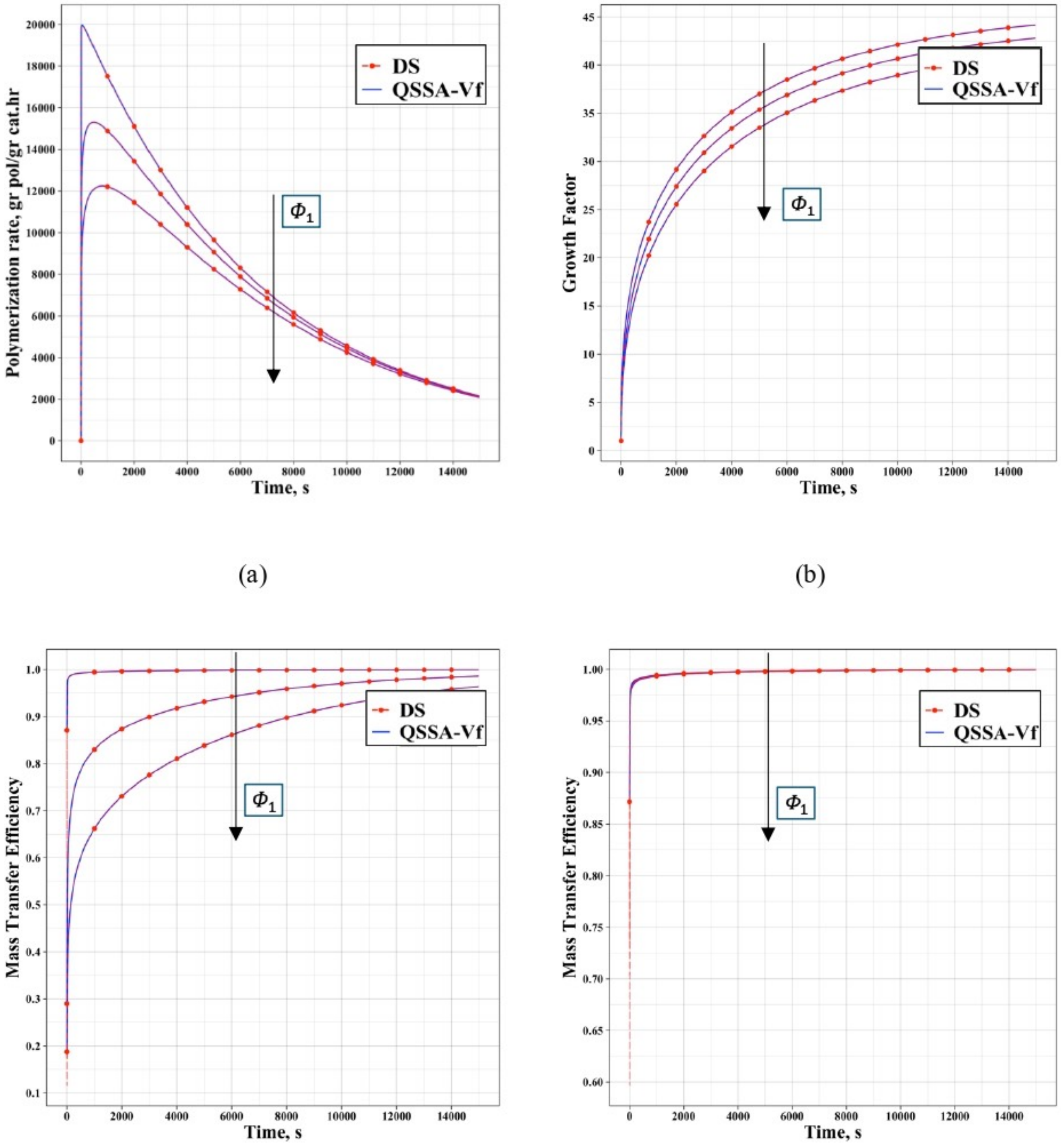

(a)

(b)

(c)

(d)

Figure B.2: Comparison between the quasi steady-state variable monomer fraction (QSSA-Vf) and dynamic solution (DS) at three different monomer Thiele moduli, Φ_1, at a constant comonomer Thiele moduli, Φ_2=0.5, a) rate of polymerization, b) particle growth, c) monomer mass transfer efficiency, and d) comonomer mass transfer efficiency.

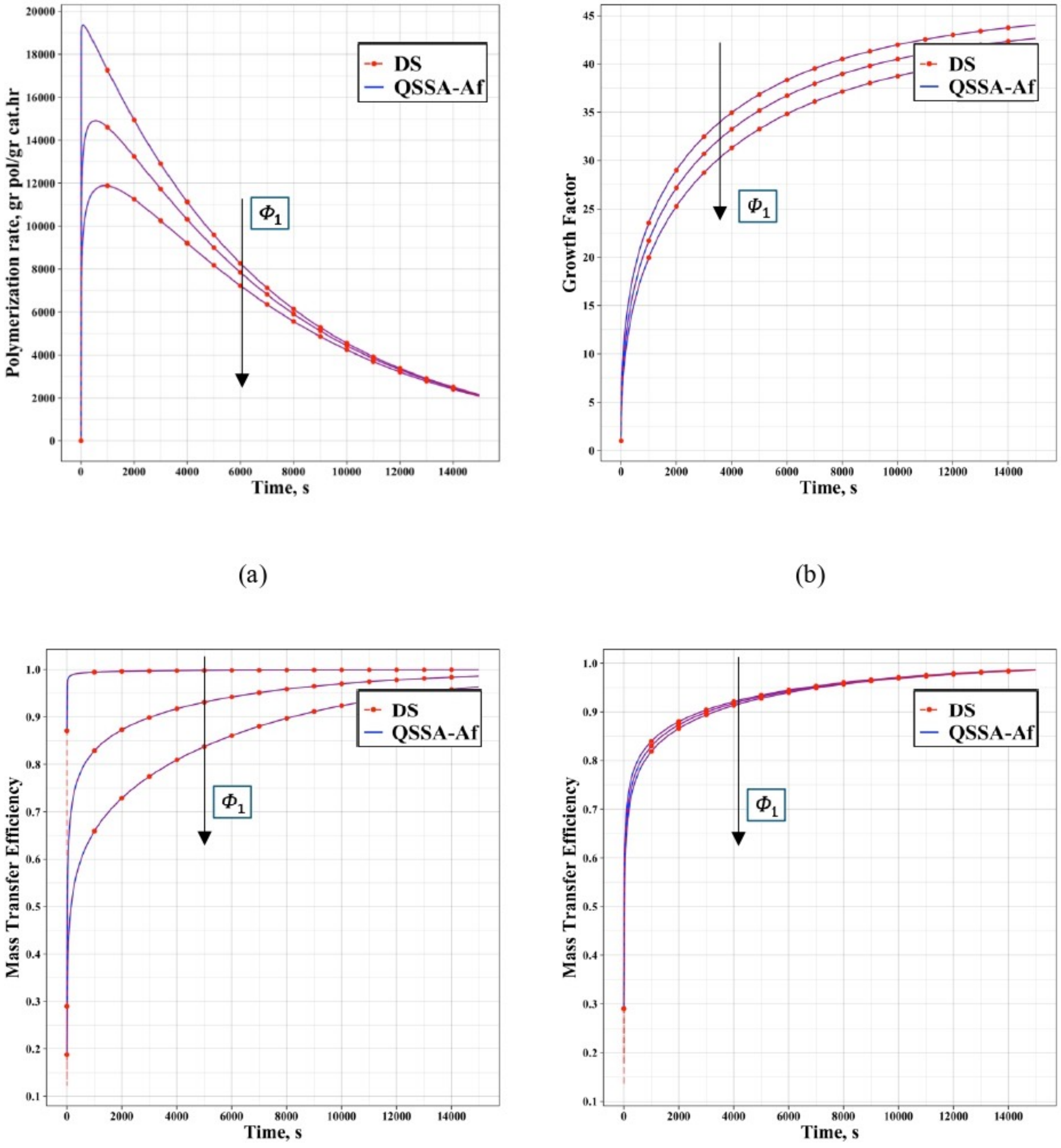

(a)

(b)

(c)

(d)

Figure B.3: Comparison between the quasi steady-state averaged monomer fraction (QSSA-Af) and dynamic solution (DS) at three different monomer Thiele moduli, Φ_1, at a constant comonomer Thiele moduli, Φ_2=3, a) rate of polymerization, b) particle growth, c) monomer mass transfer efficiency, and d) comonomer mass transfer efficiency.

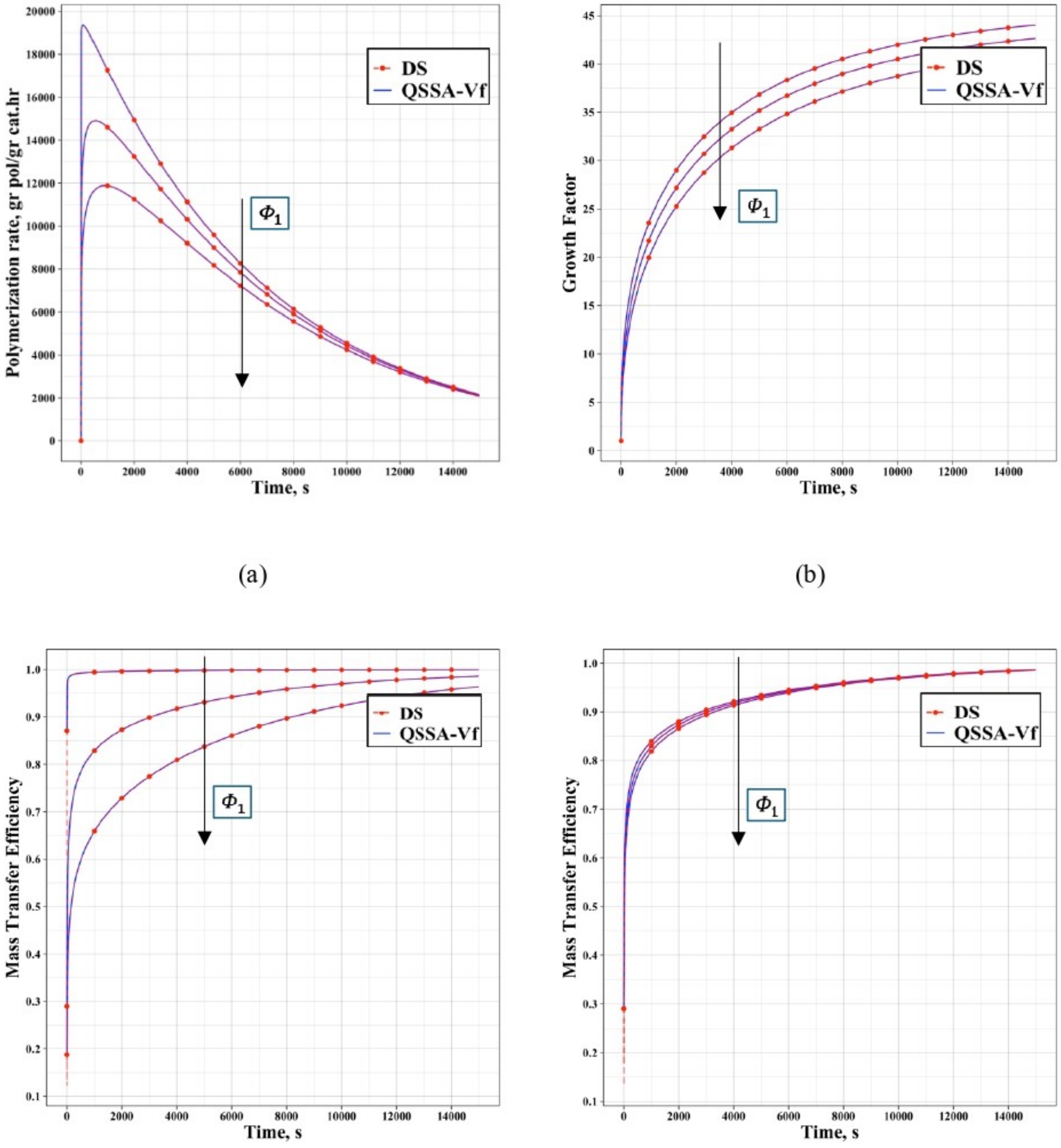

(a) (b)

(c) (d)

Figure B.4: Comparison between the quasi steady-state variable monomer fraction (QSSA-Vf) and dynamic solution (DS) at three different monomer Thiele moduli, Φ_1=0.5, 3, 5, at a constant comonomer Thiele moduli, Φ_2=3, a) rate of polymerization, b) particle growth, c) monomer mass transfer efficiency, and d) comonomer mass transfer efficiency.

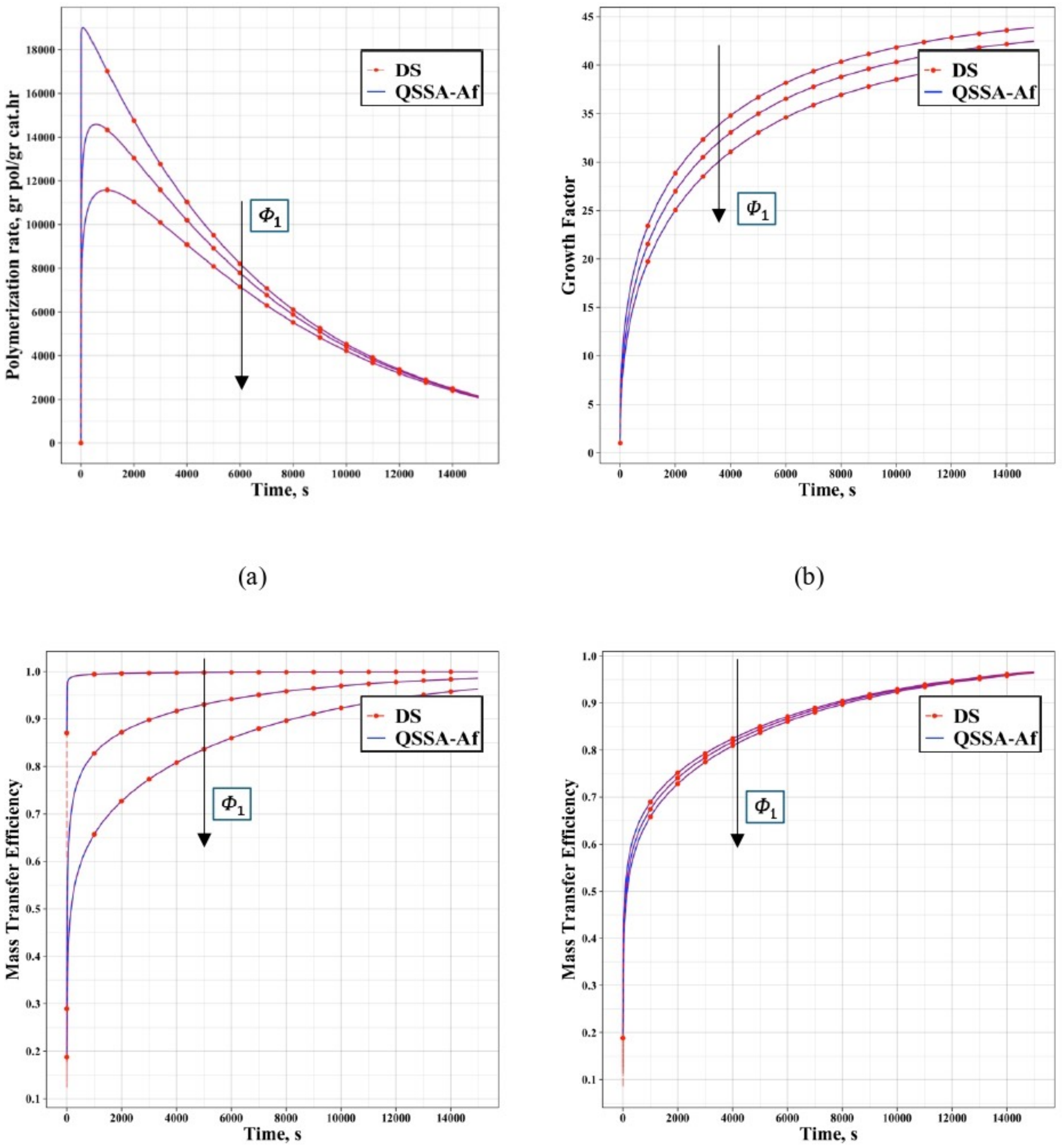

(a)

(b)

(c)

(d)

Figure B.5: Comparison between the quasi steady-state averaged monomer fraction (QSSA-Af) and dynamic solution (DS) at three different monomer Thiele moduli, Φ_1=0.5, 3, 5, at a constant comonomer Thiele moduli, Φ_2=5, a) rate of polymerization, b) particle growth, c) monomer mass transfer efficiency, and d) comonomer mass transfer efficiency.

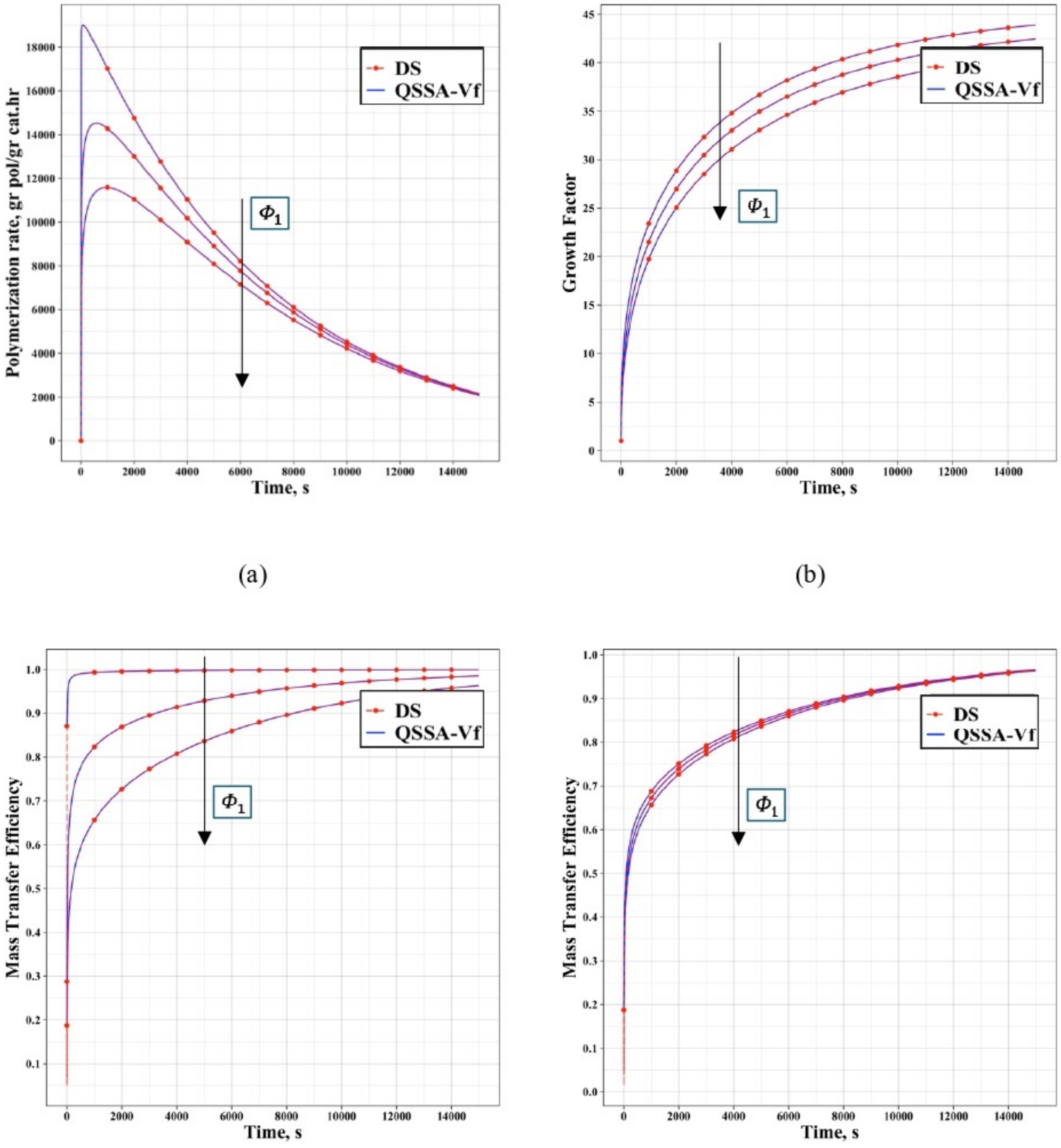

(a)

(b)

(c)

(d)

Figure B.6: Comparison between the quasi steady-state variable monomer fraction (QSSA-Vf) and dynamic solution (DS) at three different monomer Thiele moduli, Φ_1=0.5, 3, 5, at a constant comonomer Thiele moduli, Φ_2=5, a) rate of polymerization, b) particle growth, c) monomer mass transfer efficiency, and d) comonomer mass transfer efficiency.

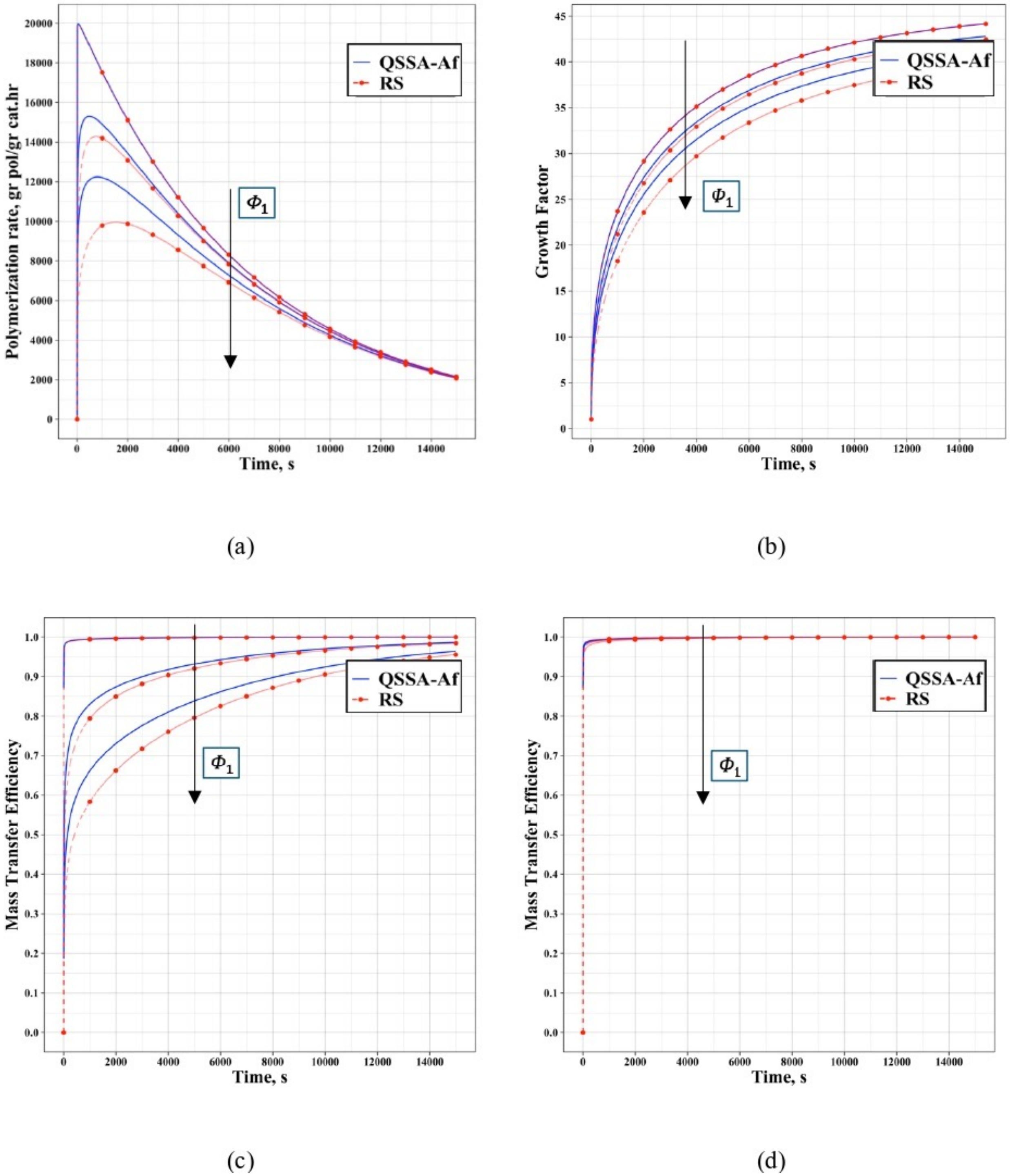

Figure B.7: Comparison between the quasi steady-state averaged monomer fraction (QSSA-Af) and rigorous solution (RS) at three different monomer Thiele moduli, Φ_1, at a constant comonomer Thiele moduli, Φ_2=0.5, a) rate of polymerization, b) particle growth, c) monomer mass transfer efficiency, and d) comonomer mass transfer efficiency.

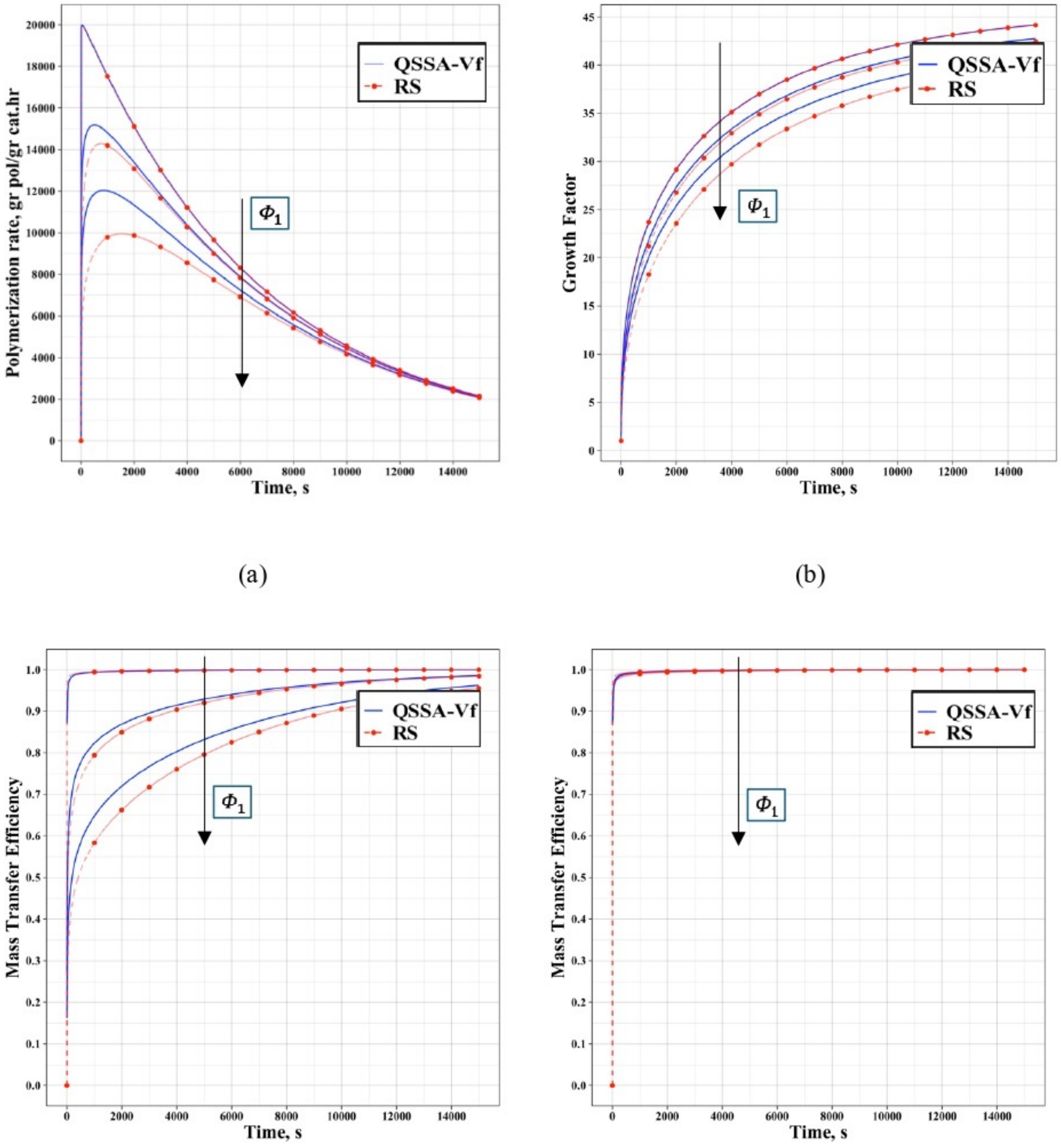

(a) (b)

(c) (d)

Figure B.8: Comparison between the quasi steady-state variable monomer fraction (QSSA-Vf) and rigorous solution (RS) at three different monomer Thiele moduli, Φ_1, at a constant comonomer Thiele moduli, Φ_2=0.5, a) rate of polymerization, b) particle growth, c) monomer mass transfer efficiency, and d) comonomer mass transfer efficiency.

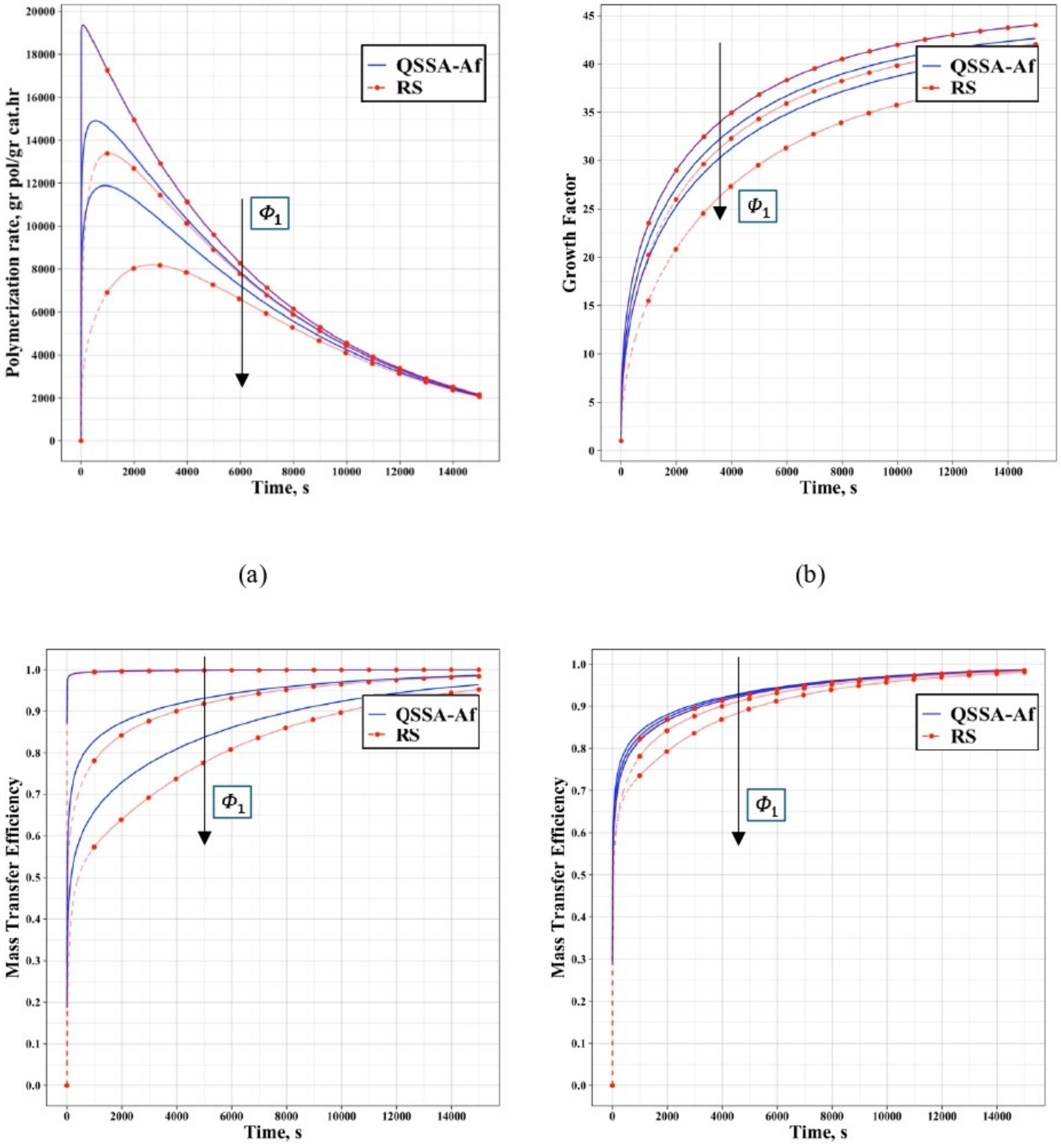

(a) (b)

(c) (d)

Figure B.9: Comparison between the quasi steady-state averaged monomer fraction (QSSA-Af) and rigorous solution (RS) at three different monomer Thiele moduli, Φ_1, at a constant comonomer Thiele moduli, Φ_2=3, a) rate of polymerization, b) particle growth, c) monomer mass transfer efficiency, and d) comonomer mass transfer efficiency.

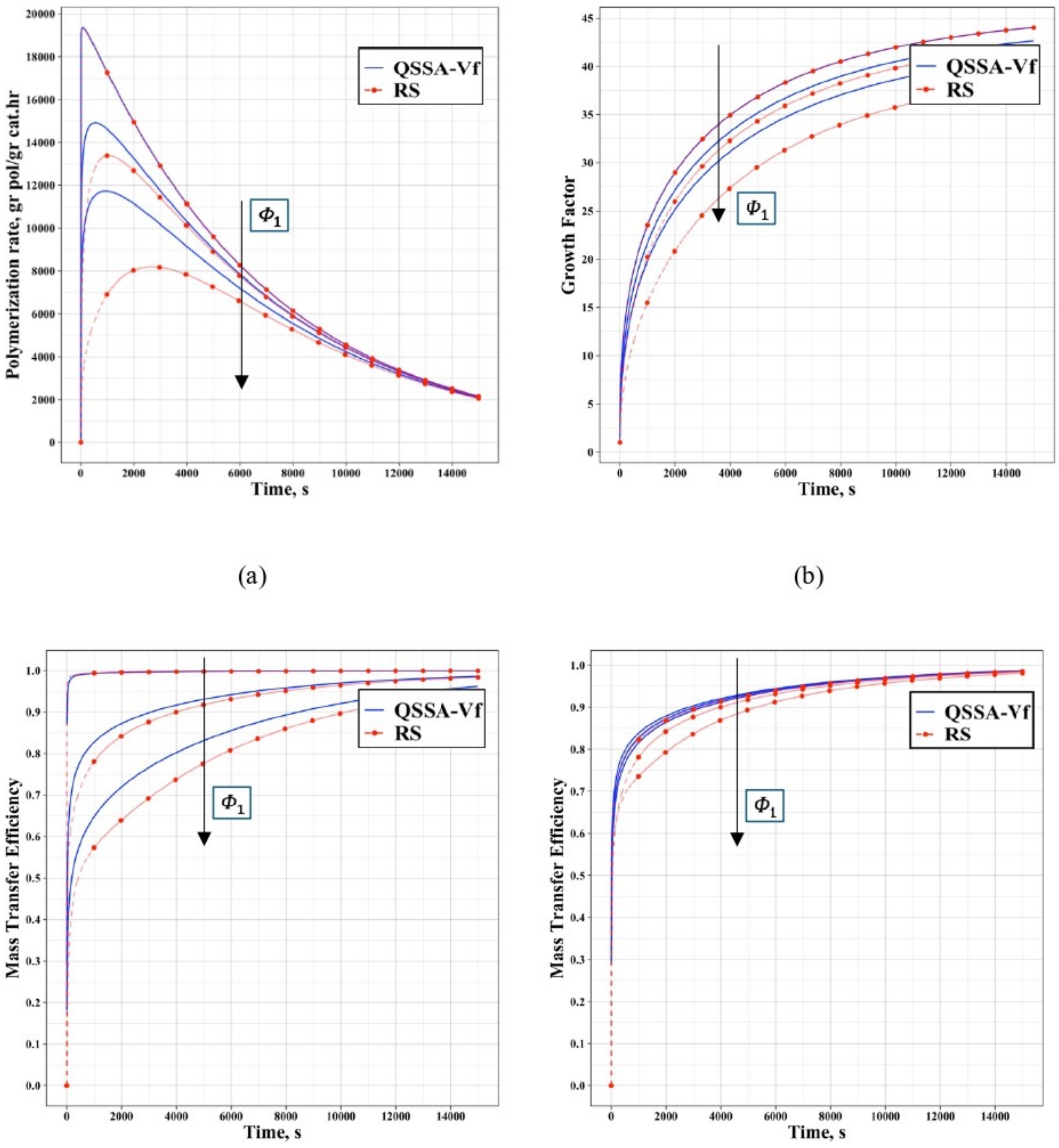

(a)

(b)

(c)

(d)

Figure B.10: Comparison between the quasi steady-state variable monomer fraction (QSSA-Vf) and rigorous solution (RS) at three different monomer Thiele moduli, Φ_1, at a constant comonomer Thiele moduli, Φ_2=3, a) rate of polymerization, b) particle growth, c) monomer mass transfer efficiency, and d) comonomer mass transfer efficiency.

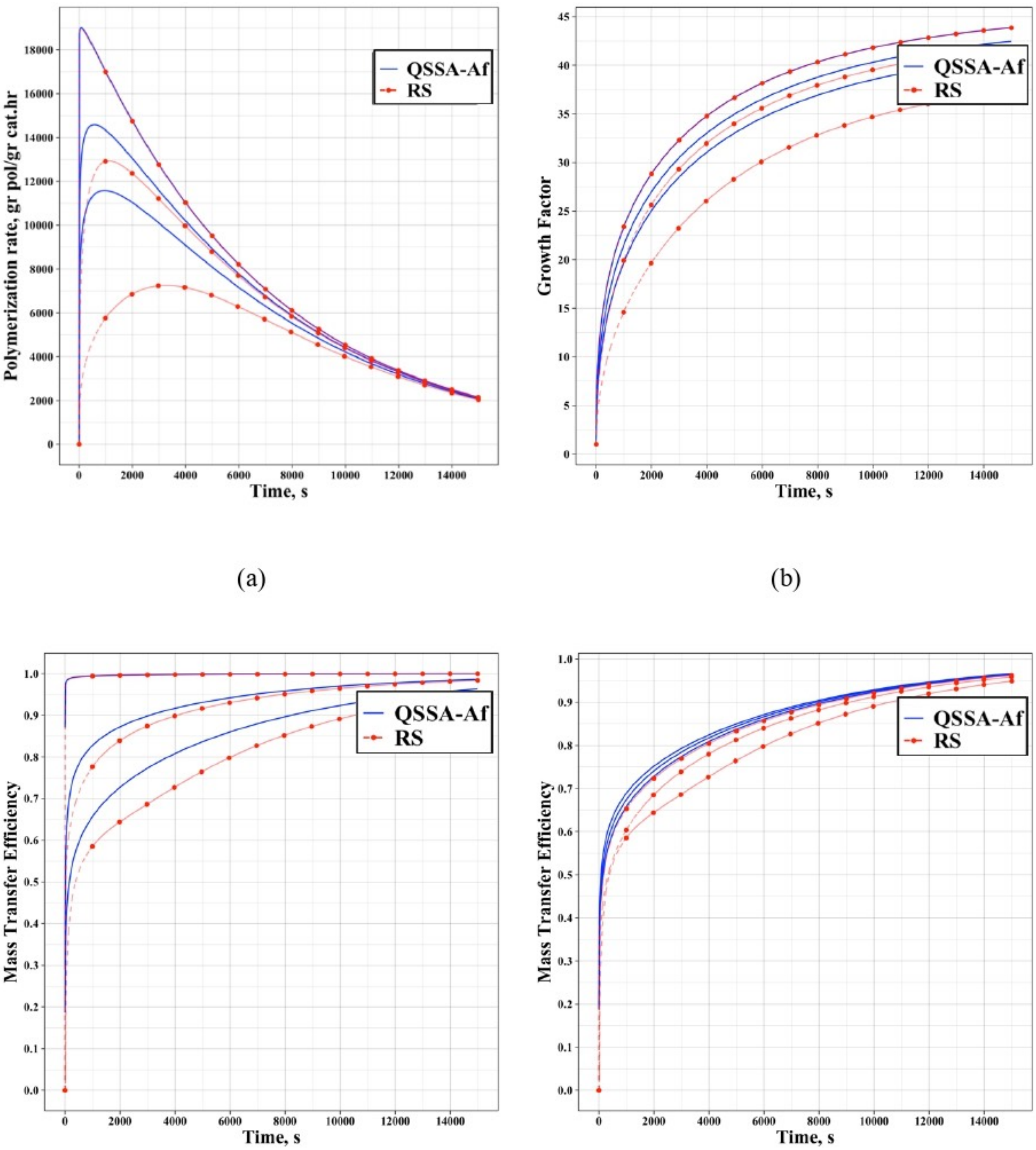

(a) (b)

(c) (d)

Figure B.11: Comparison between the quasi steady-state averaged monomer fraction (QSSA-Af) and rigorous solution (RS) at three different monomer Thiele moduli, Φ_1, at a constant comonomer Thiele moduli, Φ_2=5, a) rate of polymerization, b) particle growth, c) monomer mass transfer efficiency, and d) comonomer mass transfer efficiency.

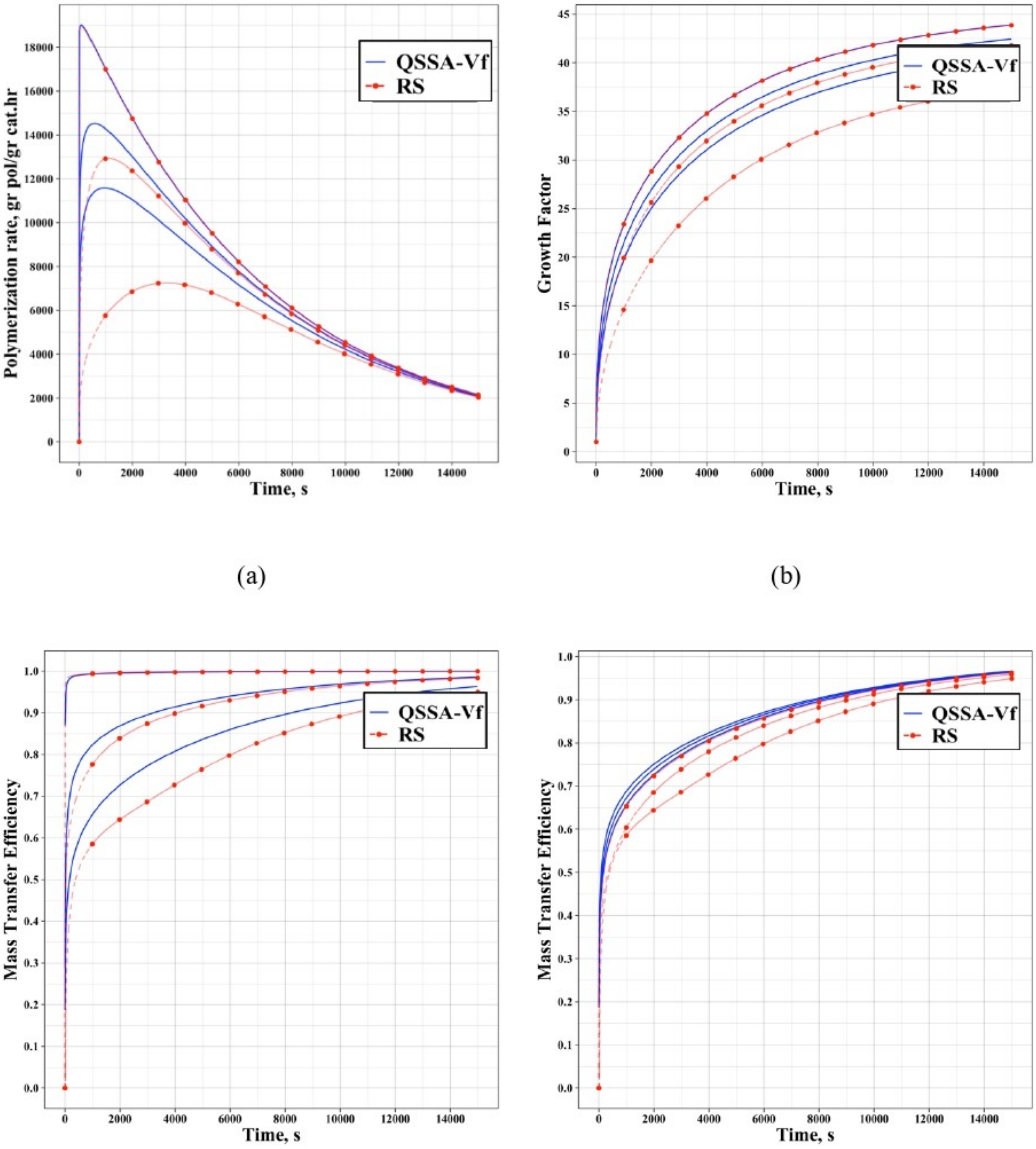

(a) (b)

(c) (d)

Figure B.12: Comparison between the quasi steady-state variable monomer fraction (QSSA-Vf) and rigorous solution (RS) at three different monomer Thiele moduli, Φ_1, at a constant comonomer Thiele moduli, Φ_2=5, a) rate of polymerization, b) particle growth, c) monomer mass transfer efficiency, and d) comonomer mass transfer efficiency.

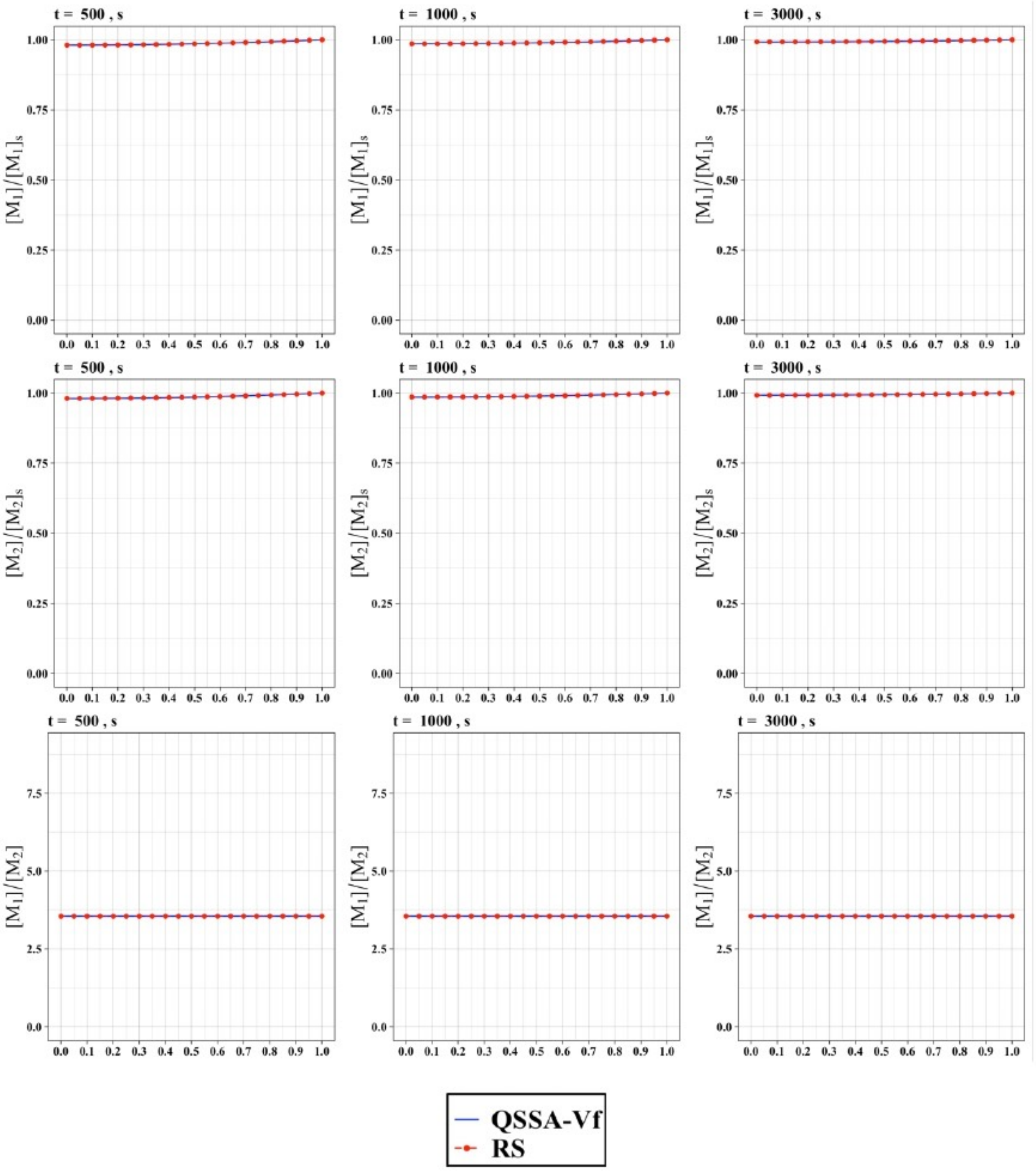

Figure B.13: Radial concentration profiles for monomer, comonomer and their ratios at three different times. Φ_1=0.5, Φ_2=0.5.

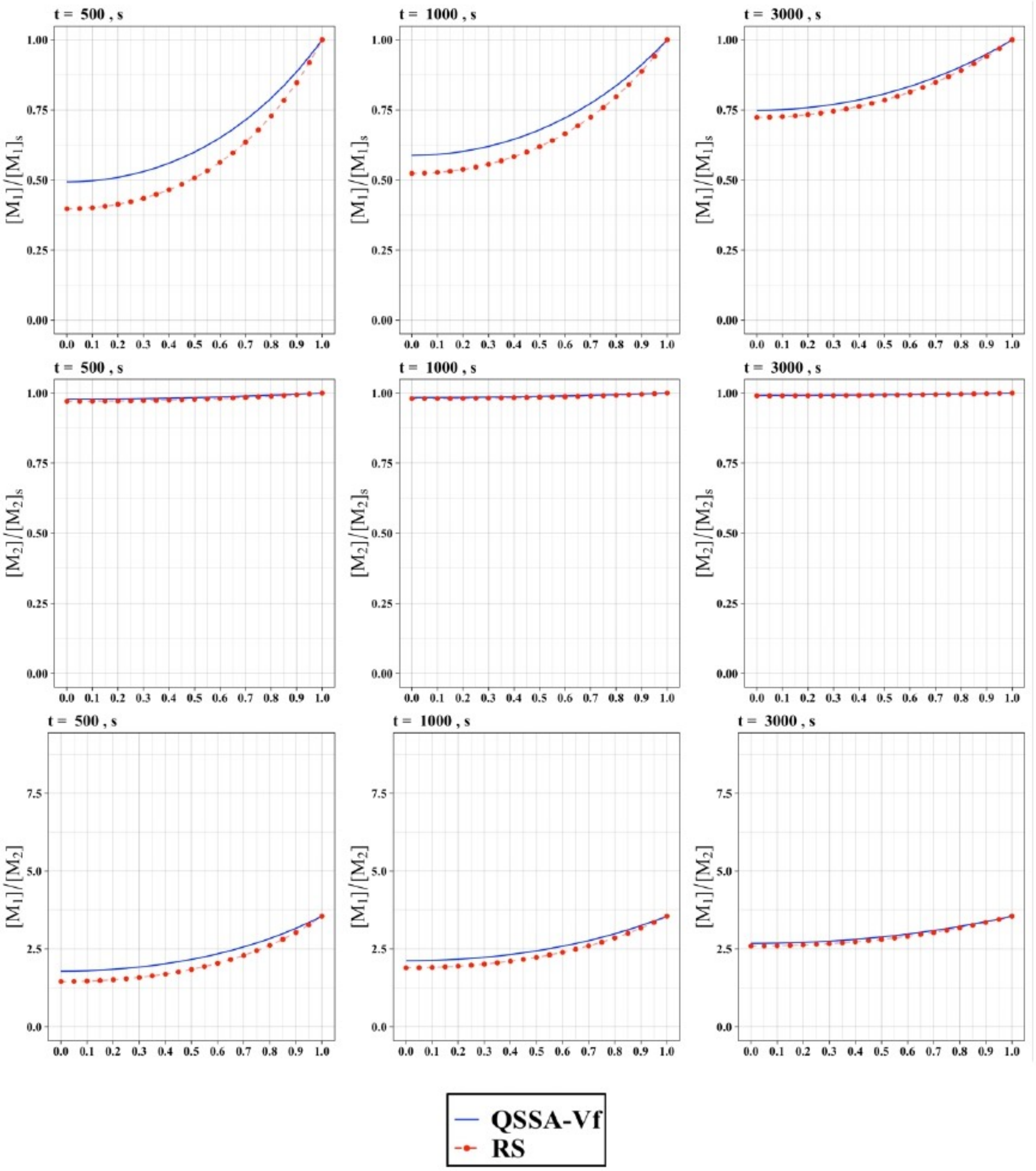

Figure B.14: Radial concentration profiles for monomer, comonomer and their ratios at three different times. Φ_1=3, Φ_2=0.5.

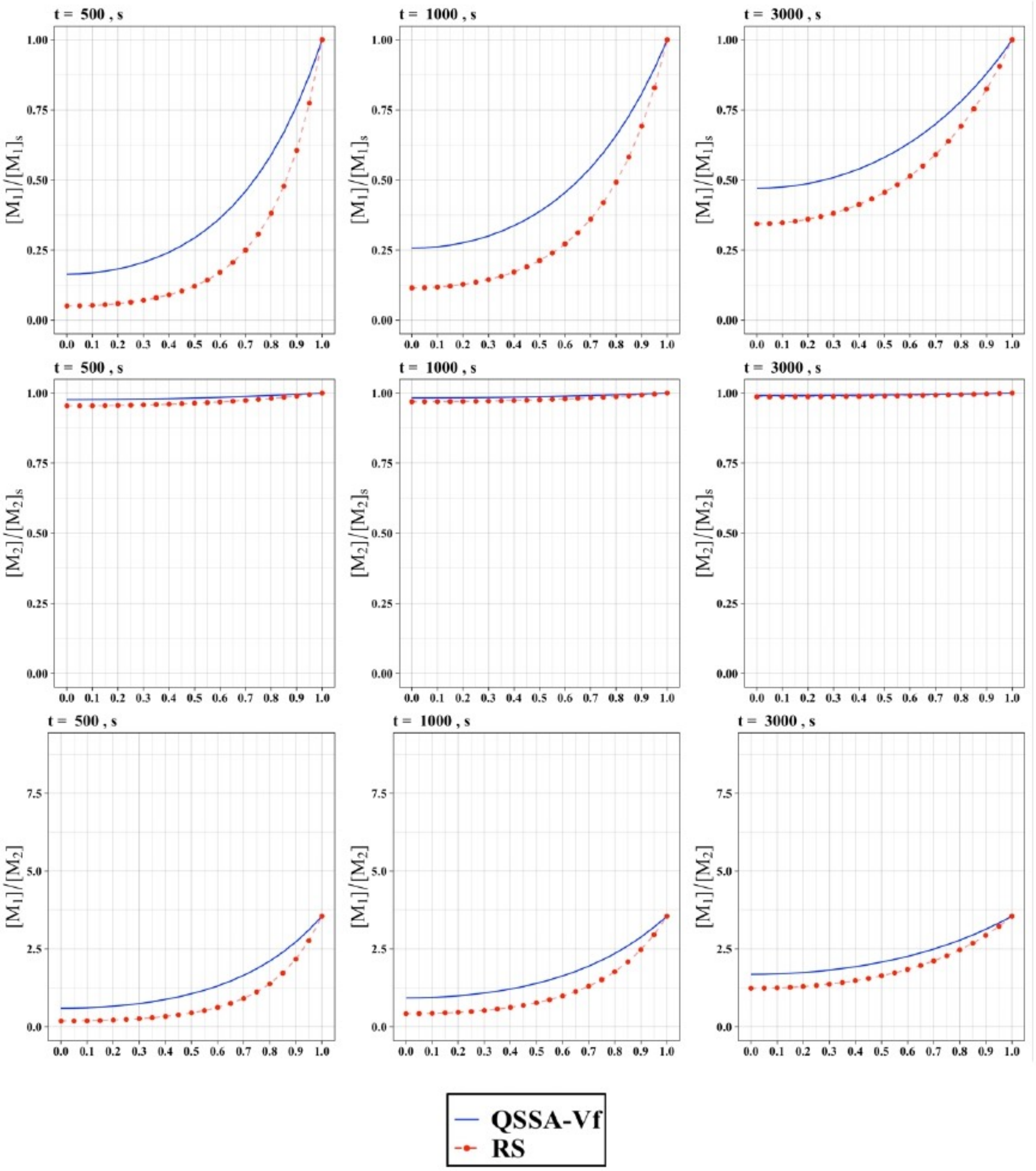

Figure B.15: Radial concentration profiles for monomer, comonomer and their ratios at three different times. Φ_1=5, Φ_2=0.5.

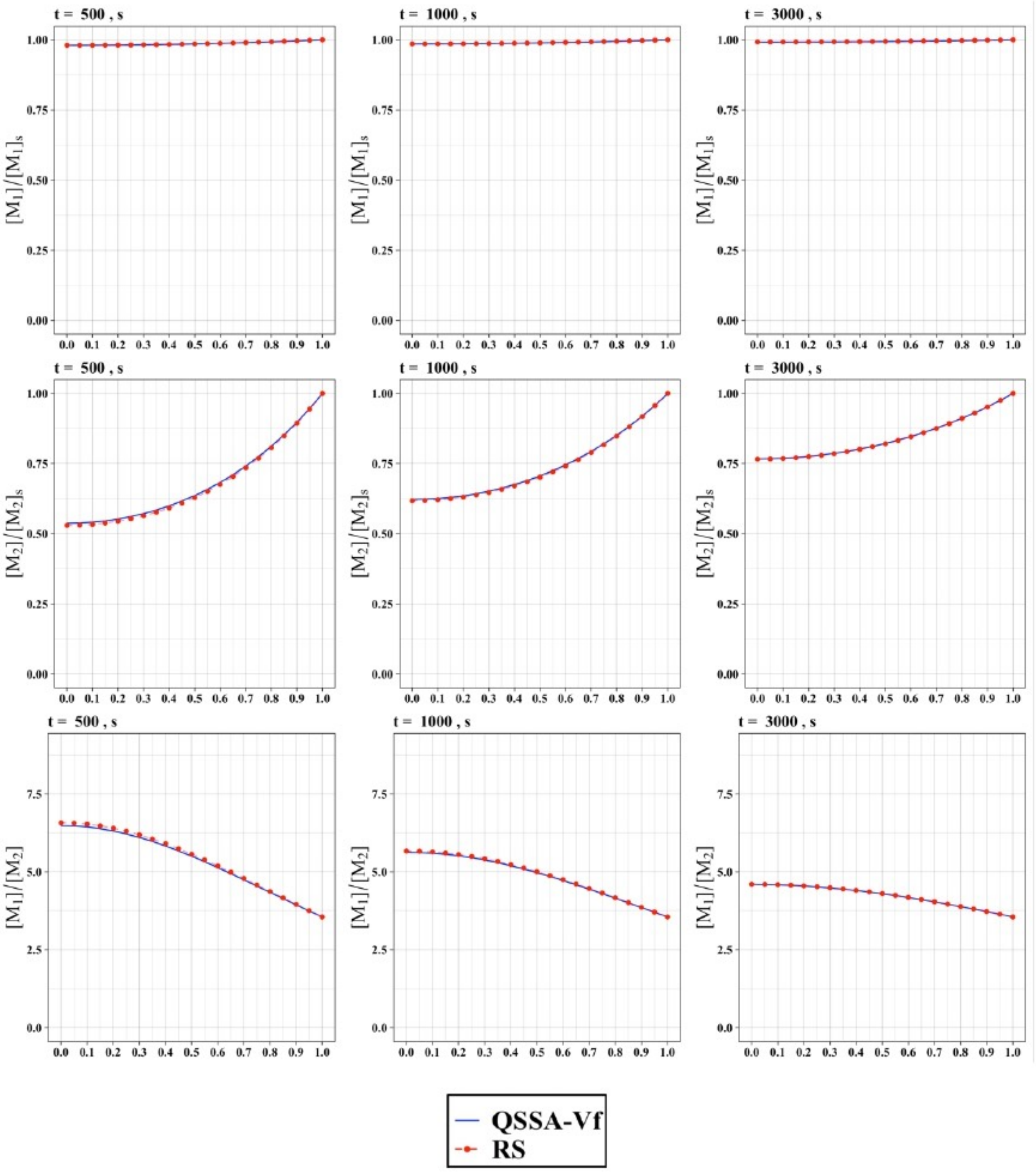

Figure B.16: Radial concentration profiles for monomer, comonomer and their ratios at three different times. Φ_1=0.5, Φ_2=3.

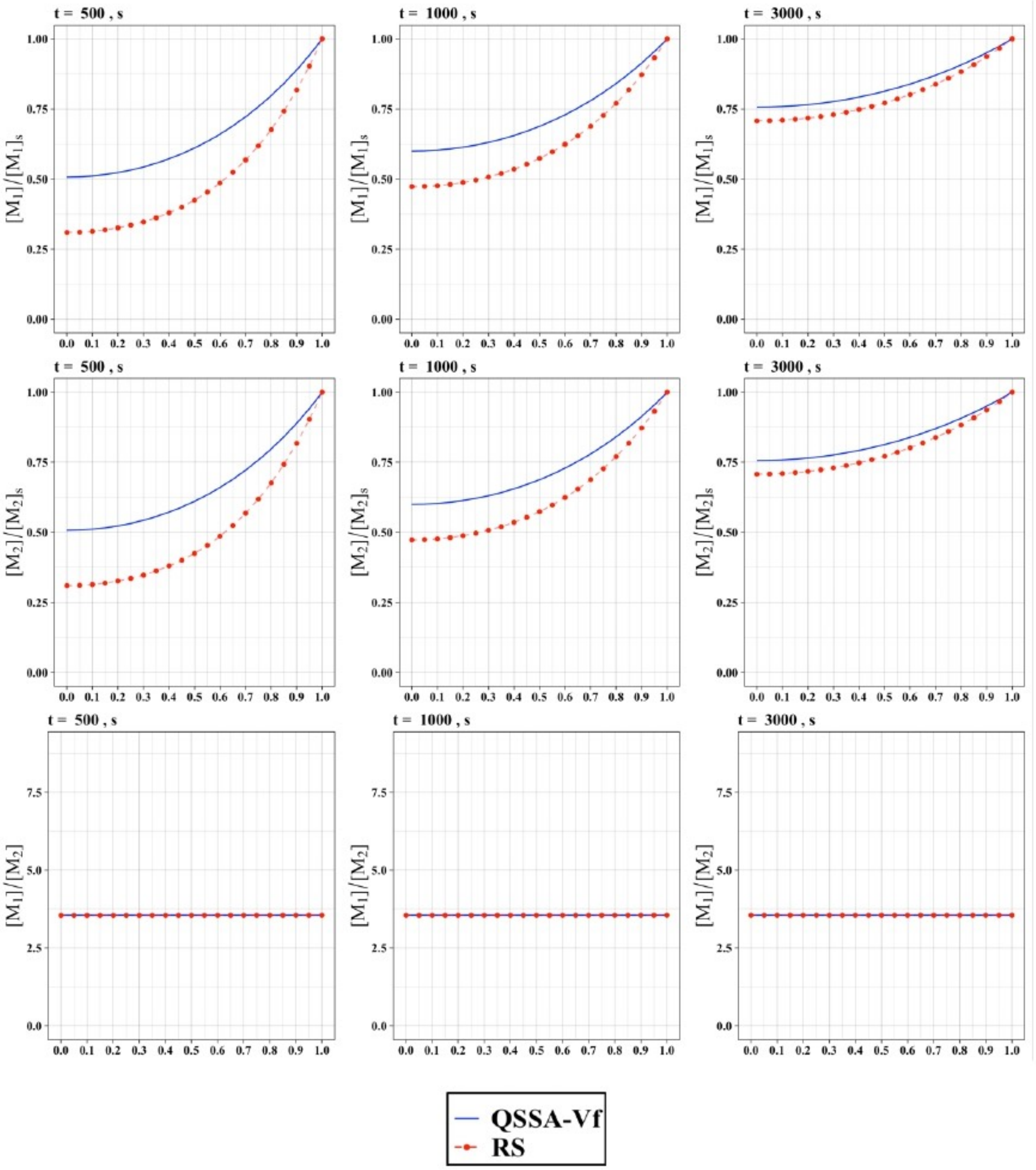

Figure B.17: Radial concentration profiles for monomer, comonomer and their ratios at three different times. Φ_1=3, Φ_2=3.}

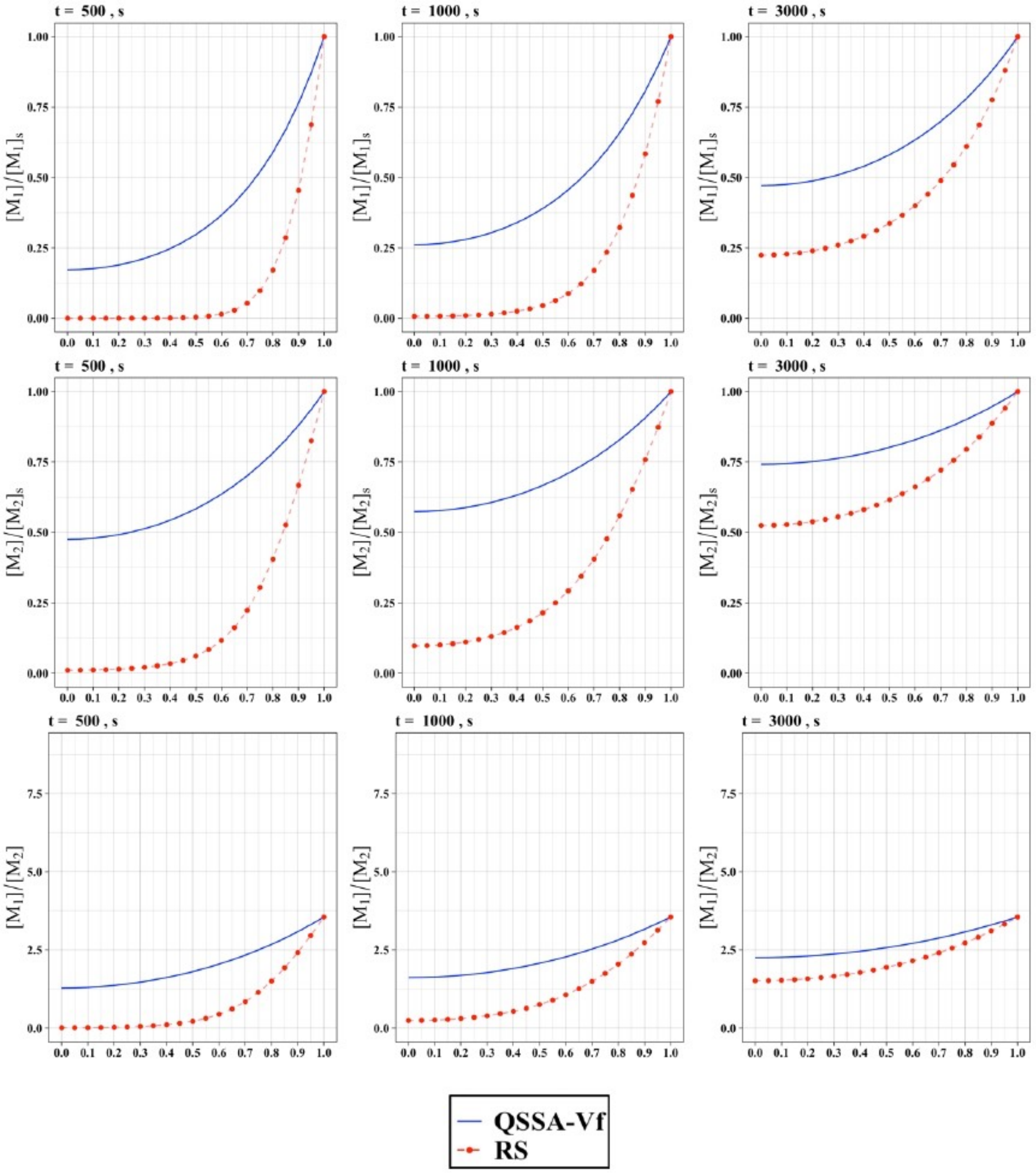

Figure B.18: Radial concentration profiles for monomer, comonomer and their ratios at three different times. Φ_1=5, Φ_2=3.

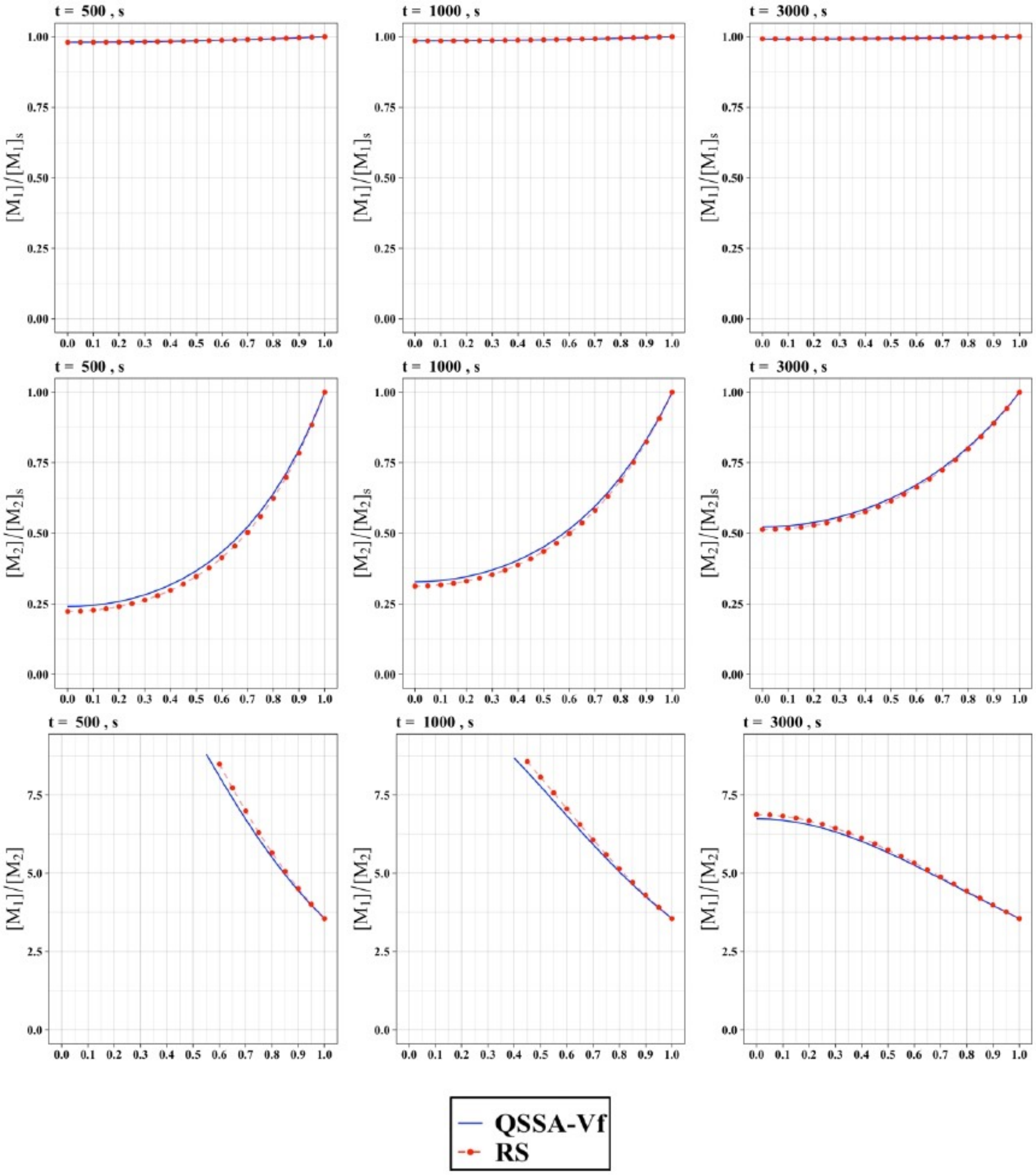

Figure B.19: Radial concentration profiles for monomer, comonomer and their ratios at three different times. Φ_1=0.5, Φ_2=5.

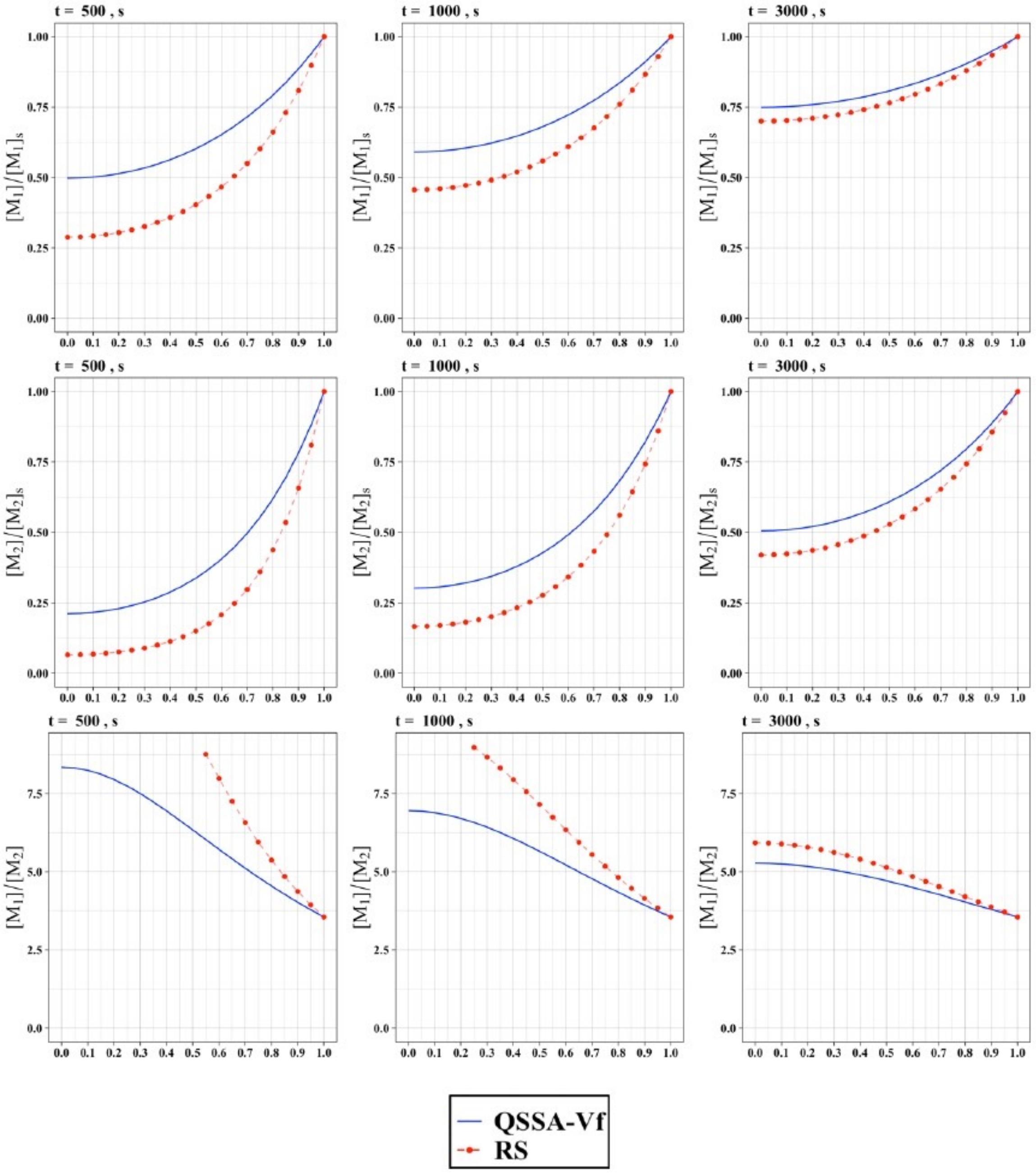

Figure B.20: Radial concentration profiles for monomer, comonomer and their ratios at three different times. Φ_1=3, Φ_2=5.

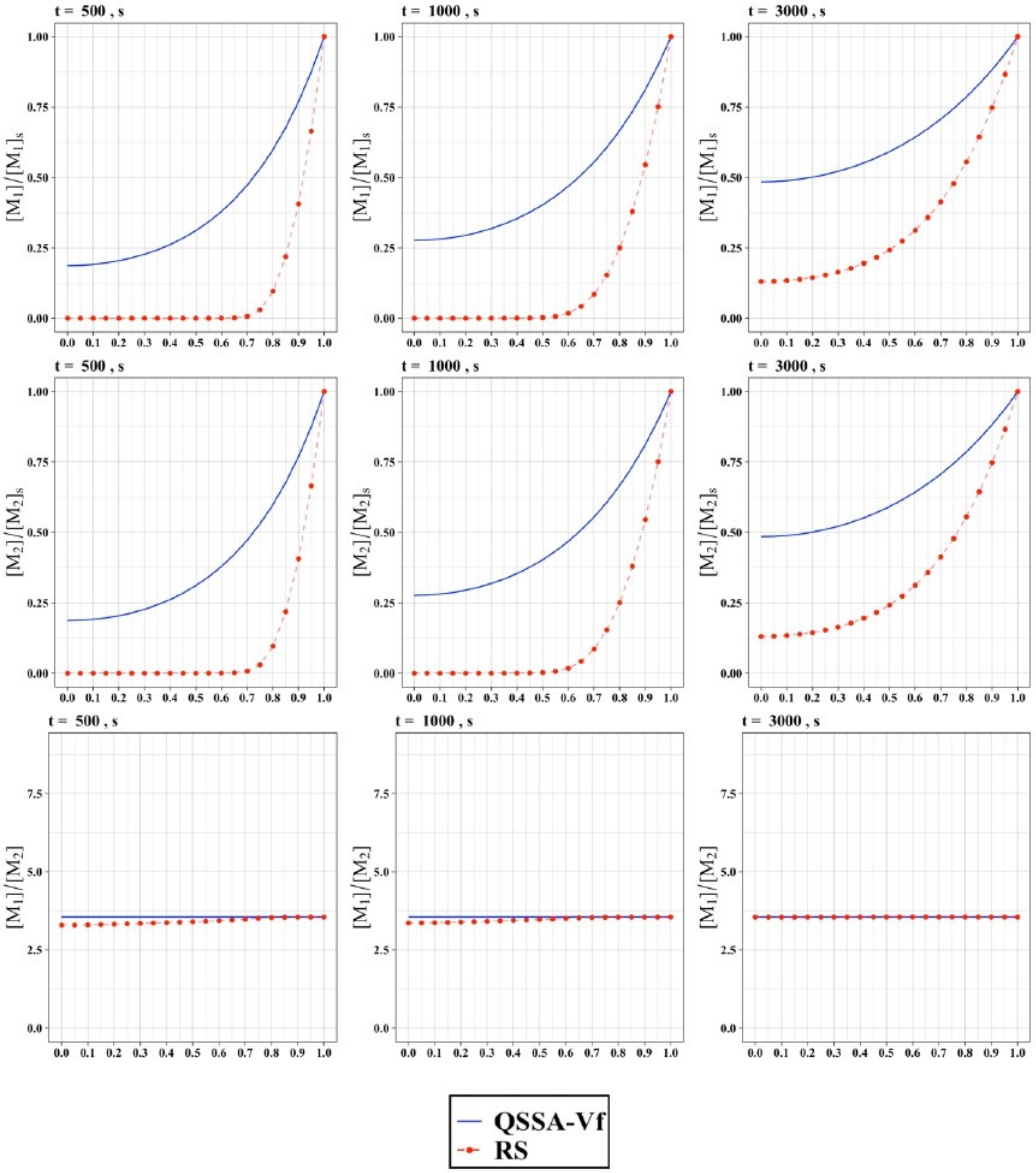

Figure B.21: Radial concentration profiles for monomer, comonomer and their ratios at three different times. Φ_1=5, Φ_2=5.

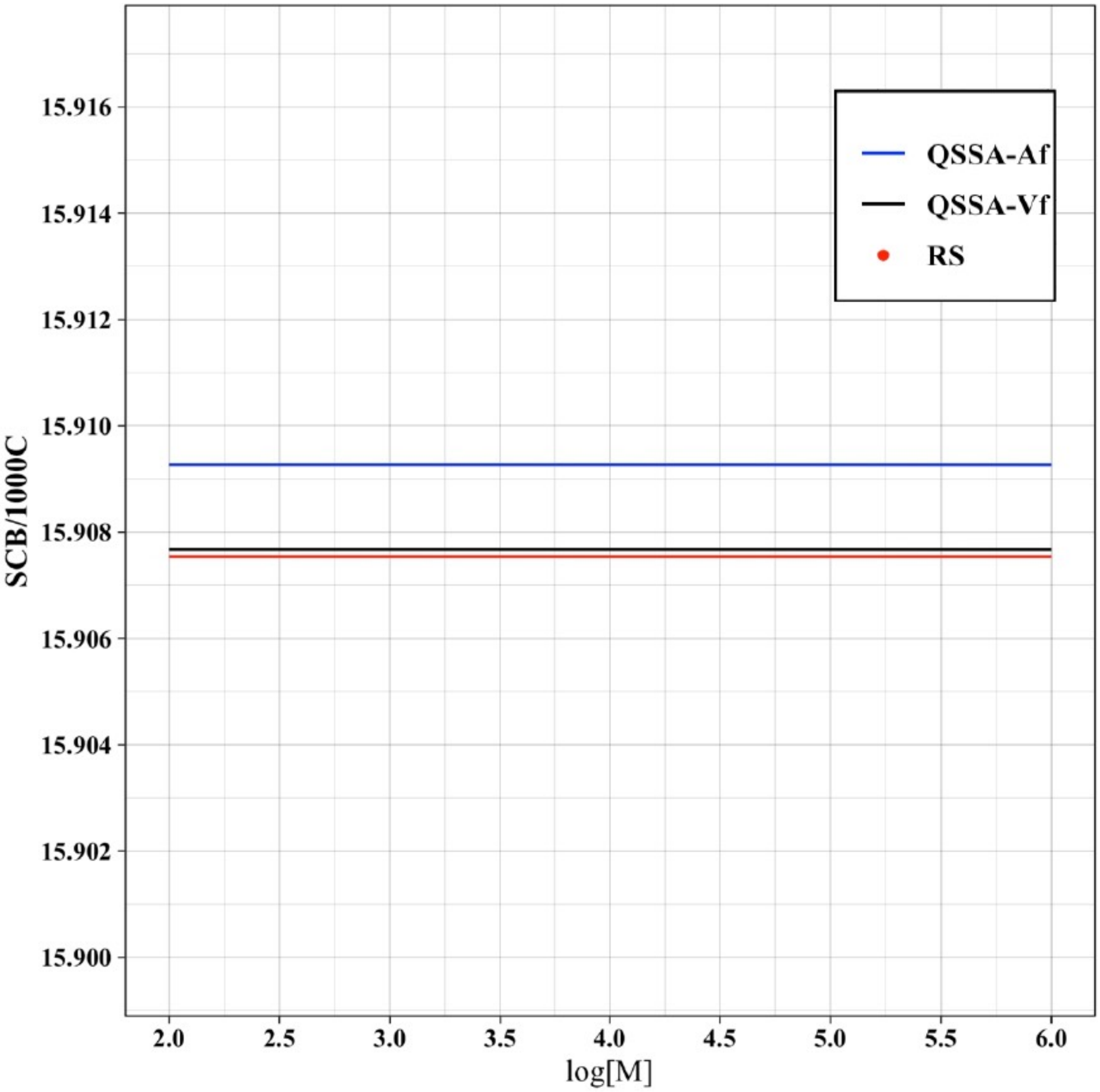

Figure B.22: Comparison of the short chain branching distribution between the quasi steady-state variable monomer fraction (QSSA-Vf) and rigorous solution (RS). Φ_1=0.5, Φ_2=0.5.

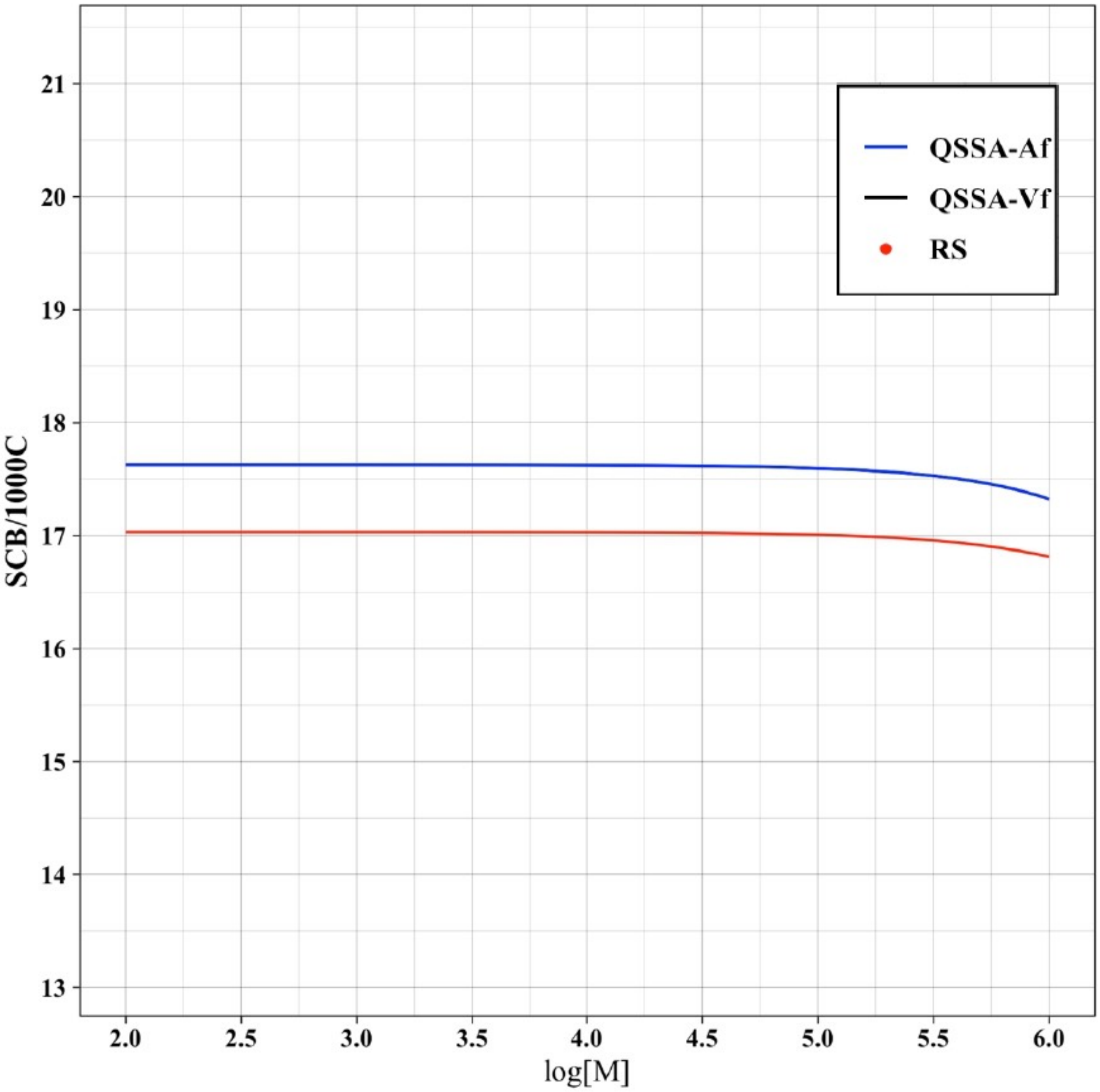

Figure B.23: Comparison of the short chain branching distribution between the quasi steady-state variable monomer fraction (QSSA-Vf) and rigorous solution (RS). Φ_1=3, Φ_2=0.5.

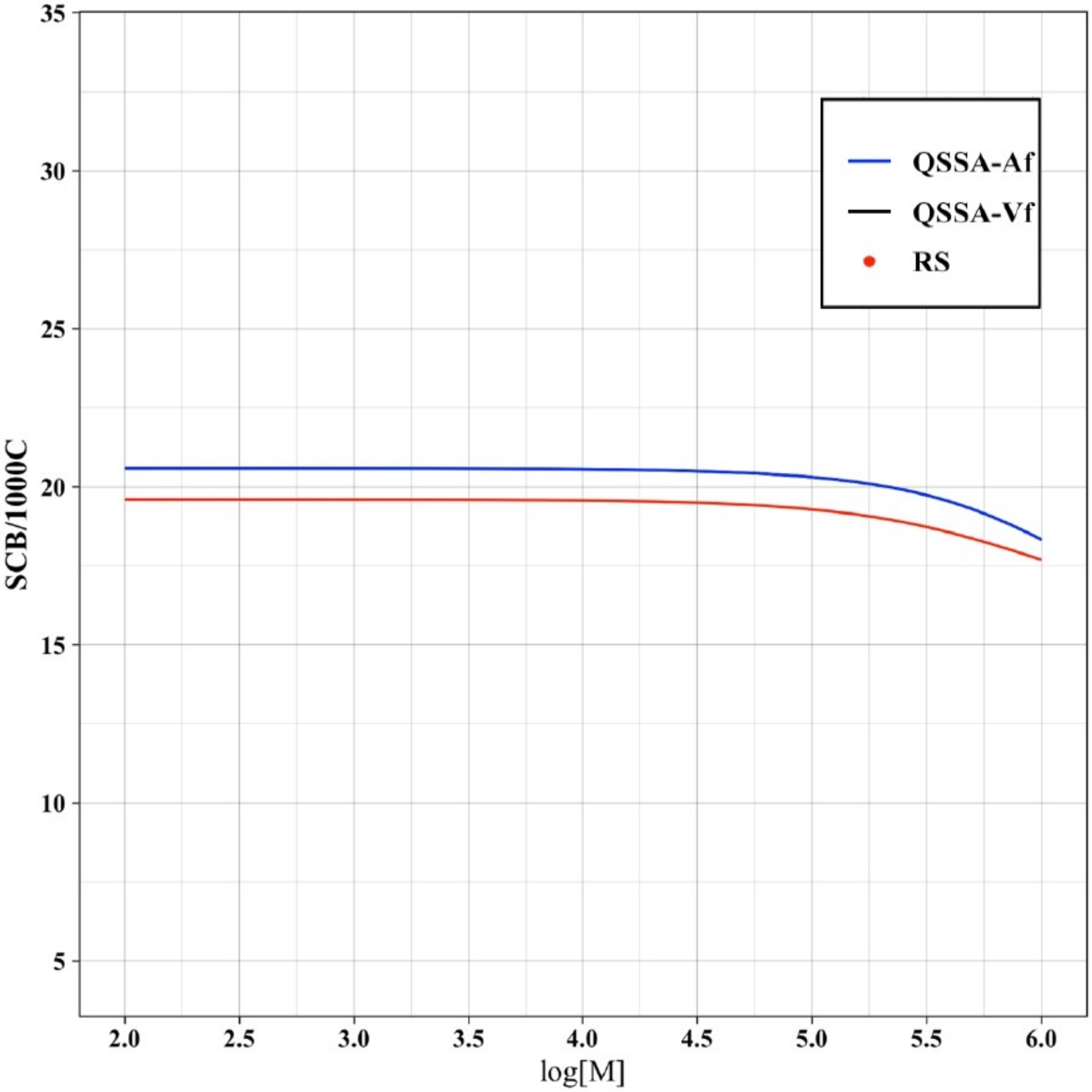

Figure B.24: Comparison of the short chain branching distribution between the quasi steady-state variable monomer fraction (QSSA-Vf) and rigorous solution (RS). Φ_1=5, Φ_2=0.5.

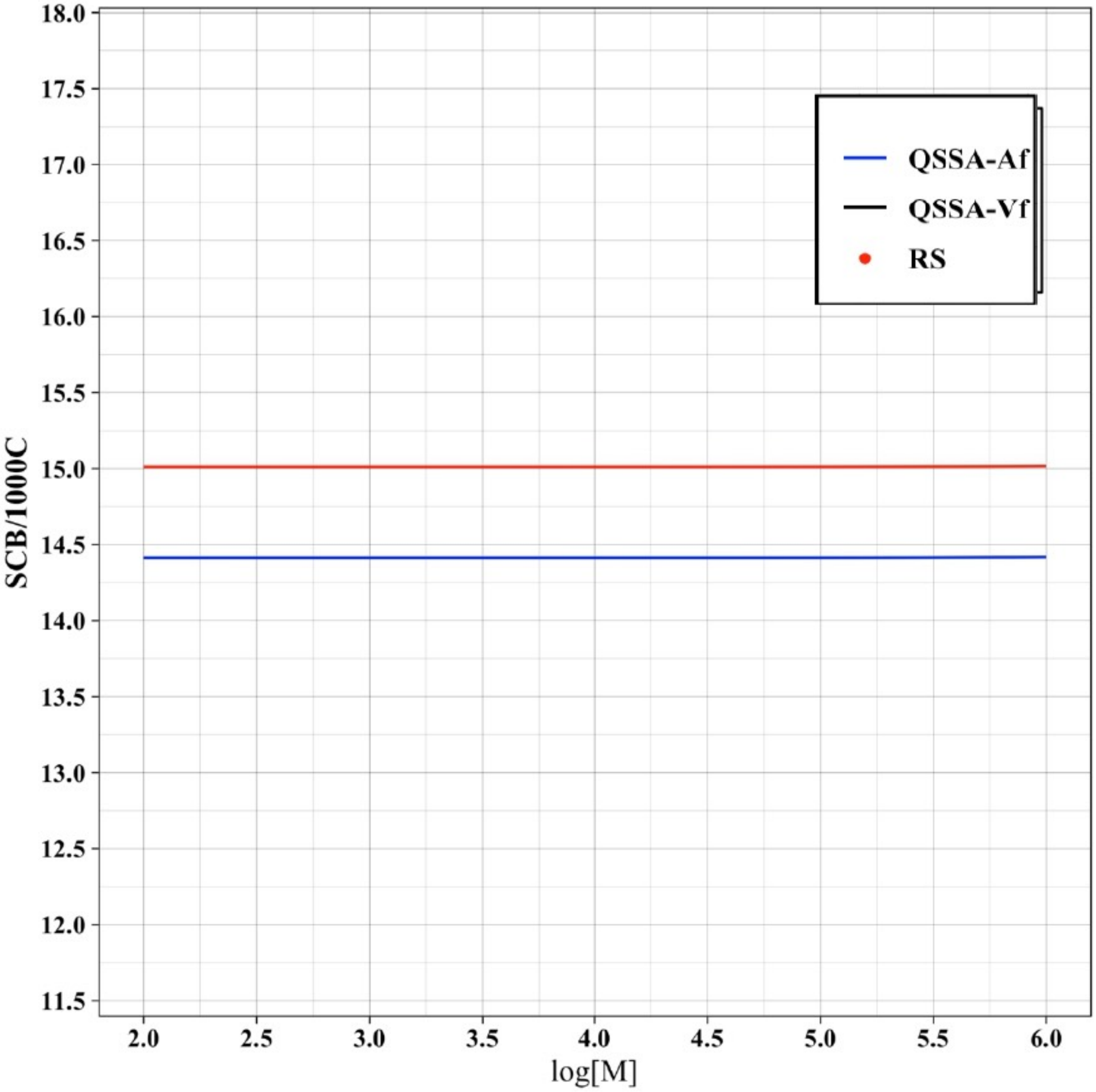

Figure B.25: Comparison of the short chain branching distribution between the quasi steady-state variable monomer fraction (QSSA-Vf) and rigorous solution (RS). Φ_1=0.5, Φ_2=3.

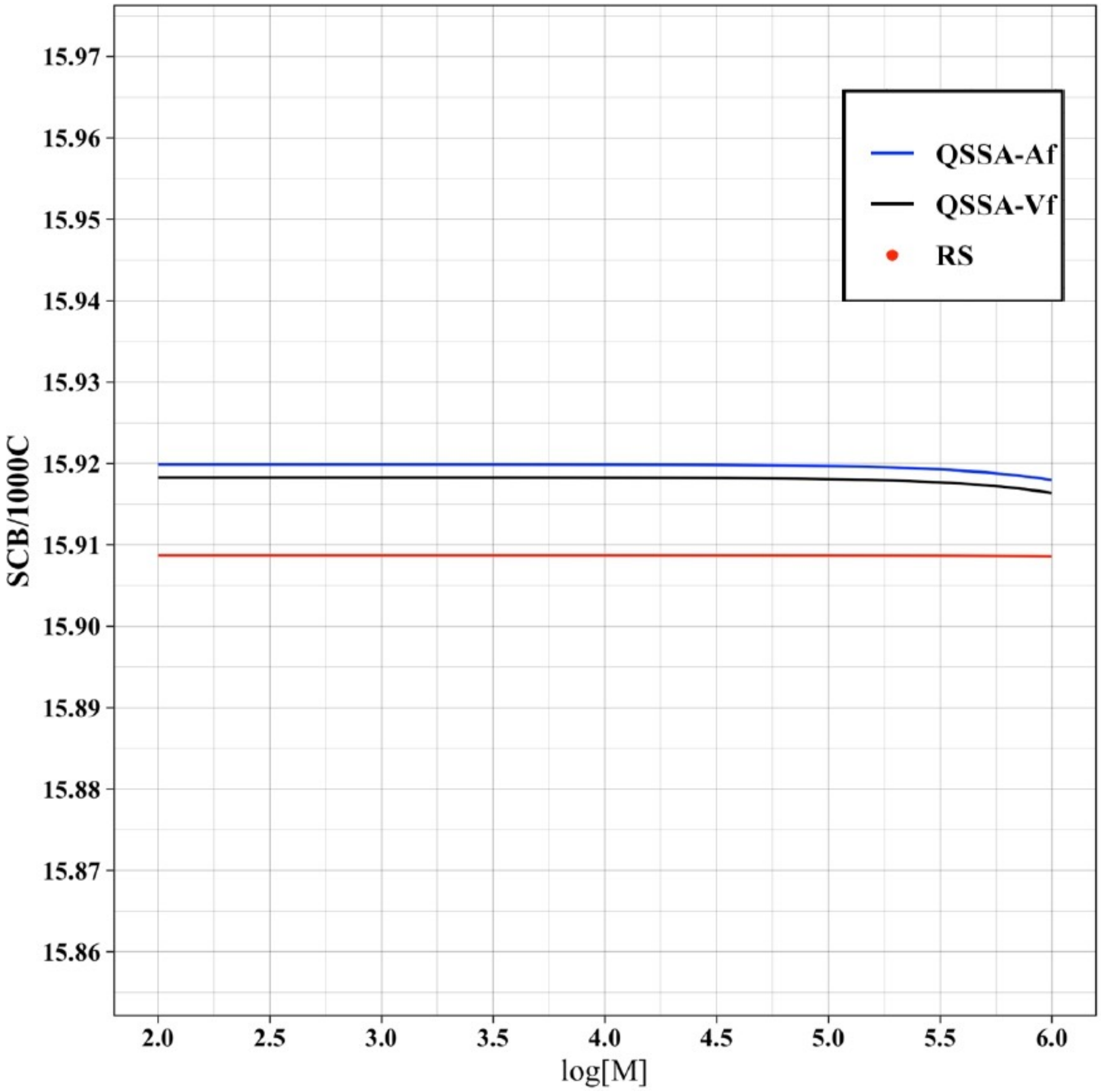

Figure B.26: Comparison of the short chain branching distribution between the quasi steady-state variable monomer fraction (QSSA-Vf) and rigorous solution (RS). Φ_1=3, Φ_2=3.

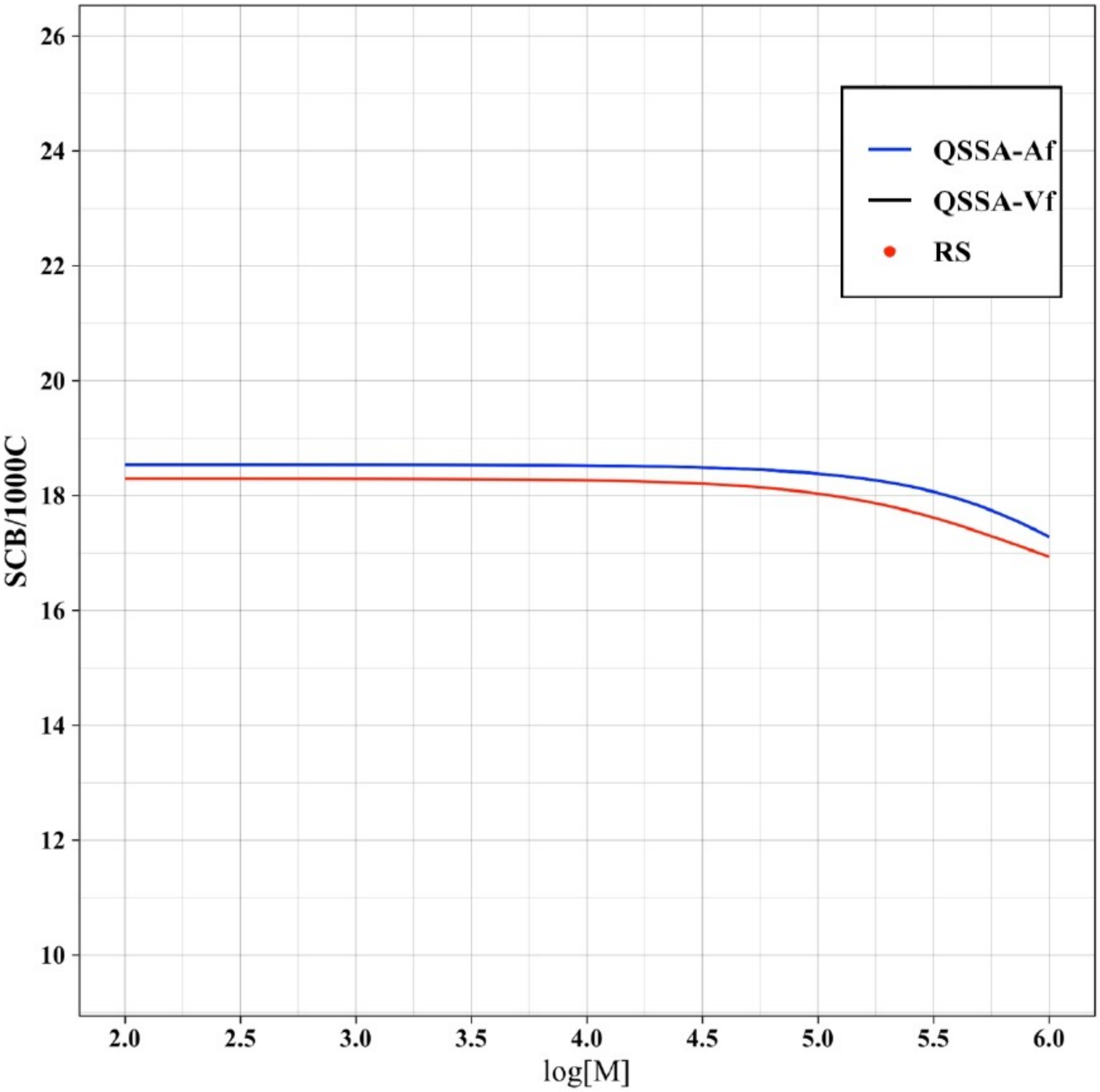

Figure B.27: Comparison of the short chain branching distribution between the quasi steady-state variable monomer fraction (QSSA-Vf) and rigorous solution (RS). Φ_1=5, Φ_2=3.

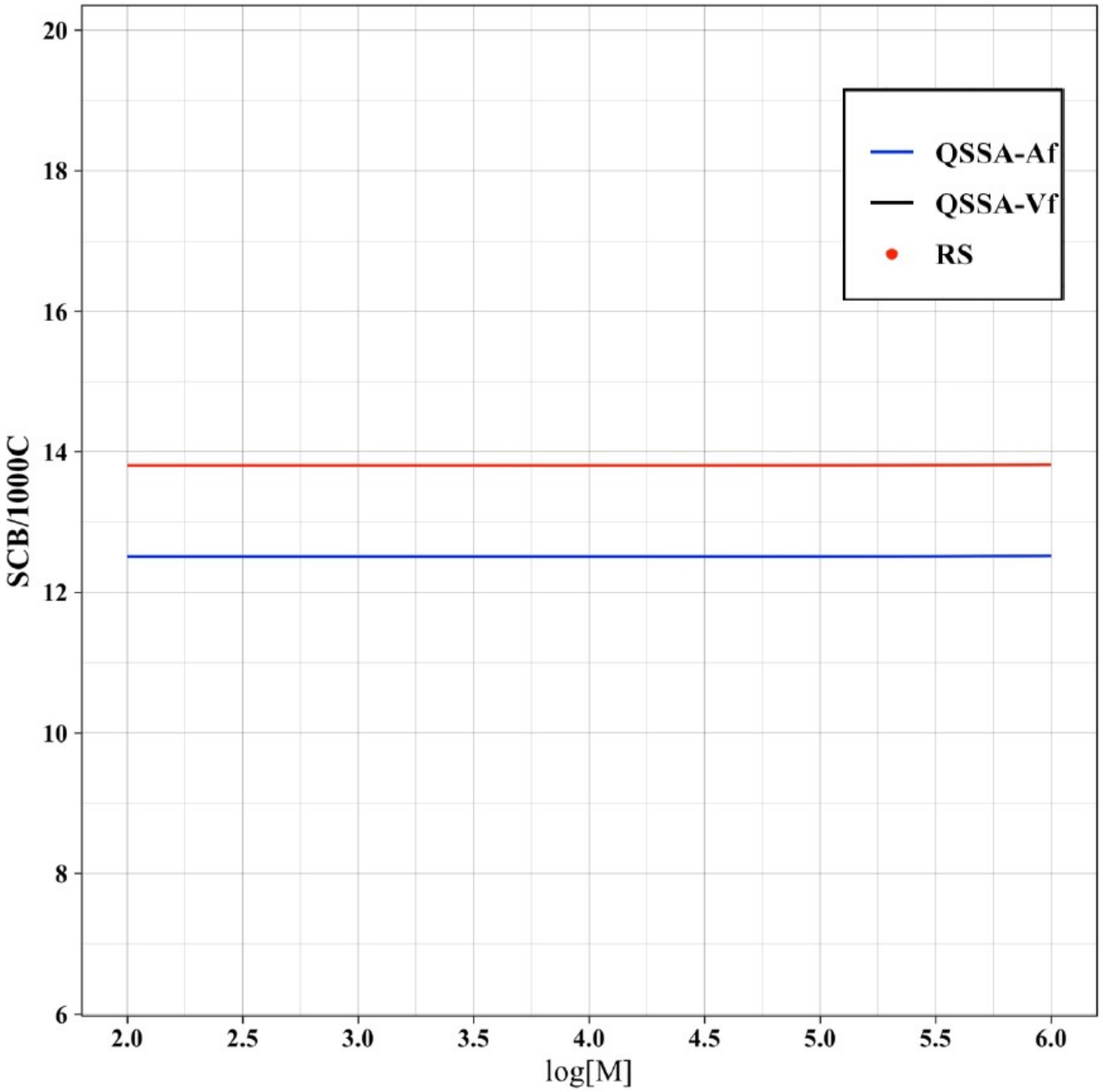

Figure B.28: Comparison of the short chain branching distribution between the quasi steady-state variable monomer fraction (QSSA-Vf) and rigorous solution (RS). Φ_1=0.5, Φ_2=5.

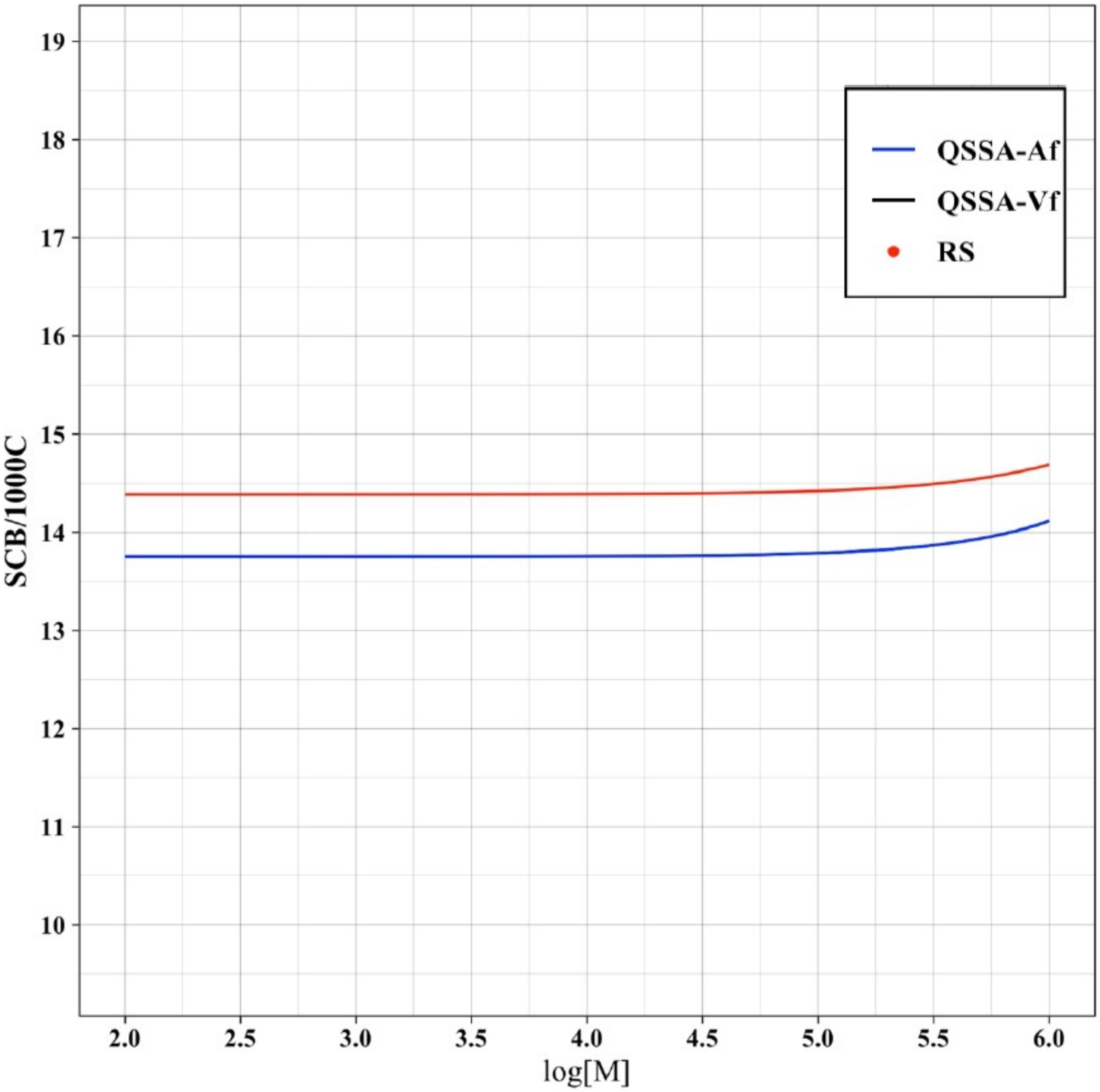

Figure B.29: Comparison of the short chain branching distribution between the quasi steady-state variable monomer fraction (QSSA-Vf) and rigorous solution (RS). Φ_1=3, Φ_2=5.

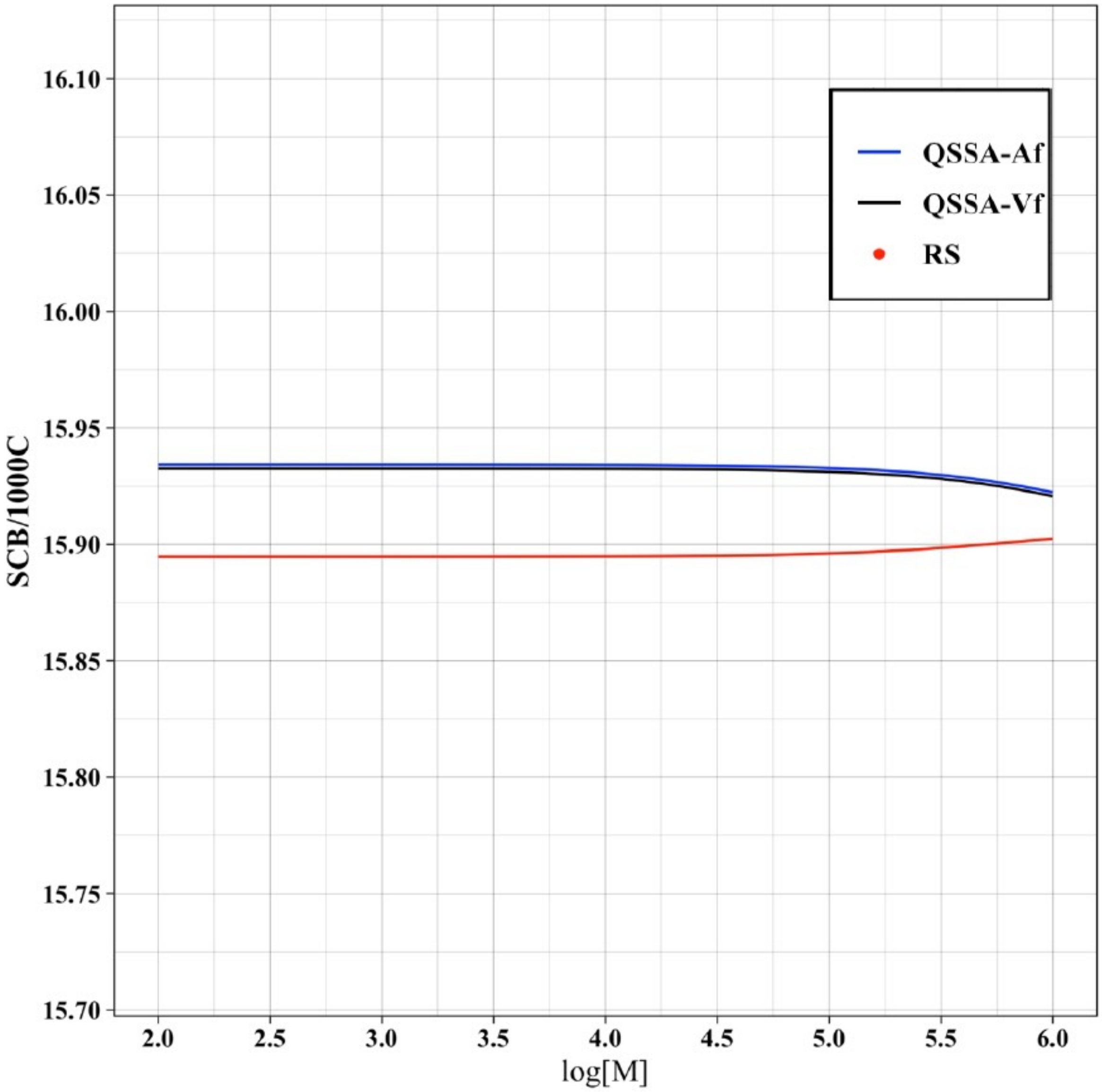

Figure B.30: Comparison of the short chain branching distribution between the quasi steady-state variable monomer fraction (QSSA-Vf) and rigorous solution (RS). Φ_1=5, Φ_2=5.